

**UCSF**

**UC San Francisco Electronic Theses and Dissertations**

**Title**

Characterization of the cellular signaling mechanisms of Tribbles pseudokinases

**Permalink**

<https://escholarship.org/uc/item/5p17x9pk>

**Author**

Kung, Jennifer Elaine

**Publication Date**

2018

Peer reviewed|Thesis/dissertation

Characterization of the cellular signaling mechanisms of Tribbles  
pseudokinases

by

Jennifer Elaine Kung

DISSERTATION

Submitted in partial satisfaction of the requirements for the degree of

DOCTOR OF PHILOSOPHY

in



Copyright 2018  
by  
Jennifer Elaine Kung

*Dedicated to my brother Michael*

## ACKNOWLEDGEMENTS

First and foremost, I would like to thank my adviser, Natalia Jura, for your unceasing encouragement and thoughtful guidance throughout my doctoral training. Without a doubt, working with you has helped me grow not only as a scientist, but also as a person. I have encountered countless challenges during graduate school, but I could always count on you to do whatever you could to help me overcome them. I feel fortunate to have such a supportive mentor and will always appreciate everything you have done for me. Your drive and your passion for science have been incredibly inspiring, and I am extremely grateful to have had this opportunity to work closely with you and to learn from you.

Thank you to all members of the Jura Lab, both past and present. I have learned so much from each and every one of you, and I am thankful for all the help and support you have provided me over the years. Thank you for sharing your advice, for being great friends, and for making the lab a fun place to be.

I would like to thank my thesis committee: Akiko Hata, John Gross, and Kevan Shokat for your enthusiasm and insightful advice. Your guidance has been invaluable in shaping my research, and I will always be grateful for the positivity and support you all have shown me throughout graduate school. Thank you to the CCB program for creating an engaging and intellectually stimulating environment. Many thanks to my CCB classmates: Kyle DeFrees, Danny Gentile, Rebecca Freilich, Alex Martinko, Sam Pollock, Izzy Taylor, and Rob Weber. Your friendship and the memories we have shared have been some the best parts of this long journey.

Finally, I would like to thank my family for their unending love and support. I would especially like to thank my parents for all the sacrifices they have made to allow me to be where I am today. Without you, none of this would be possible.

This work was supported by a National Science Foundation Graduate Research Fellowship and UCSF Discovery Fellowship.

Parts of this thesis are reproductions of material previously published in:

**Kung, J.E. & Jura, N. (2016).** Structural basis for the non-catalytic functions of protein kinases. *Structure*. 24, 7-24.

**Kung, J.E. & Jura, N. (2018).** Trb1 toggles an intramolecular switch to regulate COP1 nuclear export. (in review)

**Kung, J.E. & Jura, N. (2018).** Prospects of pharmacological targeting of pseudokinases. *Nature Reviews Drug Discovery*. (in preparation)

# **Characterization of the cellular signaling mechanisms of Tribbles pseudokinases**

by

Jennifer Elaine Kung

## **ABSTRACT**

Pseudokinases are members of the protein kinase superfamily that are predicted to be catalytically inactive despite retaining the conserved kinase domain fold. Consequently, pseudokinases have evolved to signal exclusively through non-catalytic mechanisms, such as allostery and scaffolding. Though pseudokinases have been implicated in a wide range of diseases and are known to be involved in critical cellular processes, their lack of catalytic activity has made their functions challenging to study. Members of the Tribbles family of pseudokinases have recently emerged as key regulators of diverse signaling pathways, including the MAPK cascade, proteasome-dependent degradation, the TGF- $\beta$ /BMP pathway, and the PI3K/Akt pathway. However, the molecular mechanisms underlying Tribbles-mediated signaling are poorly understood. One of the most highly conserved functions of Tribbles pseudokinases is their role in promoting ubiquitination of C/EBP transcription factors by the E3 ubiquitin ligase COP1. Dysregulation of this function has been implicated in acute myeloid leukemia, where overexpression of Trb1 or Trb2 is sufficient to induce leukemogenesis in mice through depletion of C/EBP $\alpha$ . Tribbles pseudokinases are thought to function as scaffolds to facilitate interactions between COP1 and substrates like C/EBP $\alpha$ , but the molecular basis for this function is only beginning to be uncovered. Here, we have investigated the molecular and structural determinants of regulation of COP1 by the pseudokinase Trb1. In doing so, we have uncovered a previously uncharacterized role for Trb1



in promoting COP1 nuclear localization through disrupting a conserved intramolecular regulatory interaction within COP1, and we have identified key structural elements that control COP1 localization. Collectively, these findings will deepen our understanding of the mechanisms underlying regulation of COP1 by Tribbles pseudokinases and broaden our knowledge of the diverse signaling functions of the Tribbles family.

## TABLE OF CONTENTS

<b>Chapter 1: Introduction</b> .....	1
Non-catalytic functions of protein kinases.....	2
Protein kinase structure and function.....	5
Pseudokinases.....	8
The Tribbles family of pseudokinases.....	10
References.....	14
<b>Chapter 2: Molecular basis for regulation of the E3 ubiquitin ligase COP1 by Trb1</b> .....	21
Abstract.....	22
Introduction.....	23
Results.....	25
Discussion.....	58
Materials and Methods.....	61
Acknowledgements.....	66
References.....	67
<b>Chapter 3: Structural and functional characterization of Trb1</b> .....	74
Introduction.....	75
Results.....	76
Discussion.....	85
Materials and Methods.....	87
Acknowledgements.....	90
References.....	91

## LIST OF TABLES

### Chapter 2

<b>Table 1.</b> Data collection and refinement statistics.....	51
<b>Table 2.</b> Peptides for fluorescence polarization competition assays.....	64

## LIST OF FIGURES

### Chapter 1

<b>Figure 1.</b> Kinases reported to have non-catalytic functions.....	4
<b>Figure 2.</b> Conformational transitions linked to kinase catalysis.....	6
<b>Figure 3.</b> Prevalence of pseudokinases in the kinomes of diverse species.....	9
<b>Figure 4.</b> Tribbles structure and comparison to canonical kinases.....	13

### Chapter 2

<b>Figure 1.</b> Trb1 promotes nuclear localization of COP1.....	27
<b>Figure 2.</b> COP1 and Trb1 colocalize in punctate nuclear structures.....	28
<b>Figure 3.</b> The Trb1 C-terminal tail is sufficient to promote COP1 nuclear localization.....	30
<b>Figure 4.</b> Mutations in the pseudoactive site do not affect the ability of Trb1 to promote nuclear localization of COP1.....	31
<b>Figure 5.</b> Nuclear localization of COP1 is regulated by the WD40 domain.....	33
<b>Figure 6.</b> Localization of Trb1-binding deficient COP1 WD40 mutants is unaffected By Trb1 coexpression.....	35
<b>Figure 7.</b> Trb1 competes with an intramolecular site for binding to the WD40 domain to modulate COP1 localization.....	37
<b>Figure 8.</b> Identification of an intramolecular WD40 binding site that regulates the subcellular distribution of COP1.....	39
<b>Figure 9.</b> Trb1 inhibits CRM1-mediated nuclear export of COP1.....	42
<b>Figure 10.</b> Coevolution of the COP1 pseudosubstrate latch and Tribbles.....	47
<b>Figure 11.</b> Identification of a heptad break in the COP1 coiled domain and its potential role in regulation of NES accessibility.....	49
<b>Figure 12.</b> Trb1 promotes nuclear import of COP1.....	52

<b>Figure 13.</b> N-terminal region of Trb1 is necessary for promoting COP1 nuclear localization.....	53
<b>Figure 14.</b> Cell cycle dependence of Trb1 and COP1 localization.....	55
<b>Figure 15.</b> A phosphomimetic mutation in the Trb1 C-terminal tail disrupts its interaction with COP1.....	56

### Chapter 3

<b>Figure 1.</b> Trb1 buffer optimization.....	76
<b>Figure 2.</b> Trb1 KD crystals and crystallization conditions.....	77
<b>Figure 3.</b> Trb1 does not autophosphorylate.....	78
<b>Figure 4.</b> Trb1 does not bind ATP or ATP-competitive small molecules.....	79
<b>Figure 5.</b> Analysis of Trb1 oligomerization.....	81
<b>Figure 6.</b> Effects of Trb1 KD mutations on oligomerization.....	83
<b>Figure 7.</b> Characterization of potential Trb1 dimer interface.....	84



## **Chapter 1: Introduction**

## **Non-catalytic functions of protein kinases**

By catalyzing phosphorylation, protein kinases play a central role in regulating cellular homeostasis. Dysregulation of kinase function has been linked to numerous pathologies, most notably cancer, as well as neurological, immunological, and metabolic diseases. In fact, the kinase domain is the most frequently observed domain in known oncogenes<sup>1</sup>, and a multitude of genetic alterations in kinases, including changes in expression level and mutations, have been described as driver events in malignant transformation. The enzymatic function of kinases is mediated by the conserved kinase domain fold, which is highly preserved among all protein kinases. Despite their structural conservation, protein kinases exhibit remarkable diversity in their ability to recognize unique sets of substrates, as well as other binding partners that might serve as activators or inhibitors. The specificity of these interactions is often encoded in unique binding sites within the kinase domain itself. A kinase domain therefore skillfully couples its role as a catalytic enzyme with a role as a protein scaffold in order to orchestrate an efficient and specific phosphotransfer.

Studies over the past decades have revealed that scaffolding functions of kinases extend beyond a mere supporting role in phosphorylation. This was initially suggested by observations that inhibition of kinase function can result in fundamentally different biological outputs depending on the experimental approach used to inhibit the enzyme. For example, genetic knockout of the epidermal growth factor receptor (EGFR) results in animal death soon after birth<sup>2</sup>, while loss of EGFR activity through a “kinase-dead” V743G mutation produces only mild epithelial defects<sup>3</sup>. Similarly, there are significant phenotypic discrepancies between Parkinson’s disease manifestations observed in mice in which leucine-rich repeat kinase 2 (LRRK2) is knocked out versus inactivated by a D1994S (D166 in Protein Kinase A (PKA)) mutation<sup>4</sup>. Although these discrepancies might be partially attributed to the fact that mutations or inhibitor treatment, as

opposed to gene knockdown, might still preserve a low level of kinase activity, they also suggest an alternative, more exciting, possibility that the functions of kinases are not limited to catalyzing phosphorylation but extend to other roles that are independent of enzymatic activity. These divergent outcomes of kinase inactivation have been found for an increasing number of kinases, indicating that the roles of kinases in cellular signaling are considerably more complex than we think (Figure 1).

Further evidence supporting a role for non-catalytic signaling mechanisms in kinase function comes from unbiased screens for somatic kinase mutations in cancer that have identified a surprising number of mutations that are expected to impair kinase activity by replacing conserved residues in the active site<sup>5,6</sup>. While some of these inactivating mutations occurred in kinases that act as tumor suppressors, such as LKB1, many others mapped to the kinase domains of bona fide oncogenic kinases that are typically hyperactivated in cancer, including B-RAF, EGFR, and c-Kit. In fact, kinase-inactivating mutations are the most common type of B-RAF mutation observed in non-small cell lung cancer (NSCLC)<sup>7</sup>, and recently, catalytically impaired B-RAF mutants were shown to induce the development of lung adenocarcinoma<sup>8</sup>. Subsequent insights into RAF kinase activation have revealed that these catalytically inactive B-RAF mutants allosterically activate C-RAF through heterodimerization much more efficiently than the wild type B-RAF, resulting in enhanced activation of the MAPK pathway<sup>9-11</sup>. The ability of these B-RAF kinase-inactivating mutations to drive disease underscores the importance of non-catalytic functions of kinases in signaling.

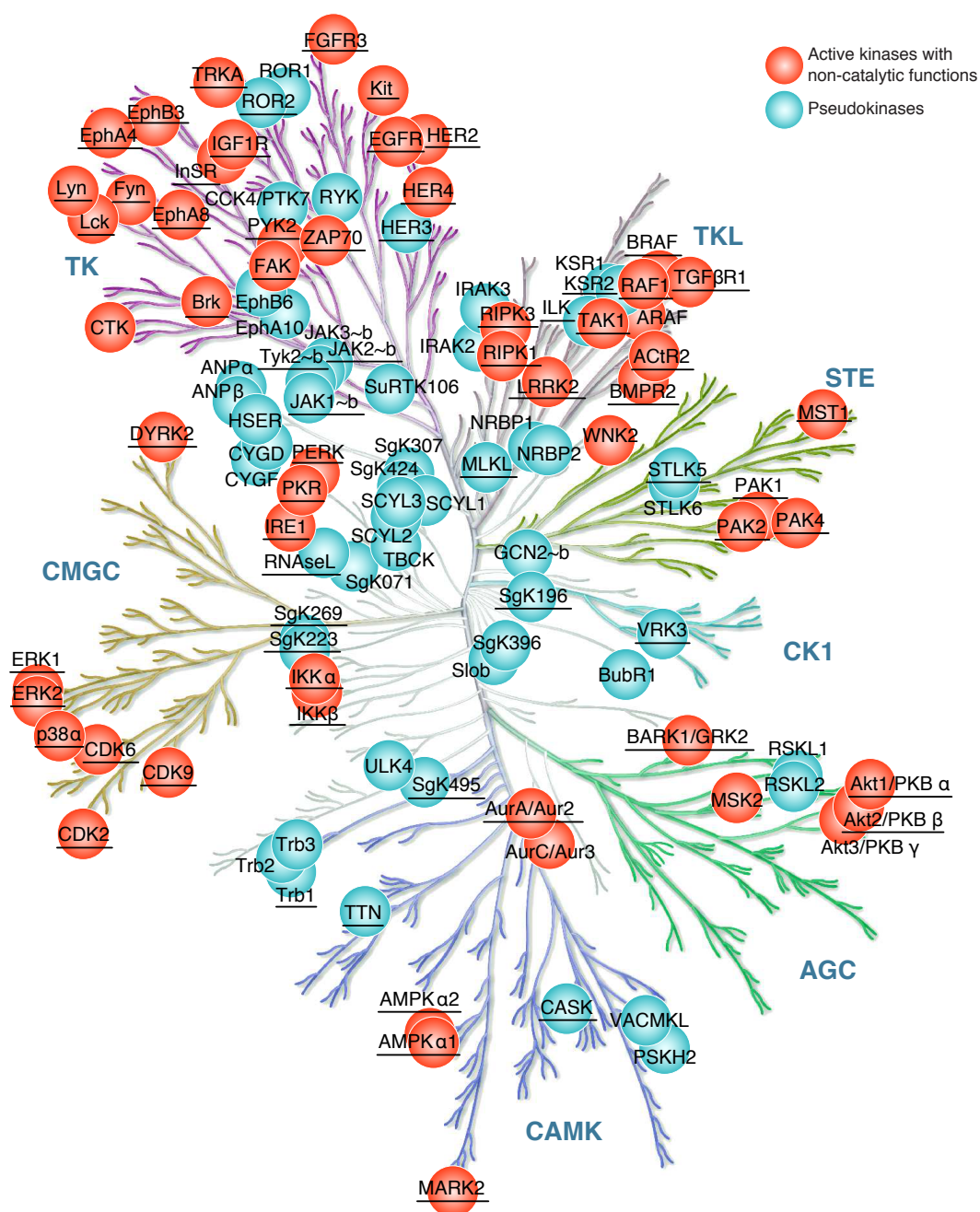


**Figure 1 | Kinases reported to have non-catalytic functions.**

This growing body of evidence indicates that many, if not all, kinases possess non-enzymatic functions in addition to their role in catalyzing phosphorylation<sup>12-14</sup>. Kinases interact with a surprisingly wide range of binding partners given the high degree of conservation of the kinase domain fold. This versatility enables kinases to perform a diverse array of non-catalytic functions, including allosterically regulating other kinases and/or unrelated enzymes, acting as molecular scaffolds to coordinate interactions between different components of signaling pathways, and regulating transcription through interactions with transcription factors or by binding directly to DNA<sup>13</sup>. Structural and functional studies in recent years have shown that each of these novel kinase functions utilizes a unique molecular mechanism, highlighting an impressive degree of adaptation.

### **Protein kinase structure and function**

Kinases exhibit a highly conserved fold with the active site located between two lobes, the N- and C-lobes, connected via the hinge region (Figure 2A). The motion of the hinge determines the relative orientation of the N- and C-lobes during the catalytic cycle. To conduct catalysis, kinases need to be dynamic to allow nucleotide binding, hydrolysis, and release in a sequential fashion, as well as binding and release of their substrates. A set of defined conformational transitions accompanies these steps and has been well characterized through decades of insightful structural and biophysical studies<sup>15,16</sup>.

In contrast to the N-lobe, which is composed primarily of  $\beta$ -strands and undergoes significant structural rearrangements during catalysis, the C-lobe, which consists mostly of  $\alpha$  helices, is more rigid and possesses less conformational flexibility except for one conserved structural element called the activation loop. The activation loop starts with a highly conserved



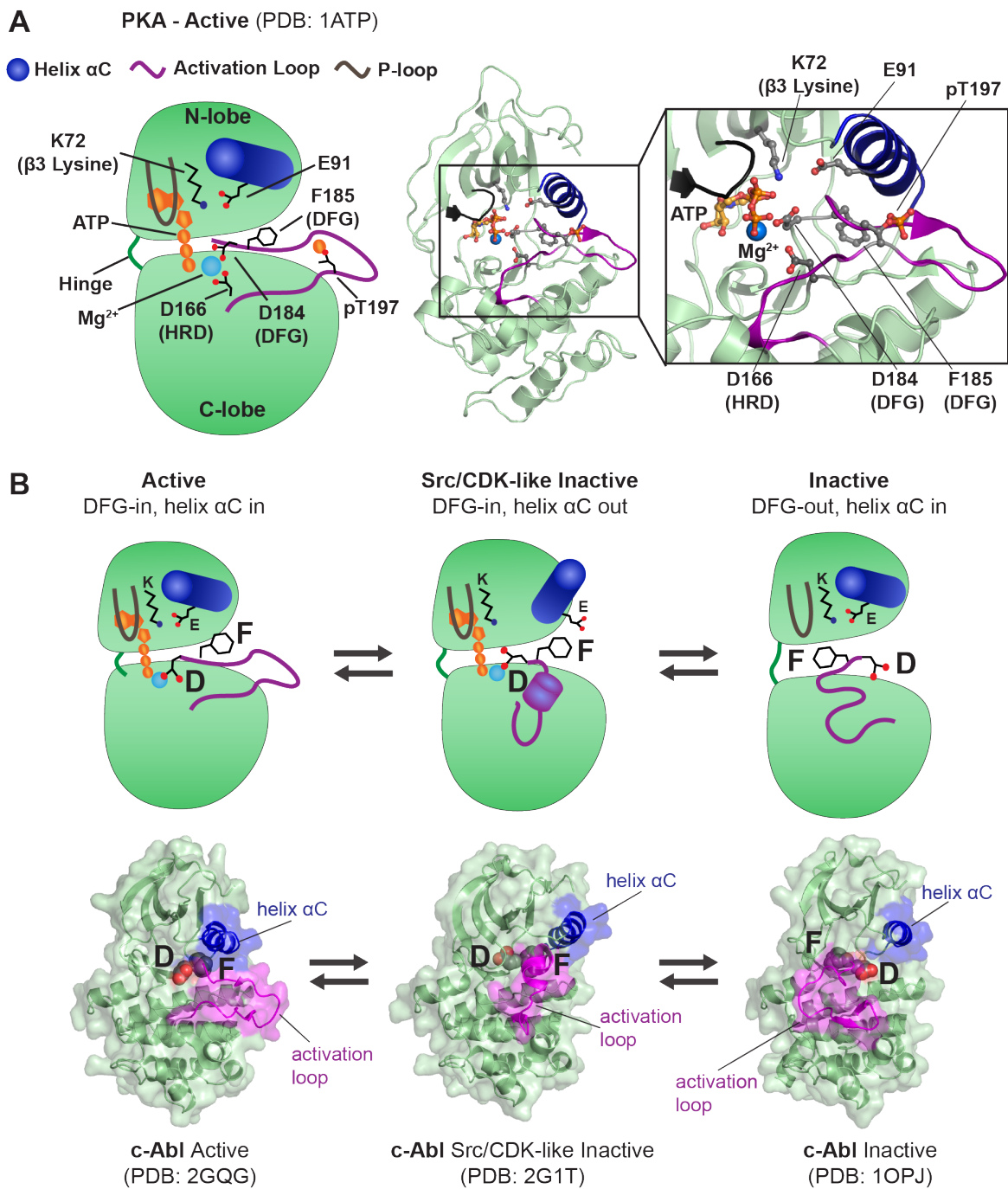


**Figure 2 | Conformational transitions linked to kinase catalysis.**

(A) Cartoon representation and crystal structure (PDB: 1ATP) of the active conformation of Protein Kinase A (PKA). The inset displays a close-up view of the active site, highlighting structural elements that are critical for catalysis.

(B) Cartoon representations (top) and crystal structures (bottom) illustrating the structural changes that occur as the c-Abl kinase domain transitions between different conformational states.

Asp-Phe-Gly (DFG) motif and extends to include one or more regulatory phosphorylation sites present in the majority of kinases. The activation loop undergoes significant conformational changes during catalysis that are intimately tied to kinase activation. In most kinases, once phosphorylated, the activation loop adopts a fully extended conformation that stabilizes the active state of the enzyme and is important for binding substrates. In this conformation, the DFG aspartate points into the active site to coordinate  $Mg^{2+}$ -ATP, while the adjacent phenylalanine points away from the catalytic cleft (Figure 2B). This position of the DFG motif is referred to as the “DFG-in” state. The aspartate and phenylalanine can exchange positions (“DFG-out”), positioning the bulky phenylalanine side chain to prevent binding of the nucleotide to the active site. This “DFG-out” state locks the kinase in the inactive conformation and is often accompanied by significant changes in the conformation of the activation loop (Figure 2B).

Conformational changes of the activation loop are tightly coupled to the movements of helix  $\alpha C$ , a conserved structural element located in the N-lobe. In the active conformation, helix  $\alpha C$  is rotated toward the active site, allowing a conserved lysine residue in the  $\beta 3$  strand within the N-lobe to form a salt bridge with a conserved glutamate in helix  $\alpha C$  (Figure 2A). Helix  $\alpha C$  also plays a critical role in stabilization of an inactive conformation of the kinase domain termed the Src/CDK-like inactive conformation, which is distinct from the “DFG-out” inactive conformation (Figure 2B). This conformation was first observed in structures of cyclin-dependent kinases (CDKs) and Src family kinases, and subsequently, in several other unrelated protein kinases, pointing to its potentially important role in the kinase catalytic cycle<sup>17</sup>. In the Src/CDK-like inactive state, helix  $\alpha C$  is rotated away from the active site such that the glutamate residue in this helix can no longer interact with the  $\beta 3$  lysine. The DFG motif adopts a DFG-in conformation, but

the remainder of the activation loop folds into a short helix rather than adopting the extended conformation seen in the active state.

While the structural steps of kinase-mediated catalysis have been studied extensively, the structural underpinnings of non-catalytic kinase functions are only beginning to be understood. Since the three structurally well-characterized kinase conformations: the active state, the inactive DFG-out state, and the Src/CDK-like inactive state, are associated with significant changes on the kinase domain surface (Figure 2B), it is therefore plausible that non-catalytic functions of kinases that rely on protein-protein interaction interfaces could be regulated by these conformational changes. Much of the pioneering work on this aspect of kinase signaling suggests that the structural transitions associated with the kinase catalytic cycle are indeed also supporting the non-catalytic functions of kinases<sup>13,14</sup>.

## **Pseudokinases**

The potential of the kinase domain fold to signal through an alternate non-catalytic mechanism is perhaps best exemplified by a subset of protein kinases that have seemingly evolved to lack catalytic activity and have thus been termed “pseudokinases”. Thus, pseudokinases provide elegant case studies to investigate the molecular basis for non-catalytic kinase functions since these functions have likely evolved in pseudokinases in isolation from the constraints that catalysis imposes on the structure of the kinase domain. Although initially thought of as evolutionary remnants that lack biological function, pseudokinases are often highly conserved in evolution and play essential roles in signaling. As such, pseudokinases represent ~10% of all human and murine kinases (Figure 1) and also comprise a notable proportion of the kinomes of diverse species, including *Arabidopsis thaliana*, *Paramecium tetraurelia*, *Dictyostelium discoideum*, and

*Toxoplasma gondii*<sup>18-24</sup> (Figure 3), underscoring the importance of the non-catalytic functions of kinases for cellular signaling. The functions of the vast majority of these pseudokinases, however, remain poorly understood, but studies conducted thus far highlight crucial roles for many of them in development, the immune response, and metabolism. Consequently, dysregulation of pseudokinases through mutations or overexpression has been linked to several developmental and morphological disorders, as well as a wide range of diseases, such as cancer, neurological disorders, metabolic disorders, and autoimmune disease<sup>25</sup>.

Pseudokinases are defined by the presence of mutations in critical catalytic residues that prevent catalysis of phosphorylation<sup>22</sup>, and the crystal structures of pseudokinase domains solved to date have revealed that pseudokinases retain the same overall kinase domain fold as their active

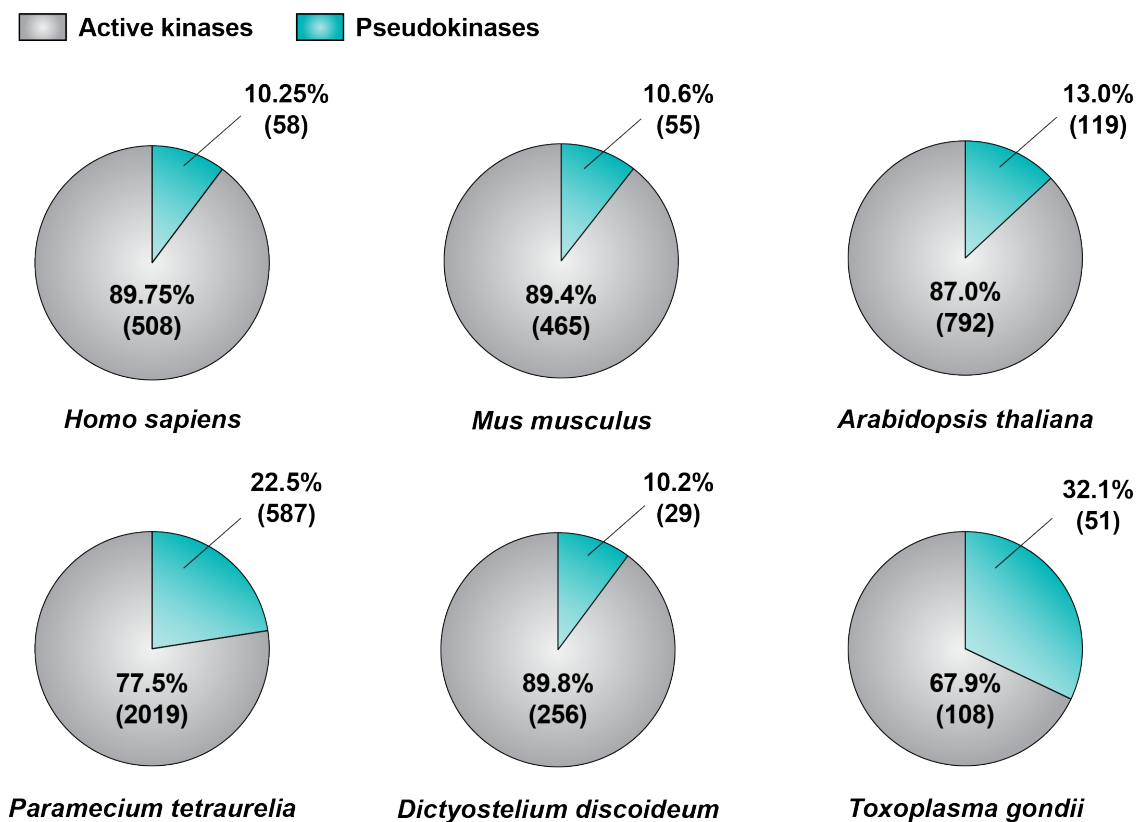


**Figure 3 | Prevalence of pseudokinases in the kinomes of diverse species.** Pie charts showing the percentages of active kinases (gray) and pseudokinases (teal) in the kinomes of the indicated species.

counterparts, though often with their own unique twist<sup>13,14</sup>. These deviations from canonical kinase domains frequently alter the accessibility of the nucleotide-binding pocket or other conserved structural elements that are usually necessary for catalysis and might affect the ability of pseudokinases to undergo the conformational transitions that regulate catalysis in their active counterparts. For instance, in several pseudokinases, such as VRK3 and ROR2, the nucleotide-binding pocket is occluded, leaving no room for ATP to bind<sup>26,27</sup>. In some pseudokinases, like PEA3 and HER3, helix  $\alpha$ C lacks the conserved glutamate residue and is shorter than in most kinases<sup>28,29</sup>, while helix  $\alpha$ C in Pragmin not only lacks the conserved glutamate but is also completely disordered<sup>30,31</sup>. The activation loops of a number of pseudokinases, including RNase L and Tyk2, are also unusually short, likely precluding the conformational transitions typically observed in active kinases<sup>32-34</sup>. The activation loop can also adopt atypical conformations in pseudokinases as seen in structures of murine MLKL in which the activation loop forms a short  $\alpha$ -helix that takes the position normally occupied by helix  $\alpha$ C in the active conformation of active kinases<sup>35</sup>.

### **The Tribbles family of pseudokinases**

The *tribbles* gene was first identified in *Drosophila* as a novel regulator of the cell cycle during development through its ability to promote proteasomal degradation of the C/EBP homolog Slbo and the CDC25 homolog String<sup>36-39</sup>. The Tribbles family of pseudokinases has since been found to be conserved in all metazoans, with humans expressing three Tribbles family members: Trb1, Trb2, and Trb3, which have all been found to regulate diverse signaling processes and have been implicated in a variety of diseases, including several types of cancer and metabolic disease<sup>40</sup>.



Tribbles pseudokinases are characterized by a highly conserved pseudokinase domain flanked by disordered N- and C-terminal regions that are not homologous to any known protein domains (Figure 4A). The three Tribbles family members share a high degree of sequence similarity (Trb1/Trb2: 71.3%, Trb1/Trb3: 53.7%, Trb2/Trb3: 53.7%), especially in the pseudokinase domain, which is homologous to those of Ser/Thr kinases and has the same overall architecture as a canonical kinase domain<sup>41</sup> (Figure 4C). Despite this, the sequences of conserved kinase motifs in the putative active site of the Tribbles pseudokinase domain deviate significantly from what is observed in canonical active kinases (Figure 4B). Mammalian Tribbles homologs retain the lysine in the VAIK motif, which coordinates the  $\alpha$  and  $\beta$  phosphates of ATP, as well as the aspartate in the HRD motif, which serves as a catalytic base in active kinases. However, the rest of the VAIK motif diverges markedly from the canonical sequence. Even more striking differences occur in the glycine-rich loop and the DFG motif, which are important for binding ATP and chelating  $Mg^{2+}$ . In particular, the presence of acidic residues in the glycine-rich loop is expected to prevent nucleotide-binding, and crystal structures of the Trb1 pseudokinase domain have revealed that the glycine-rich loop is three residues shorter than in most other kinases, resulting in an unusually shallow putative nucleotide-binding pocket<sup>41</sup>. Helix  $\alpha C$  in Trb1 is also shorter than in catalytically active kinases and displays an unusual kink not observed in other kinase crystal structures (Figure 4C). Because of these deviations from canonical active kinases, all members of the Tribbles family were predicted to be catalytically inactive and unable to bind ATP. This was confirmed in biochemical studies of Trb1, but Trb2 has been reported to bind ATP and to retain measurable catalytic activity in the presence of EDTA *in vitro*<sup>41,42</sup>. The role of nucleotide binding in Tribbles function remains unknown, but a recent report demonstrating

destabilization of the Trb2 pseudokinase domain by ATP-competitive small molecules suggests that nucleotide binding might serve a structural role in stabilizing the pseudokinase domain<sup>43</sup>.

The C-terminal tails of Tribbles pseudokinases contain a highly conserved motif that recruits the E3 ubiquitin ligase COP1, which then ubiquitinates substrates, such as the transcription factor C/EBP $\alpha$  and the metabolic enzyme acetyl CoA carboxylase, that bind to the Tribbles pseudokinase domains<sup>44-47</sup>. Dysregulation of this function has been implicated in acute myeloid leukemia where overexpression of Trb1 or Trb2 induces leukemogenesis in mice through COP1-mediated depletion of C/EBP $\alpha$ , as well as in lung cancer, where Trb2 overexpression has been linked to degradation of C/EBP $\alpha$ <sup>44,46,48,49</sup>. Additionally, genome-wide association studies have identified variants at the Trb1 locus that significantly associate with plasma lipid traits and cardiovascular disease, possibly due to the role of Trb1 in degradation of C/EBP $\alpha$ , a key regulator of lipogenesis<sup>119-122</sup>. Structural studies of Trb1 revealed that its C-terminal tail binds to a pocket formed by helix  $\alpha$ C in the N-lobe of the pseudokinase domain<sup>41</sup> (Figure 4C). Some of the same residues in the tail that are required for COP1 binding also appear to be necessary for this intramolecular interaction with the pseudokinase domain, suggesting a potential autoinhibitory role of the pseudokinase domain in regulating interaction of the C-terminal tail with COP1<sup>41,50</sup>. Biochemical studies of Trb2 indicate that its pseudokinase domain and C-terminal tail might participate in a similar intramolecular interaction<sup>43</sup>. Binding of the C-terminal tail to the pseudokinase domain is disrupted by binding of C/EBP $\alpha$  to the C-lobe of Trb1, demonstrating a role for substrate binding in allosteric regulation of the interaction of Trb1 with COP1<sup>47</sup>.

In addition to regulating ubiquitination, Tribbles pseudokinases also modulate other kinases, within the MAPK and Akt pathways<sup>51,52</sup>. All three Tribbles pseudokinases interact with MEK through a conserved motif in their C-lobes, which leads to enhanced ERK phosphorylation<sup>53</sup>.

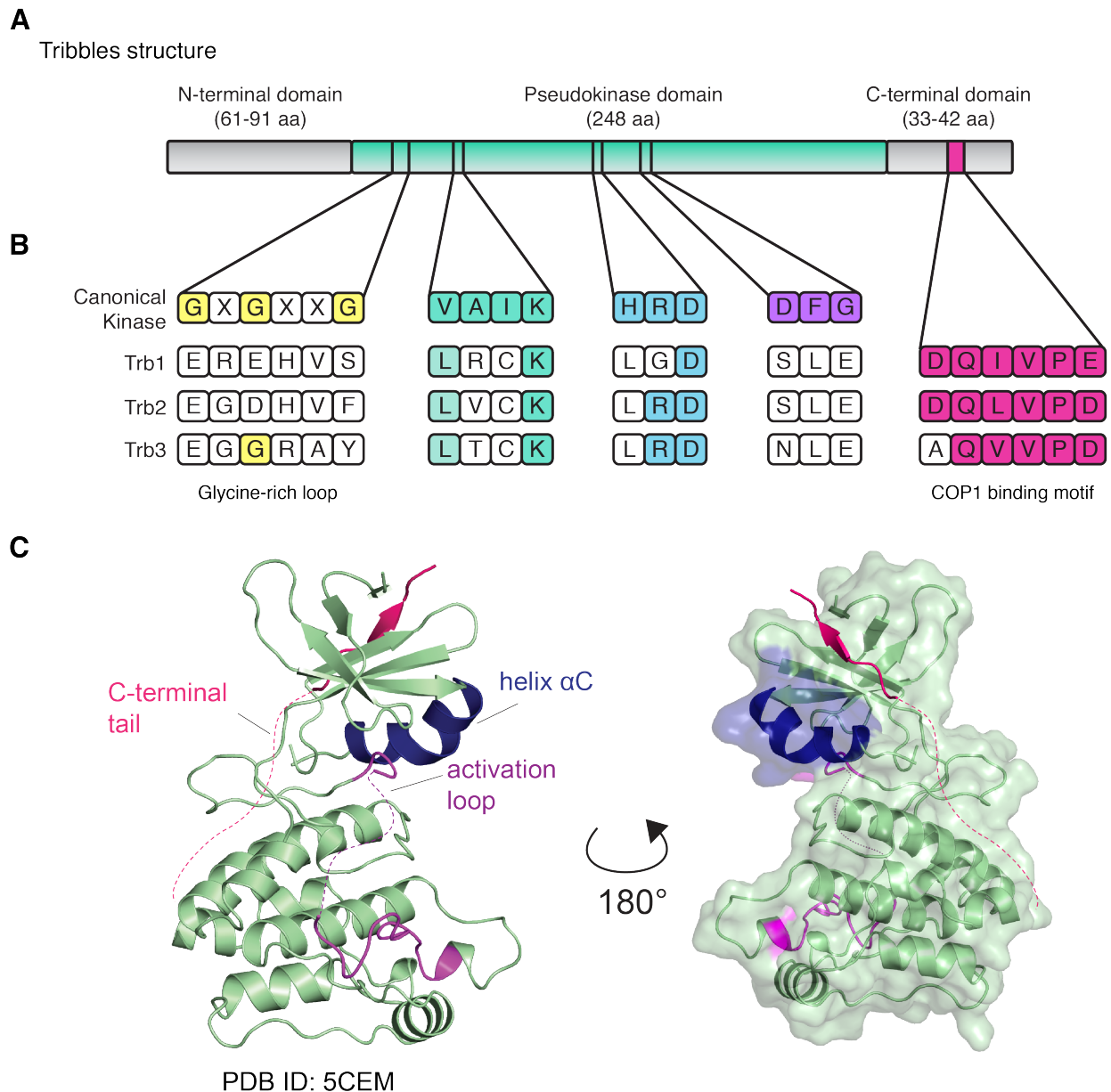


**Figure 4 | Tribbles structure and comparison to canonical kinases.**

(A) Tribbles family members have a conserved architecture that consists of a central pseudokinase domain flanked by N- and C-terminal domains.

(B) All three Tribbles isoforms diverge markedly from canonical kinases in conserved catalytic motifs. Conserved residues are shaded. All three Tribbles isoforms also have a conserved COP1 binding motif in their C-terminal domains.

(C) Crystal structure of Trb1 pseudokinase domain and C-terminal tail (PDB: 5CEM).

Dysregulation of this process has been implicated in both leukemia and breast cancer<sup>53,54</sup>. Trb3 has also been reported to promote insulin resistance by binding to and inhibiting Akt<sup>52</sup>, a function that is also conserved for the *Drosophila* Tribbles homolog<sup>55</sup>. Elevated levels of Trb3 and the resulting inhibition of Akt have been shown to promote apoptosis and has been associated with neuronal cell death in Parkinson's disease<sup>56,57</sup>. In contrast, Trb2 is believed to activate Akt signaling, and overexpression of Trb2 promotes drug resistance in cancer cells<sup>58</sup>.

Collectively, these findings demonstrate that Tribbles pseudokinases have emerged as critical regulators of a variety of signaling pathways and that their functions are frequently dysregulated in disease. Despite this, the structural and molecular basis for these functions are only beginning to be uncovered. Elucidating the mechanisms underlying Tribbles-mediated signaling will be imperative not only for understanding the role of Tribbles in disease and developing therapeutics that can modulate their function, but will also provide insights into the non-catalytic functions of other pseudokinases and active kinases.

## References

1. Futreal, P. A. *et al.* A census of human cancer genes. *Nat Rev Cancer* **4**, 177–183 (2004).
2. Miettinen, P. J. *et al.* Epithelial immaturity and multiorgan failure in mice lacking epidermal growth factor receptor. *Nature* **376**, 337–341 (1995).
3. Luetkeke, N. C. *et al.* The mouse waved-2 phenotype results from a point mutation in the EGF receptor tyrosine kinase. *Genes & Development* **8**, 399–413 (1994).
4. Herzig, M. C. *et al.* LRRK2 protein levels are determined by kinase function and are crucial for kidney and lung homeostasis in mice. *Human Molecular Genetics* **20**, 4209–4223 (2011).

5. Greenman, C. *et al.* Patterns of somatic mutation in human cancer genomes. *Nature* **446**, 153–158 (2007).
6. Creixell, P. *et al.* Kinome-wide decoding of network-attacking mutations rewiring cancer signaling. *Cell* **163**, 202–217 (2015).
7. Chang, M. T. *et al.* Identifying recurrent mutations in cancer reveals widespread lineage diversity and mutational specificity. *Nature Biotechnology* **34**, 155–163 (2016).
8. Nieto, P. *et al.* A Braf kinase-inactive mutant induces lung adenocarcinoma. *Nature* (2017). doi:10.1038/nature23297
9. Wan, P. T. C. *et al.* Mechanism of activation of the RAF-ERK signaling pathway by oncogenic mutations of B-RAF. *Cell* **116**, 855–867 (2004).
10. Garnett, M. J. *et al.* Wild-Type and Mutant B-RAF Activate C-RAF through Distinct Mechanisms Involving Heterodimerization. *Molecular Cell* **20**, 963–969 (2005).
11. Yao, Z. *et al.* Tumours with class 3 BRAF mutants are sensitive to the inhibition of activated RAS. *Nature* **548**, 234–238 (2017).
12. Jacobsen, A. V. & Murphy, J. M. The secret life of kinases: insights into non-catalytic signalling functions from pseudokinases. *Biochem. Soc. Trans.* **45**, 665–681 (2017).
13. Kung, J. E. & Jura, N. Structural Basis for the Non-catalytic Functions of Protein Kinases. *Structure* **24**, 7–24 (2016).
14. Shaw, A. S., Kornev, A. P., Hu, J., Ahuja, L. G. & Taylor, S. S. Kinases and pseudokinases: lessons from RAF. *Molecular and Cellular Biology* **34**, 1538–1546 (2014).
15. Huse, M. & Kuriyan, J. The conformational plasticity of protein kinases. *Cell* **109**, 275–282 (2002).

16. Taylor, S. S. & Kornev, A. P. Protein kinases: evolution of dynamic regulatory proteins. *Trends in Biochemical Sciences* **36**, 65–77 (2011).
17. Jura, N. *et al.* Catalytic Control in the EGF Receptor and Its Connection to General Kinase Regulatory Mechanisms. *Molecular Cell* **42**, 9–22 (2011).
18. Caenepeel, S., Charydczak, G., Sudarsanam, S., Hunter, T. & Manning, G. The mouse kinome: discovery and comparative genomics of all mouse protein kinases. *Proceedings of the National Academy of Sciences* **101**, 11707–11712 (2004).
19. Castells, E. & Casacuberta, J. M. Signalling through kinase-defective domains: the prevalence of atypical receptor-like kinases in plants. *J. Exp. Bot.* **58**, 3503–3511 (2007).
20. Bemm, F., Schwarz, R., Förster, F. & Schultz, J. A kinome of 2600 in the ciliate *Paramecium tetraurelia*. *FEBS Letters* **583**, 3589–3592 (2009).
21. Goldberg, J. M. *et al.* The dictyostelium kinome--analysis of the protein kinases from a simple model organism. *PLoS Genet.* **2**, e38 (2006).
22. Manning, G., Whyte, D. B., Martinez, R., Hunter, T. & Sudarsanam, S. The protein kinase complement of the human genome. *Science* **298**, 1912–1934 (2002).
23. Peixoto, L. *et al.* Integrative genomic approaches highlight a family of parasite-specific kinases that regulate host responses. *Cell Host & Microbe* **8**, 208–218 (2010).
24. Hunter, T. & Manning, G. in *Receptor Tyrosine Kinases: Structure, Functions and Role in Human Disease* 1–15 (Springer, New York, NY, 2015). doi:10.1007/978-1-4939-2053-2\_1
25. Reiterer, V., Eysers, P. A. & Farhan, H. Day of the dead: pseudokinases and pseudophosphatases in physiology and disease. *Trends in Cell Biology* **24**, 489–505 (2014).

26. Scheeff, E. D., Eswaran, J., Bunkoczi, G., Knapp, S. & Manning, G. Structure of the Pseudokinase VRK3 Reveals a Degraded Catalytic Site, a Highly Conserved Kinase Fold, and a Putative Regulatory Binding Site. *Structure* **17**, 128–138 (2009).
27. Artim, S. C., Mendrola, J. M. & Lemmon, M. A. Assessing the range of kinase autoinhibition mechanisms in the insulin receptor family. *Biochem. J.* **448**, 213–220 (2012).
28. Jura, N., Shan, Y., Cao, X., Shaw, D. E. & Kuriyan, J. Structural analysis of the catalytically inactive kinase domain of the human EGF receptor 3. *Proc. Natl. Acad. Sci. U.S.A.* **106**, 21608–21613 (2009).
29. Ha, B. H. & Boggon, T. J. The crystal structure of pseudokinase PEAK1 (Sugen Kinase 269) reveals an unusual catalytic cleft and a novel mode of kinase fold dimerization. *J. Biol. Chem.* jbc.RA117.000751 (2017). doi:10.1074/jbc.RA117.000751
30. Patel, O. *et al.* Structure of SgK223 pseudokinase reveals novel mechanisms of homotypic and heterotypic association. *Nat Comms* **8**, 1157 (2017).
31. Lecointre, C. *et al.* Dimerization of the Pragmin Pseudo-Kinase Regulates Protein Tyrosine Phosphorylation. *Structure* **26**, 545–554.e4 (2018).
32. Huang, H. *et al.* Dimeric Structure of Pseudokinase RNase L Bound to 2-5A Reveals a Basis for Interferon-Induced Antiviral Activity. *Molecular Cell* **53**, 221–234 (2014).
33. Han, Y. *et al.* Structure of human RNase L reveals the basis for regulated RNA decay in the IFN response. *Science* **343**, 1244–1248 (2014).
34. Lupardus, P. J. *et al.* Structure of the pseudokinase-kinase domains from protein kinase TYK2 reveals a mechanism for Janus kinase (JAK) autoinhibition. *Proc. Natl. Acad. Sci. U.S.A.* **111**, 8025–8030 (2014).

35. Murphy, J. M. *et al.* The Pseudokinase MLKL Mediates Necroptosis via a Molecular Switch Mechanism. *Immunity* **39**, 443–453 (2013).
36. Mata, J., Curado, S., Ephrussi, A. & Rørth, P. Tribbles coordinates mitosis and morphogenesis in *Drosophila* by regulating string/CDC25 proteolysis. *Cell* **101**, 511–522 (2000).
37. Seher, T. C., Seher, T. C., Leptin, M. & Leptin, M. Tribbles, a cell-cycle brake that coordinates proliferation and morphogenesis during *Drosophila* gastrulation. *Curr. Biol.* **10**, 623–629 (2000).
38. Grosshans, J. & Wieschaus, E. A genetic link between morphogenesis and cell division during formation of the ventral furrow in *Drosophila*. *Cell* **101**, 523–531 (2000).
39. Rørth, P., Szabo, K., Szabo, K., Texido, G. & Texido, G. The level of C/EBP protein is critical for cell migration during *Drosophila* oogenesis and is tightly controlled by regulated degradation. *Molecular Cell* **6**, 23–30 (2000).
40. Yokoyama, T. & Nakamura, T. Tribbles in disease: Signaling pathways important for cellular function and neoplastic transformation. *Cancer Science* **102**, 1115–1122 (2011).
41. Murphy, J. M. *et al.* Molecular Mechanism of CCAAT-Enhancer Binding Protein Recruitment by the TRIB1 Pseudokinase. *Structure* **23**, 2111–2121 (2015).
42. Bailey, F. P. *et al.* The Tribbles 2 (TRB2) pseudokinase binds to ATP and autophosphorylates in a metal-independent manner. *Biochem. J.* (2015).  
doi:10.1042/BJ20141441
43. Foulkes, D. M. *et al.* Repurposing covalent EGFR/HER2 inhibitors for on-target degradation of human Tribbles 2 (TRIB2) pseudokinase. *bioRxiv* 305243 (2018).  
doi:10.1101/305243



44. Dedhia, P. H. *et al.* Differential ability of Tribbles family members to promote degradation of C/EBP $\alpha$  and induce acute myelogenous leukemia. *Blood* **116**, 1321–1328 (2010).
45. Qi, L. *et al.* TRB3 links the E3 ubiquitin ligase COP1 to lipid metabolism. *Science* **312**, 1763–1766 (2006).
46. Keeshan, K. *et al.* Transformation by Tribbles homolog 2 (Trib2) requires both the Trib2 kinase domain and COP1 binding. *Blood* **116**, 4948–4957 (2010).
47. Jamieson, S. A. *et al.* Substrate binding allosterically relieves autoinhibition of the TRIB1 pseudokinase. *bioRxiv* 313767 (2018). doi:10.1101/313767
48. Keeshan, K. *et al.* Tribbles homolog 2 inactivates C/EBP $\alpha$  and causes acute myelogenous leukemia. *Cancer Cell* **10**, 401–411 (2006).
49. Yoshida, A., Kato, J.-Y., Nakamae, I. & Yoneda-Kato, N. COP1 targets C/EBP $\alpha$  for degradation and induces acute myeloid leukemia via Trib1. *Blood* **122**, 1750–1760 (2013).
50. Uljon, S. *et al.* Structural Basis for Substrate Selectivity of the E3 Ligase COP1. *Structure* **24**, 687–696 (2016).
51. Kiss-Toth, E. *et al.* Human Tribbles, a Protein Family Controlling Mitogen-activated Protein Kinase Cascades. *Journal of Biological Chemistry* **279**, 42703–42708 (2004).
52. Du, K., Herzig, S., Kulkarni, R. N. & Montminy, M. TRB3: a tribbles homolog that inhibits Akt/PKB activation by insulin in liver. *Science* **300**, 1574–1577 (2003).
53. Yokoyama, T. *et al.* Trib1 links the MEK1/ERK pathway in myeloid leukemogenesis. *Blood* **116**, 2768–2775 (2010).
54. Izrailit, J., Berman, H. K., Datti, A., Wrana, J. L. & Reedijk, M. High throughput kinase inhibitor screens reveal TRB3 and MAPK-ERK/TGF $\beta$  pathways as fundamental Notch

- regulators in breast cancer. *Proceedings of the National Academy of Sciences* **110**, 1714–1719 (2013).
55. Das, R., Sebo, Z., Pence, L. & Dobens, L. L. Drosophila Tribbles Antagonizes Insulin Signaling-Mediated Growth and Metabolism via Interactions with Akt Kinase. *PLoS ONE* **9**, e109530 (2014).
56. Zareen, N. *et al.* A feed-forward loop involving Trib3, Akt and FoxO mediates death of NGF-deprived neurons. *Cell Death Differ* **20**, 1719–1730 (2013).
57. Aimé, P. *et al.* Trib3 Is Elevated in Parkinson's Disease and Mediates Death in Parkinson's Disease Models. *J. Neurosci.* **35**, 10731–10749 (2015).
58. Hill, R. *et al.* TRIB2 confers resistance to anti-cancer therapy by activating the serine/threonine protein kinase AKT. *Nat Comms* **8**, 14687 (2017).

## **Chapter 2: Molecular basis for regulation of the E3 ubiquitin ligase COP1 by Trb1**

## **ABSTRACT**

COP1 is a highly conserved ubiquitin ligase that regulates diverse cellular processes in plants and metazoans. Tribbles pseudokinases, which only exist in metazoans, act as scaffolds that interact with COP1 and its substrates to facilitate ubiquitination. Here, we report that, in addition to this scaffolding role, Trb1 promotes nuclear localization of COP1 by disrupting an intramolecular interaction between the WD40 domain and a previously uncharacterized regulatory site within COP1. This site, which we have termed the pseudosubstrate latch (PSL), resembles the consensus COP1-binding motif present in known COP1 substrates. Our findings support a model in which binding of the PSL to the WD40 domain stabilizes a conformation of COP1 that is conducive to CRM1-mediated nuclear export, and Trb1 displaces this intramolecular interaction to induce nuclear retention of COP1. Coevolution of Tribbles and the PSL in metazoans further underscores the importance of this role of Tribbles in regulating COP1 function.

## INTRODUCTION

Constitutive Photomorphogenic 1 (COP1), also known as RFWD2, is a RING domain-containing E3 ubiquitin ligase that is essential for mammalian embryonic development. COP1 regulates diverse cellular processes, including cell proliferation and the DNA damage response, by promoting the degradation of key transcription factors<sup>1,2</sup>. Overexpression of COP1 is observed in breast and ovarian adenocarcinomas, as well as hepatocellular carcinoma and pancreatic cancer<sup>3-5</sup>. Deletion of the COP1 locus has also been reported in many cancer types, such as prostate cancer and melanoma<sup>1,6</sup>. These findings indicate that COP1 can have pro-oncogenic or tumor-suppressing functions depending on the cellular context. The opposing effects of COP1 in cancer are likely reflective of the ability of COP1 to target for degradation both transcription factors that function as tumor suppressors, such as C/EBP $\alpha$  and p53, as well as proto-oncogenes, such as c-Jun and ETS family members<sup>6-9</sup>.

COP1 is highly conserved in metazoans, as well as in plants. The domain organization of COP1 is the same in these multicellular eukaryotes and, in addition to the N-terminal RING domain, includes a coiled coil domain and a C-terminal WD40 domain, consisting of seven WD40 repeats. First identified as a key repressor of photomorphogenesis in plants<sup>10</sup>, COP1 influences the expression of the majority of light-controlled genes in *Arabidopsis*, which accounts for >20% of the genome<sup>11</sup>. COP1 achieves this by ubiquitinating and promoting the degradation of transcription factors, such as HY5, LAF1, and HFR, that positively regulate light signaling<sup>12</sup>. This activity of COP1 is itself regulated by light, which controls trafficking of COP1 between the nucleus and cytoplasm. In dark-grown plants, COP1 localizes to the nucleus where it binds to and ubiquitinates transcription factors. Light inhibits COP1 activity by triggering its nuclear export, away from its

substrates<sup>13,14</sup>. Thus, shuttling between the cytosol and nucleus is an essential mechanism for regulation of COP1 activity in plants.

Like plant COP1, mammalian COP1 localizes to both the nucleus and cytoplasm. However, the mechanisms governing COP1 localization in mammalian cells are not well understood, and in the absence of the light/dark cycle, they would need to be different than those in plants. In contrast to the light-controlled binary pattern of either cytosolic or nuclear localization of COP1 in plant cells, the partitioning of COP1 in mammalian cells under steady state growth conditions varies quite markedly from cell to cell, ranging from primarily nuclear to primarily cytoplasmic<sup>15,16</sup>. Since many substrates of mammalian COP1 are also transcription factors, partitioning of COP1 between the nucleus and cytoplasm is likely important for regulation of its activity as it is in plants.

Pseudokinases in the Tribbles family (Trb1, Trb2, Trb3) have been identified as critical regulators of COP1 function in mammals and are not present in plants. In particular, Trb1 and Trb2 are essential for COP1-mediated ubiquitination of the tumor suppressor C/EBP $\alpha$ <sup>7,17,18</sup>. Dysregulation of Tribbles expression can be pathogenic in a COP1-dependent manner. In acute myeloid leukemia, overexpression of Trb1 or Trb2 has been shown to induce leukemogenesis in mice through excessive COP1-dependent degradation of C/EBP $\alpha$ <sup>7,17,18</sup>. Loss of Trb1 expression is also detrimental. Mice that have Trb1-deficient hematopoietic cells experience defects in myeloid cell differentiation due to aberrant levels of C/EBP $\alpha$  and develop metabolic disorders, such as hypertriglyceridemia and insulin resistance, when fed a high-fat diet<sup>19</sup>.

All three Tribbles family members possess a highly conserved pseudokinase domain flanked by an N-terminal extension and a C-terminal tail. Tribbles interact directly with the WD40 domain of COP1 via a conserved COP1-binding motif in their C-terminal tails that conforms to the consensus sequence (D/E)(D/E)(X)XXVP(D/E), present in numerous COP1 substrates<sup>17,20,21</sup>.

Through this motif, Tribbles recruit substrates to COP1 lacking a canonical COP1-binding motif, such as C/EBP $\alpha$ . Thus, Tribbles pseudokinases have been proposed to regulate COP1 by functioning as scaffolds that interact directly with both COP1 and its substrates to facilitate ubiquitination<sup>7,20,22</sup>.

In this study, we show that in addition to this scaffolding role, Trb1 emulates the regulatory control that light exerts on COP1 localization in plants and modulates the extent of COP1 nuclear localization. We demonstrate that Trb1 blocks nuclear export of COP1 through disruption of an intramolecular interaction within COP1. We identify a regulatory site in COP1, which we have termed the “pseudosubstrate latch”, that closely resembles the canonical COP1-binding motif used by COP1 binding partners. The pseudosubstrate latch in COP1 appears to have coevolved with Tribbles pseudokinases in animals and, notably, is missing in plants, which use light to control COP1 nucleocytoplasmic shuttling. Our work highlights how two orthogonal mechanisms have evolved in different kingdoms to regulate the same process.

## RESULTS

### **Trb1 promotes nuclear accumulation of COP1**

To investigate the effects of Trb1 expression on COP1 localization, we transiently expressed GFP-tagged human COP1 in COS7 cells and examined its subcellular distribution in the presence and absence of co-transfected human Trb1 via confocal microscopy. In the absence of Trb1, COP1 localized to both the nucleus and cytoplasm, while Trb1 localized primarily to the nucleus<sup>23,24</sup>. Consistent with previous studies, the distribution of COP1 between these two compartments varied considerably within the cell population<sup>15,16</sup> (Figures 1A and B). Strikingly, when Trb1 and COP1 were coexpressed, COP1 shifted to being predominantly nuclear (Figure

1C). To quantify this effect, we measured the ratio of nuclear to cytoplasmic COP1 fluorescence and found that coexpression of Trb1 markedly increased the ratio of nuclear to cytoplasmic COP1 across the entire cell population (Figure 1D).

Notably, we found that in approximately half of the cells co-transfected with COP1 and Trb1, both proteins colocalize in punctate structures in the nucleus (Figure 2A), a phenomenon previously observed for *Arabidopsis* COP1<sup>13</sup>. These structures colocalized with DAXX, a component of PML bodies (Figure 2B), but not with markers of other types of subnuclear compartments (Figure 2C). *Arabidopsis* COP1 recruits its substrates and binding partners to nuclear puncta<sup>25-27</sup>. Thus, we tested whether the COP1 substrate, C/EBP $\alpha$ , is also recruited to the COP1 and Trb1-positive nuclear puncta in mammalian cells by co-transfecting Trb1, COP1, and C/EBP $\alpha$  in COS7 cells and examining their localization via immunofluorescence. Surprisingly, however, upon C/EBP $\alpha$  coexpression, Trb1 and COP1 no longer localized in nuclear puncta (Figure 2D). These results demonstrate a potential difference in the composition of the punctate nuclear structures that COP1 localizes to in plants versus mammals and show that binding of C/EBP $\alpha$  to the Trb1/COP1 complex results in the redistribution of this complex between subnuclear compartments. Previously, targeting of COP1 nuclear puncta had been reported to be abolished through mutation of R356 and K358<sup>15</sup>. However, we found that COP1 R356A/K358A still localized to nuclear puncta in the presence of Trb1 (Figure 2E). Thus, it remains unclear what structural elements of COP1 and Trb1 enable their localization to nuclear puncta.



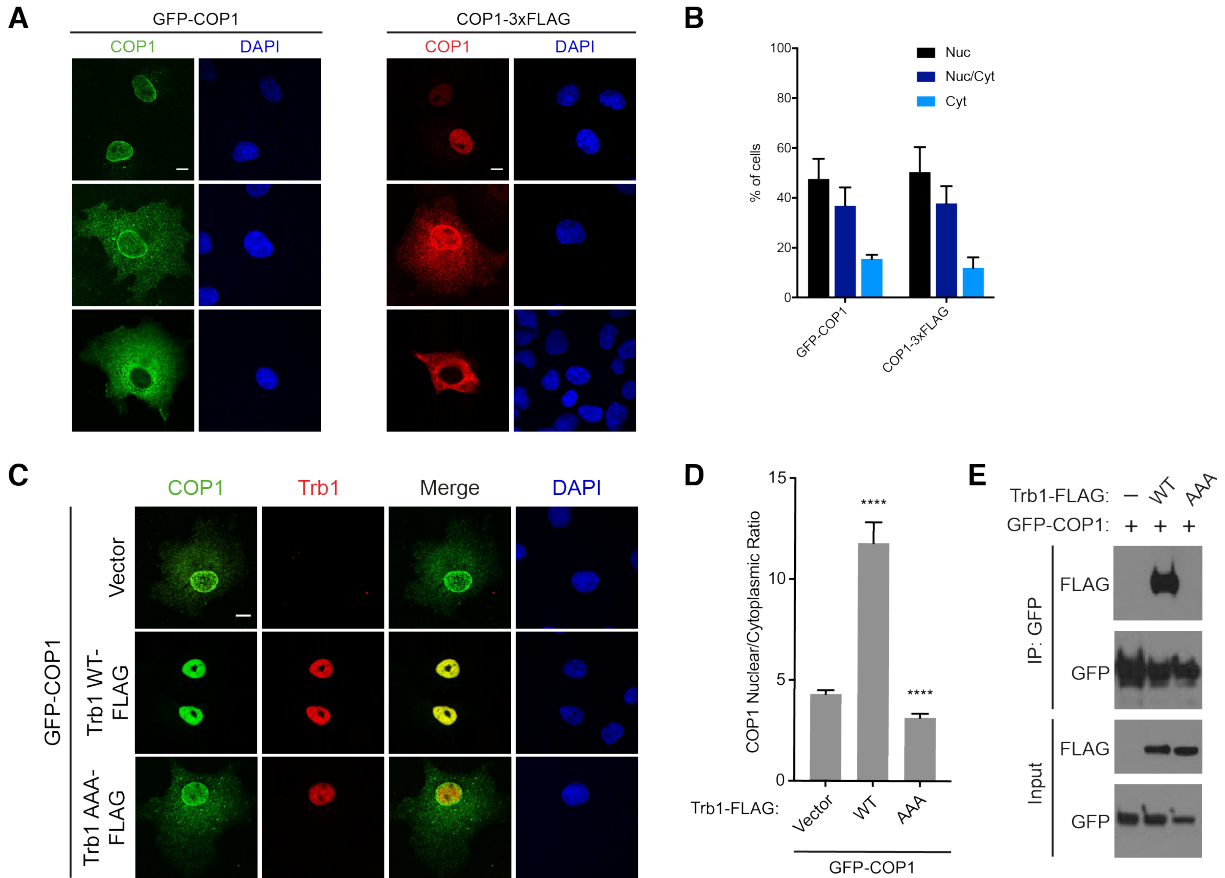


**Figure 1 | Trb1 promotes nuclear localization of COP1.**

- (A) Representative immunofluorescence images of COS7 cells expressing GFP-COP1 (green) or COP1-3xFLAG (red) showing the different patterns of localization (nuclear, nuclear & cytoplasmic, and cytoplasmic) typically observed within a cell population. For visualizing COP1-3xFLAG, the cells were stained with anti-FLAG (Sigma) and anti-mouse Alexa Fluor 568. Nuclei were counterstained with DAPI (blue). Scale bar, 10  $\mu$ m.
- (B) Quantification of percentage of cells observed in (A) with the indicated COP1 construct exhibiting nuclear (Nuc), nuclear and cytoplasmic (Nuc/Cyt), or cytoplasmic (Cyt) localization. Mean values  $\pm$  S.E.M. are shown for three independent experiments where 50 individual cells per experiment were analyzed.
- (C) Representative images of COS7 cells expressing GFP-COP1 (green) co-transfected with empty vector or the indicated Trb1-FLAG construct (red). Cells were stained with anti-FLAG (Sigma) and anti-mouse Alexa Fluor 568. Nuclei were counterstained with DAPI (blue). Scale bar, 10  $\mu$ m.
- (D) Quantification of the average ratio of nuclear/cytoplasmic fluorescence of GFP-COP1 in (A). Mean values  $\pm$  S.E.M. are shown for three independent experiments where 50 individual cells per experiment were analyzed. Significance relative to GFP-COP1 with empty vector was calculated using the Student t test (\*\*\*\* $p < 0.00001$ ).
- (E) Coimmunoprecipitation of GFP-COP1 with Trb1-FLAG in COS7 cells showing that the AAA mutation ablates the Trb1/COP1 interaction.

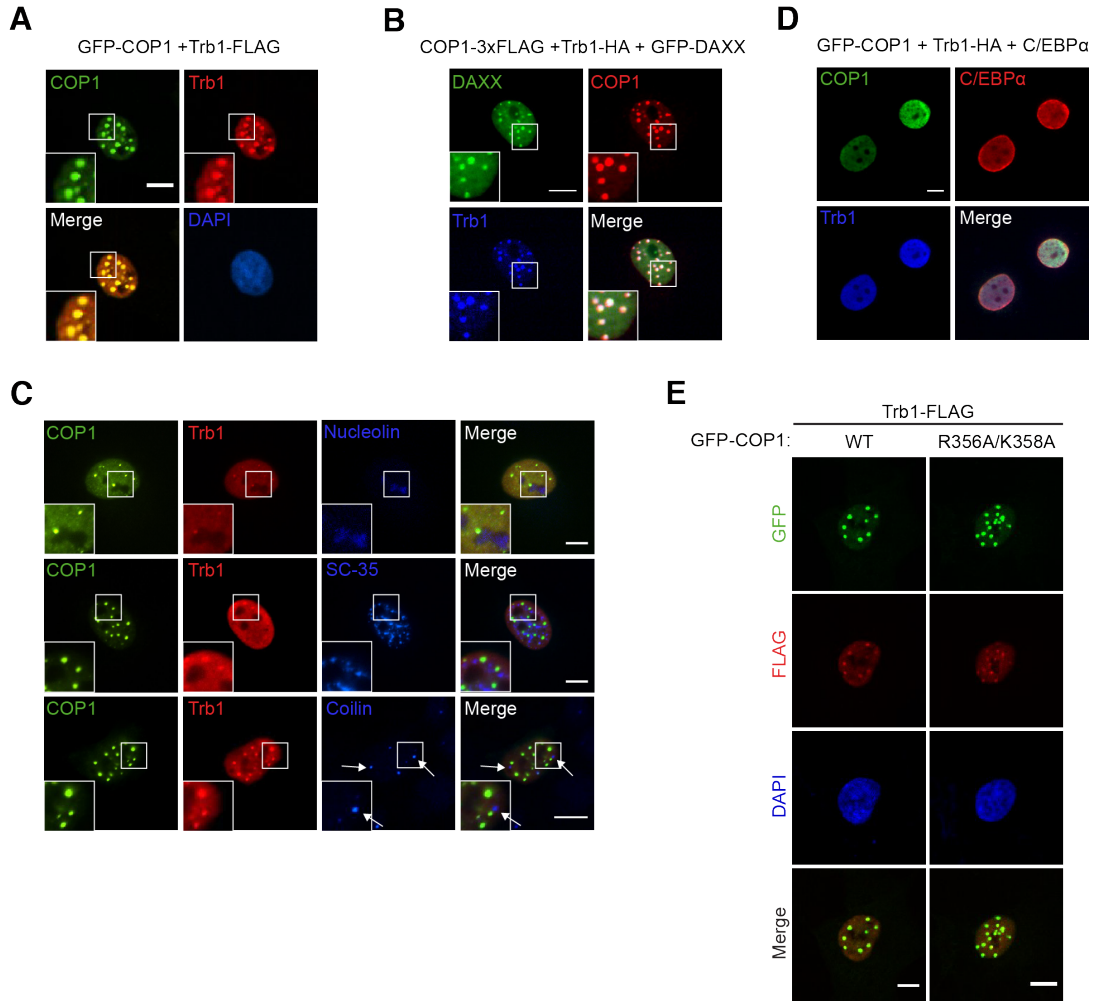


**Figure 2 | COP1 and Trb1 colocalize in punctate nuclear structures.**

- (A) Representative images of COS7 cells showing GFP-COP1 (green) and Trb1-FLAG (red) colocalizing in punctate nuclear structures. Insets show enlarged images of these nuclear puncta. Cells were stained with anti-FLAG and anti-mouse Alexa Fluor 568. Nuclei were counterstained with DAPI (blue). Scale bar, 10  $\mu$ m.
- (B) Representative images of COS7 cells showing that GFP-COP1 (green) and Trb1-HA (blue) are diffuse in the nucleoplasm when coexpressed with C/EBPα (red). Cells were stained with anti-HA (Santa Cruz), anti-C/EBPα (Cell Signaling), anti-mouse Alexa Fluor 405, and anti-rabbit Alexa Fluor 680. Scale bar, 10  $\mu$ m.
- (C) Representative images of COS7 cells showing that COP1-3xFLAG (red) and Trb1-HA (blue) colocalize with GFP-DAXX (green). Insets show enlarged images of nuclear puncta. Cells were stained with anti-FLAG (Cell Signaling), anti-HA (Santa Cruz), anti-mouse Alexa Fluor 405, and anti-rabbit Alexa Fluor 680. Scale bar, 10  $\mu$ m.
- (D) Representative images of COS7 cells showing that GFP-COP1 (green) and Trb1-FLAG (red) do not colocalize with markers (blue) for nucleoli (nucleolin), nuclear speckles (SC-35), or Cajal bodies (coilin). Cells were stained with anti-FLAG (Cell Signaling), anti-mouse Alexa Fluor 405, anti-rabbit Alexa Fluor 680, and either anti- nucleolin, anti-SC-35, or anti-coilin, as indicated. Scale bar, 10  $\mu$ m.

### **The Trb1 C-terminal tail is sufficient to promote nuclear localization of COP1**

To test if a direct interaction between Trb1 and COP1 is required for promoting nuclear localization of COP1, we generated a mutant, Trb1 AAA, in which the COP1-binding motif in the Trb1 C-terminal tail is mutated from DQIVPE to AQIAAE. An analogous set of mutations abolishes the interaction between murine Trb2 and COP1<sup>28</sup>, and we confirmed through coimmunoprecipitation that Trb1 AAA also failed to interact with COP1 (Figure 1E). Although Trb1 AAA localized to the nucleus like Trb1 WT, this mutant failed to increase COP1 nuclear localization (Figures 1C and D). Hence, a direct interaction between Trb1 and COP1 via the COP1-binding motif in the Trb1 C-terminal tail is required for Trb1-mediated COP1 nuclear accumulation.

To determine if the tail of Trb1 is sufficient for regulation of COP1 localization, we fused the C-terminal tail of Trb1 (residues 343-372) to GFP and tested the ability of this construct to modulate the localization of a FLAG-tagged COP1 construct. For comparison, we also fused full-length Trb1 to GFP and created AAA mutants of both the full-length and tail fusion constructs. Both GFP-Trb1 WT and GFP-Trb1 AAA localized exclusively to the nucleus. In contrast, GFP-tail WT and GFP-tail AAA, which lack the NLS present in the N-terminal extension of Trb1 were both found in the nucleus and cytoplasm. In accordance with our earlier results, GFP-Trb1 WT potentiated COP1 nuclear localization, whereas GFP alone and GFP-Trb1 AAA did not. Remarkably, however, GFP-Trb1 tail was sufficient to promote COP1 nuclear localization. This effect was abrogated by the AAA mutation, which eliminates COP1 binding (Figures 3A and B).

These findings reveal that the Trb1 C-terminal tail is both necessary and sufficient to enhance COP1 nuclear localization.

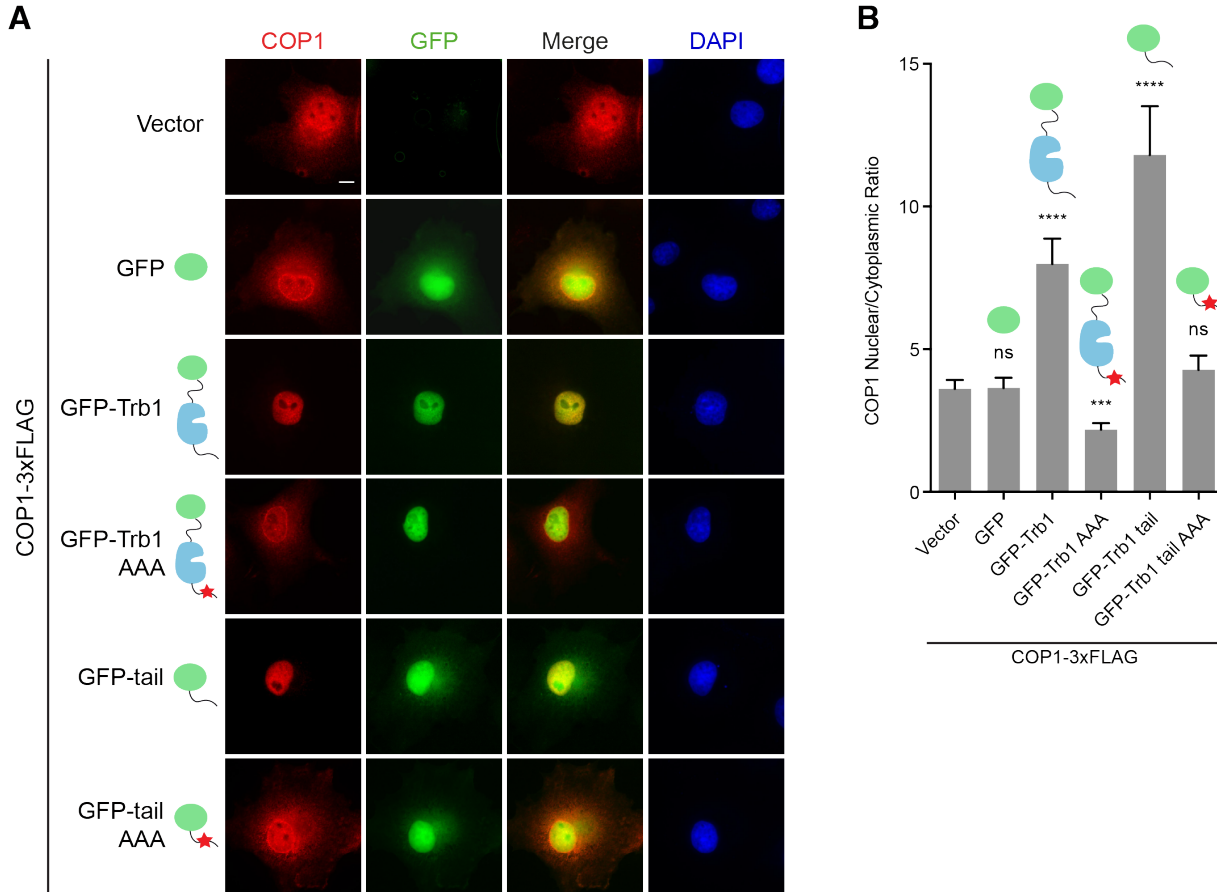


**Figure 3 | The Trb1 C-terminal tail is sufficient to promote COP1 nuclear localization.**

**(A)** Representative images of COS7 cells expressing COP1-3xFLAG (red) co-transfected with empty vector, GFP, or the indicated GFP-Trb1 constructs (green). Cells were stained with anti-FLAG (Sigma) and anti-mouse Alexa Fluor 568. Nuclei were counterstained with DAPI (blue). Scale bar, 10  $\mu$ m.

**(B)** Quantification of the average ratio of nuclear/cytoplasmic fluorescence of COP1-3xFLAG in (A). Mean values  $\pm$  S.E.M. are shown for three independent experiments where 50 individual cells per experiment were analyzed. Significance relative to GFP-COP1 with empty vector was calculated using the Student t test (ns, not significant; \*\*\* $p < 0.0001$ ; \*\*\*\* $p < 0.00001$ ).

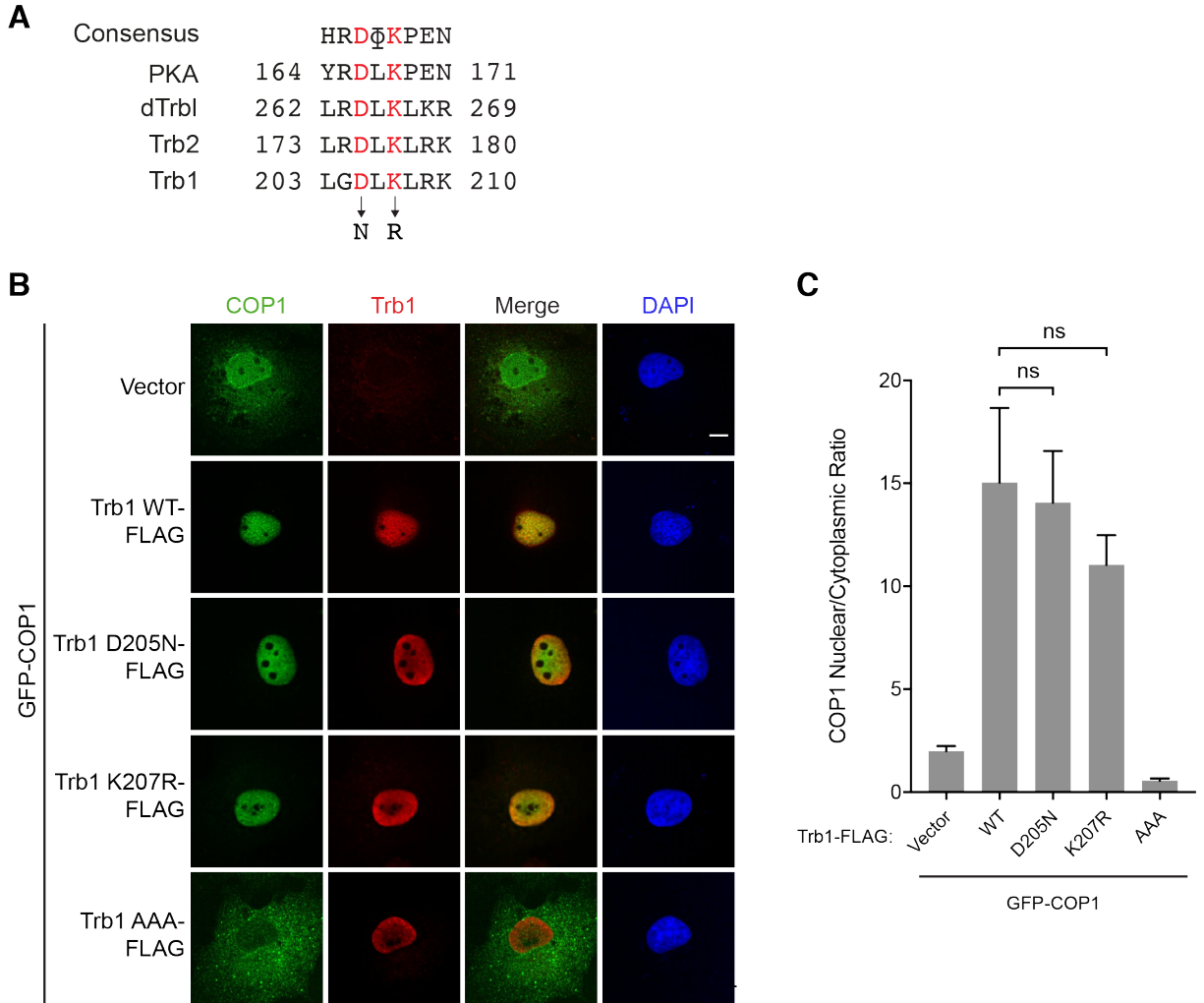


**Figure 4 | Mutations in the pseudoactive site do not affect the ability of Trb1 to promote nuclear localization of COP1.**

- (A) Sequence alignment of the catalytic loop in Trb1, Trb2, *Drosophila* Tribbles (dTrbl), and PKA.
- (B) Representative images of COS7 cells showing GFP-COP1 (green) co-transfected with empty vector or the indicated Trb1-FLAG constructs (red). Cells were stained with anti-FLAG (Sigma) and anti-mouse Alexa Fluor 568. Nuclei were counterstained with DAPI (blue). Scale bar, 10  $\mu$ m.
- (C) Quantification of the average ratio of nuclear/cytoplasmic fluorescence of GFP-COP1 in (B). Mean values  $\pm$  S.E.M. are shown for three independent experiments where 50 individual cells per experiment were analyzed. Significance relative to GFP-COP1 coexpressed with Trb1 WT was calculated using the Student t test (ns, not significant).

Though the C-terminal tail of Trb1 was sufficient for promoting COP1 nuclear localization, we next tested whether the pseudokinase domain of Trb1 could play an additional regulatory role in this process. Several studies have shown that mutations in the pseudokinase domain affect interactions between Tribbles and its binding partners. The pseudokinase domain retains several conserved motifs important for catalysis in catalytically competent kinases, including the HRD motif in the catalytic loop. A mutation within the HRD motif in the *Drosophila* Tribbles homolog ablates its interactions with Akt and the C/EBP homolog Slbo<sup>29,30</sup>. Similarly, mutations in the catalytic loop of murine Trb2 impair binding of C/EBP $\alpha$ <sup>7</sup>. Although Trb1 is catalytically inactive<sup>31</sup>, these mutations might bias the pseudokinase domain to adopt different conformations and thereby affect the ability of Trb1 to interact with its binding partners. We generated point mutations in the pseudoactive site of Trb1 corresponding to those analyzed in *Drosophila* Tribbles (D205N) and in murine Trb2 (K207R) (Figure 4A). Neither of these mutations, however, caused a significant change in the ability of Trb1 promote COP1 nuclear localization (Figure 4B and C).

### **Nuclear localization of COP1 is regulated by the WD40 domain**

The Trb1 tail binds to the WD40 domain of COP1<sup>20</sup>. Therefore, we expected that mutations in the Trb1-binding site in the COP1 WD40 domain would prevent Trb1 from promoting COP1 nuclear localization. We generated several COP1 WD40 point mutants (K472E, R515E, W517A, K600E, E642R) to test this hypothesis. Each of these residues is highly conserved, and analogous mutations in *Arabidopsis* COP1 affect binding of substrates containing a COP1-binding motif<sup>21</sup>.

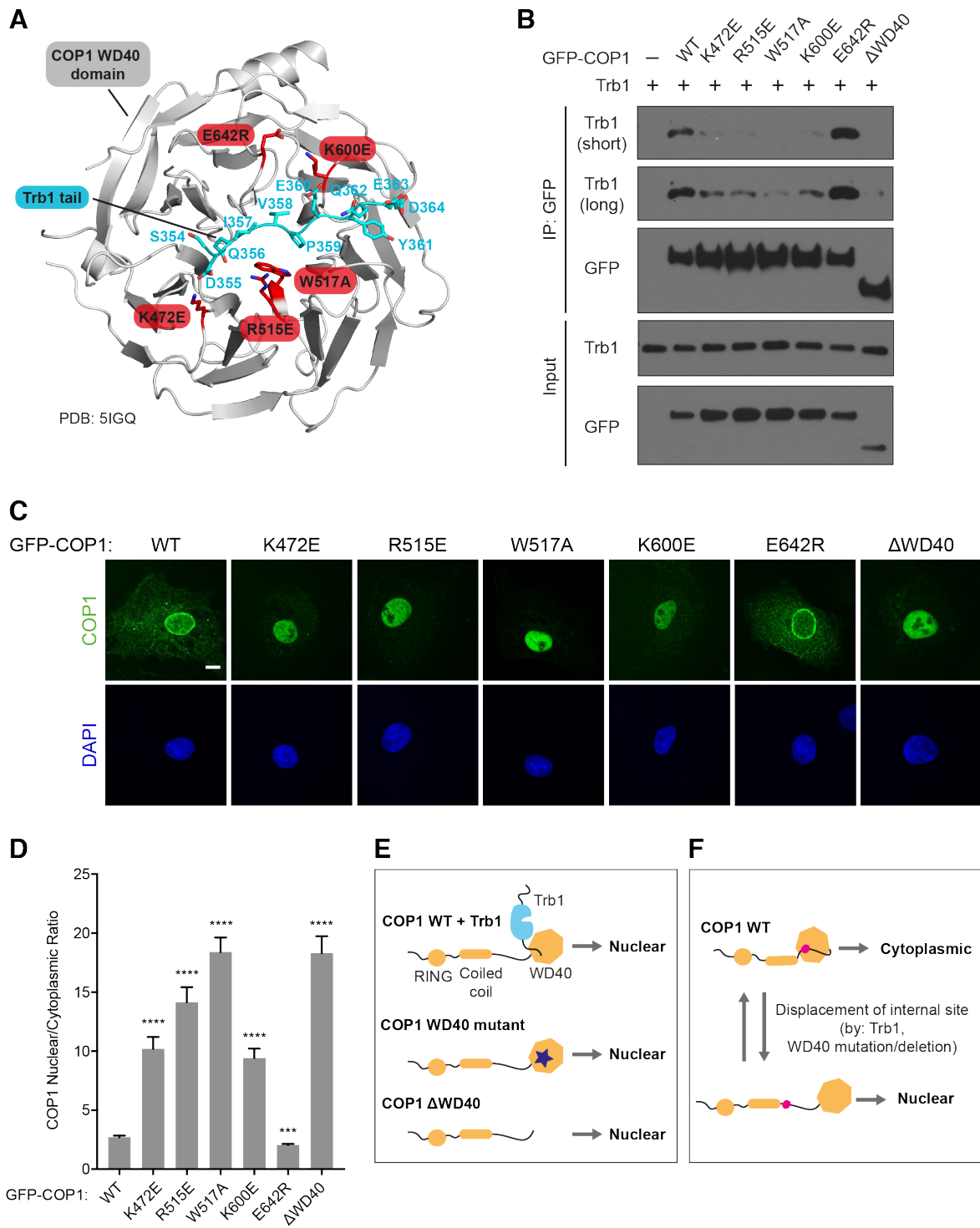


**Figure 5 | Nuclear localization of COP1 is regulated by the WD40 domain.**

- (A) A cartoon representation of a crystal structure of the COP1 WD40 domain (grey) in complex with the Trb1 tail (cyan) (PDB: 5IGQ). Point mutations introduced in the WD40 domain are shown in red.
- (B) Coimmunoprecipitation of COP1 WD40 mutants with Trb1 from COS7 cells transiently transfected with the indicated GFP-COP1 constructs and untagged Trb1.
- (C) Representative images of COS7 cells transiently transfected with the indicated GFP-COP1 constructs (green). Nuclei were counterstained with DAPI (blue). Scale bar, 10  $\mu$ m. See also Figure 6A for corresponding images of these GFP-COP1 constructs coexpressed with Trb1-FLAG.
- (D) Quantification of the average ratio of nuclear/cytoplasmic fluorescence of GFP-COP1 constructs in (C). Mean values  $\pm$  S.E.M. are shown for three independent experiments where 50 individual cells per experiment were analyzed. Significance relative to GFP-COP1 WT was calculated using the Student t test (\*\*p < 0.0001; \*\*\*\*p < 0.00001).
- (E) Cartoons summarizing the effects of Trb1 binding and WD40 domain mutation/deletion on COP1 localization.
- (F) Proposed model for regulation of COP1 subcellular localization by an intramolecular regulatory site that competes with Trb1 for binding to the WD40 domain.

The crystal structure of the COP1 WD40 domain in complex with the Trb1 tail revealed that four of these residues (K472, R515, W517, K600) directly engage the Trb1 tail, and their mutation should therefore prevent Trb1 binding, while E642 is not involved in the interaction (Figure 5A).

We confirmed through coimmunoprecipitation that K472E, R515E, W517A, and K600E mutations indeed markedly weakened the interaction between Trb1 and COP1, while E642R did not (Figure 5B). Counterintuitively, however, all four COP1 WD40 mutants that exhibited impaired Trb1 binding localized primarily to the nucleus even in the absence of Trb1 (Figures 5C and D). Coexpression with Trb1 did not result in a significant change in the localization of these mutants (Figures 6A and B). COP1 E642R, on the other hand, behaved similarly to COP1 WT and accumulated exclusively in the nucleus only in the presence of Trb1 coexpression (Figures 5C and D, 6A and B). The WD40 domain mutations that interfere with Trb1 binding mimicked the effect of deleting the entire WD40 domain (Figs 5C and D), which was previously shown to cause



mammalian COP1 to localize exclusively to the nucleus<sup>15,16</sup>. These findings reveal that an intact Trb1 binding site is necessary for proper nucleocytoplasmic shuttling of COP1.

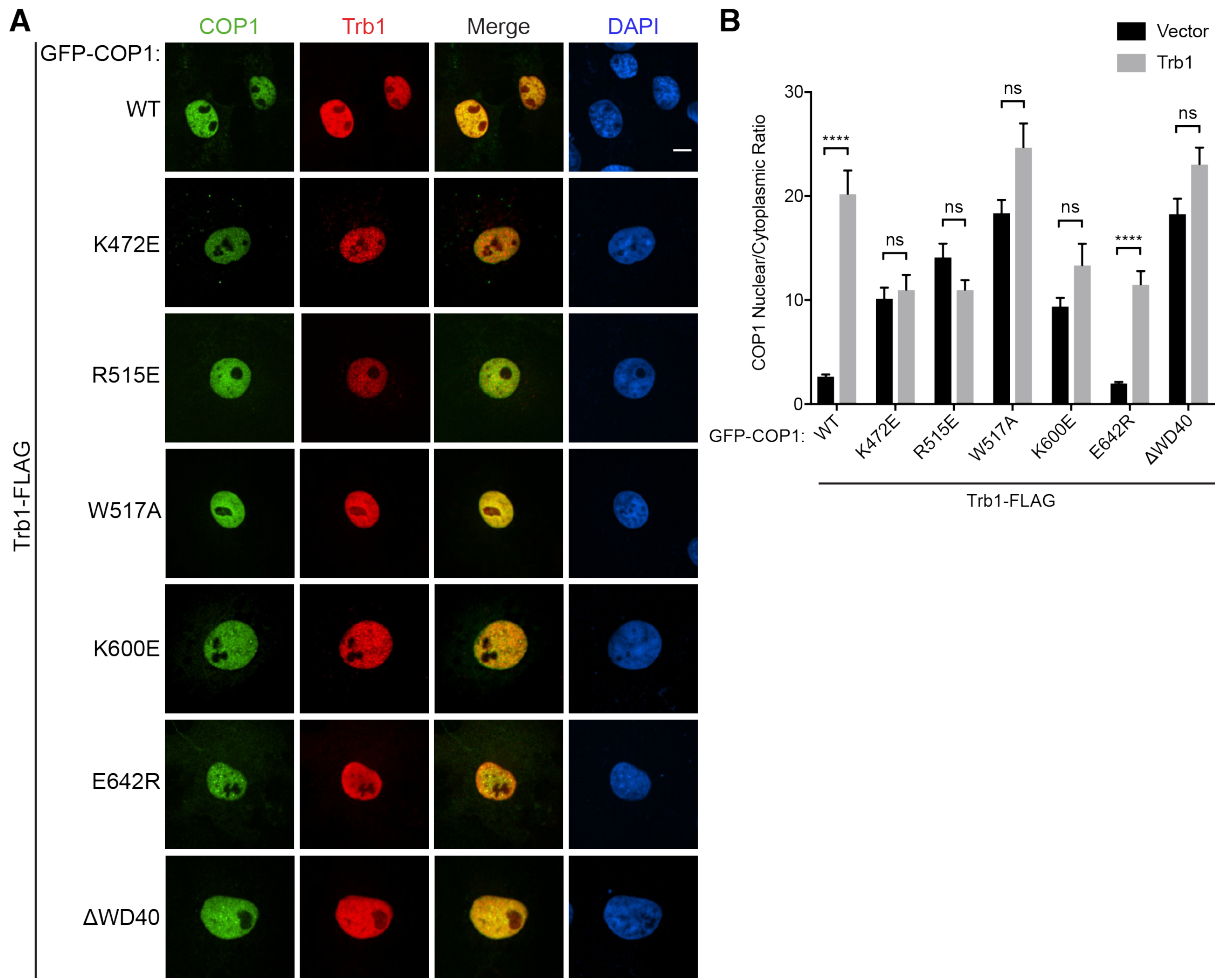


**Figure 6 | Localization of Trb1-binding deficient COP1 WD40 mutants is unaffected by Trb1 coexpression.**

- (A) Representative images of COS7 cells co- transfected with Trb1-FLAG (red) and the indicated GFP-COP1 constructs (green). Cells were stained with anti-FLAG (Sigma) and anti-mouse Alexa Fluor 568. Nuclei were counterstained with DAPI (blue). Scale bar, 10  $\mu$ m.
- (B) Quantification of the average ratio of nuclear/cytoplasmic fluorescence for each of the indicated GFP-COP1 constructs co- transfected with empty vector (Figure 5C) or with Trb1-FLAG (Figure 6A). Mean values  $\pm$  S.E.M. are shown for three independent experiments where 50 individual cells per experiment were analyzed. Significance was calculated using the Student t test (ns, not significant; \*\*\*\*p,  $p < 0.00001$ ).

## **Identification of an intramolecular WD40 binding site that regulates the subcellular distribution of COP1**

Our findings demonstrate that association of Trb1 with the WD40 domain and disruption of the Trb1 binding site on the WD40 domain paradoxically both cause COP1 to be retained in the nucleus (Figure 5E). These seemingly contradictory observations could be explained by a model in which the Trb1 binding site on the WD40 domain participates in an intramolecular interaction that promotes COP1 nuclear export such that the Trb1 C-terminal tail competes with this interaction, causing nuclear retention (Figure 5F). We hypothesized that this intramolecular site resembles the consensus COP1-binding motif found in numerous COP1 binding partners. By examining the sequence of COP1, we identified a sequence, EDSTVPQ, which contains key structural features of the COP1-binding motif, including the “VP” motif and acidic residues a few positions N-terminal to the VP motif (Figure 7A). This site is located within the linker between the coiled coil and WD40 domains and spans residues 308-314 (Figure 5F).

If this putative intramolecular site is responsible for interacting with the WD40 domain to enable COP1 nuclear export, then its mutation should result in increased COP1 nuclear localization, mimicking the effect of Trb1 binding or mutating/deleting the WD40 domain. Indeed, mutation of this site (COP1 4A) (Figure 7A) resulted in enhanced nuclear localization of COP1 (Figures 7B and C). In addition, deletions in the linker between the coiled coil and WD40 domains resulted in increased nuclear localization only if they included the EDSTVPQ sequence (Figure 8). Together, these data support a role for this intramolecular WD40 binding site in regulation of COP1 nuclear export. Because of the similarity between the intramolecular site and the COP1-binding motifs in COP1 substrates, we have termed this site the pseudosubstrate latch (PSL).

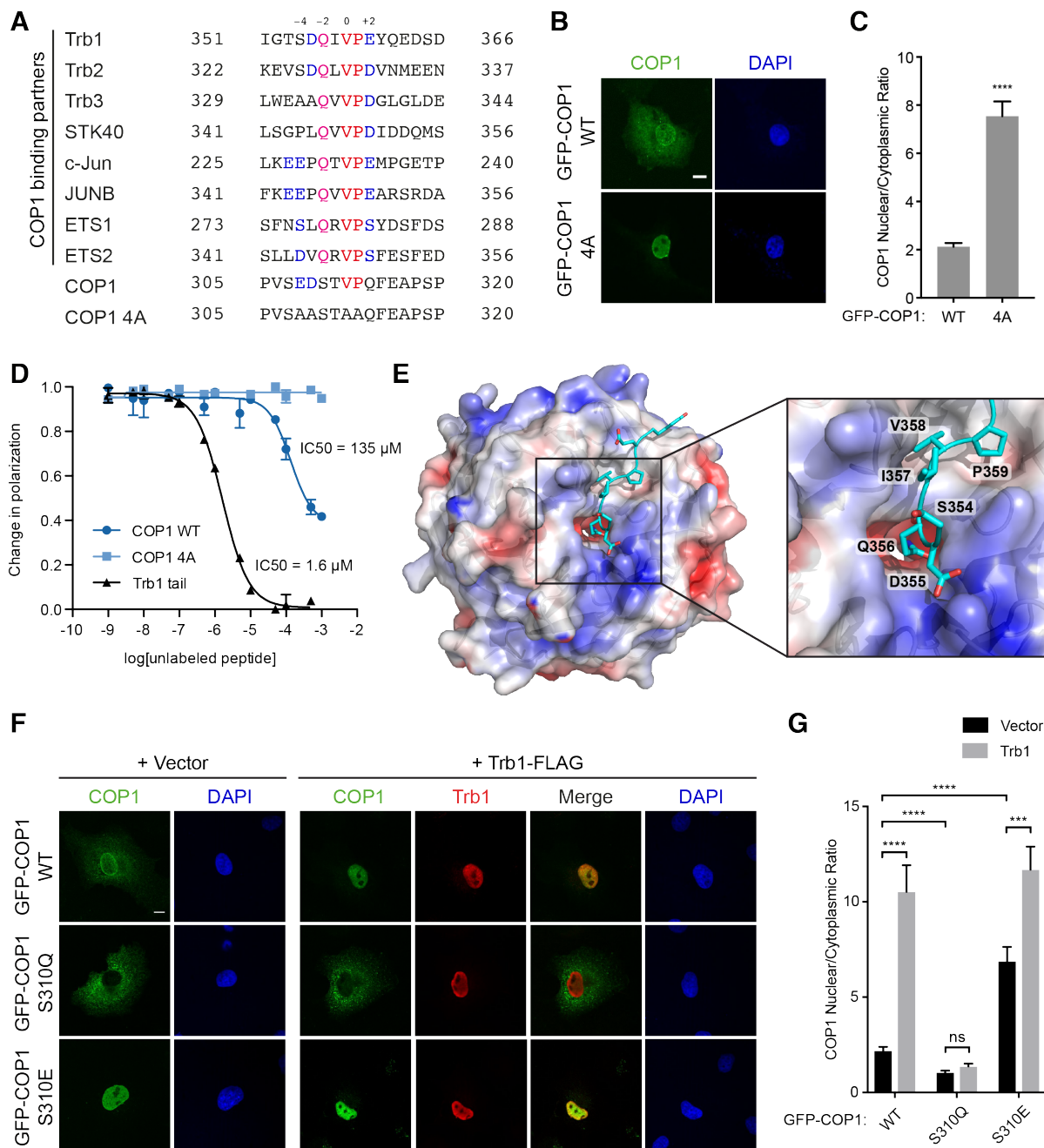


**Figure 7 | Trb1 competes with an intramolecular site for binding to the WD40 domain to modulate COP1 localization.**

- (A) Sequence alignment of COP1 pseudosubstrate latch with the COP1 4A mutant and COP1-binding motifs from previously identified COP1 binding partners. Residues in the sequences are colored to indicate residues conserved in the COP1-binding motif: Val-Pro dipeptide (red), acidic residues (blue), conserved Gln (magenta).
- (B) Representative images of COS7 cells transiently transfected with GFP-COP1 WT or GFP-COP1 4A (green). Nuclei were counterstained with DAPI (blue). Scale bar, 10  $\mu$ m.

- (C) Quantification of the average ratio of nuclear/cytoplasmic fluorescence of GFP-COP1 in (B). Mean values  $\pm$  S.E.M. are shown for three independent experiments where 50 individual cells per experiment were analyzed. Significance relative to GFP-COP1 WT was calculated using the Student t test (\*\*\*\* $p < 0.00001$ ).
- (D) Fluorescence polarization competition assay measuring the ability of unlabeled COP1 PSL, COP1 PSL 4A, and Trb1 tail peptides to compete with FITC-Trb1 tail for binding to the COP1 WD40 domain (376-731). The COP1 WD40 domain was preincubated with FITC-Trb1 tail before addition of the indicated concentrations of unlabeled peptide. The change in polarization is plotted as a function of unlabeled peptide concentration. Curves were fit to a sigmoidal dose-response curve. Error bars represent the S.E.M.
- (E) Surface representation of the crystal structure (PDB: 5IGQ) of the COP1 WD40 domain colored according to electrostatic surface potential, calculated by APBS <sup>32</sup>, in complex with the Trb1 tail (cyan). Inset shows zoomed view of Trb1 Q356 inserting its side chain into the central channel of the COP1 WD40 domain.
- (F) Representative images of COS7 cells transiently transfected with the indicated GFP-COP1 constructs (green) and empty vector or Trb1-FLAG (red). Nuclei were counterstained with DAPI (blue). Scale bar, 10  $\mu$ m.
- (G) Quantification of the average ratio of nuclear/cytoplasmic fluorescence of GFP-COP1 constructs in (F). Mean values  $\pm$  S.E.M. are shown for three independent experiments where 50 individual cells per experiment were analyzed. Significance was calculated using the Student t test (ns, not significant, \*\*\* $p < 0.0001$ ; \*\*\*\* $p < 0.00001$ ).

We next used a fluorescence polarization competition assay to directly measure whether the PSL binds to the same interface on the WD40 domain as the Trb1 tail. An unlabeled COP1 PSL peptide was able to compete with a FITC-labeled Trb1 tail peptide for binding to recombinant human COP1 WD40 domain with an IC<sub>50</sub> of 135  $\mu$ M, whereas a COP1 PSL 4A peptide did not displace FITC-Trb1 tail even at millimolar concentrations (Figure 7D). These results demonstrate that the COP1 PSL binds to the WD40 domain in a manner dependent on the COP1-binding motif within the PSL. An unlabeled Trb1 tail peptide competed with FITC-Trb1 tail with an IC<sub>50</sub> of 1.6  $\mu$ M. Although the PSL binds to the WD40 domain with ~100-fold lower affinity than the Trb1 tail, the PSL/WD40 interaction can occur in *cis* in the context of full-length COP1, which would increase its effective affinity in a cellular environment.

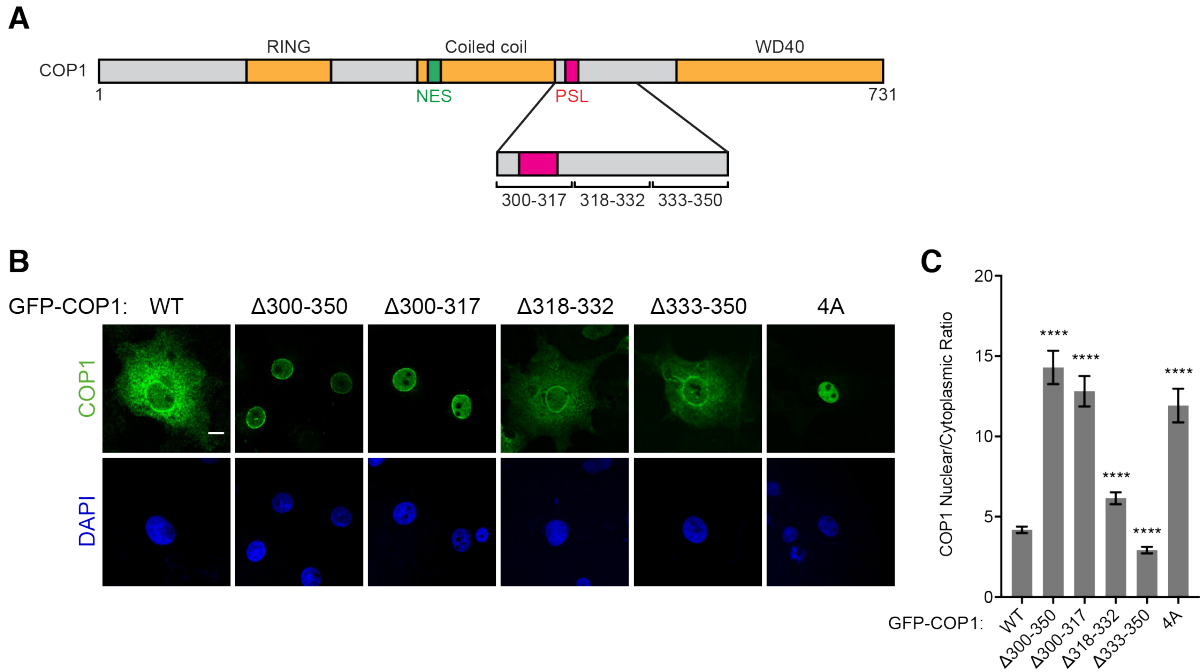


**Figure 8 | Identification of an intramolecular WD40 binding site that regulates the subcellular distribution of COP1.**

- (A) Schematic of COP1 illustrating locations of the coiled coil-WD40 domain linker deletions and PSL.
- (B) Representative images of COS7 cells transfected with the indicated GFP-COP1 constructs (green). Nuclei were counterstained with DAPI (blue). Scale bar, 10  $\mu$ m.
- (C) Quantification of the average ratio for nuclear/cytoplasmic fluorescence for each of the indicated GFP-COP1 constructs. Mean values  $\pm$  S.E.M. are shown for three independent experiments where 50 individual cells per experiment were analyzed. Significance relative to GFP-COP1 WT was calculated using the Student t test (ns, not significant; \*\*\*\*p,  $p < 0.00001$ ).

The lower affinity of the intramolecular PSL/WD40 interaction could be in place to allow the Trb1 tail to outcompete it. To test this model, we sought to reengineer the PSL into a stronger WD40 binding site, which would be expected to decrease the ability of Trb1 to promote COP1 nuclear localization. We compared the COP1-binding motif in the PSL to those in known COP1 binding partners and found that a unique feature of the PSL is its lack of a glutamine residue in the -2 position relative to the VP motif (Q356 in Trb1) (Figure 7A). Examination of the electrostatic surface potential of the WD40 domain in the crystal structure of the Trb1 tail/COP1 WD40 domain complex reveals that the side chain of Trb1 Q356 inserts into the negatively charged central channel of the COP1 WD40 domain and forms a hydrogen bond with Y491 (Figure 7E). In the COP1 PSL, the corresponding residue is a serine (S310), which is expected not to engage as well in hydrogen bonding with Y491 due to its shorter side chain and lower polarity. We therefore reasoned that mutating S310 to glutamine (S310Q) would strengthen the interaction between the PSL and WD40 domain, and consequently, enhance the ability of the PSL to compete with Trb1 for binding to the WD40 domain. Indeed, COP1 S310Q exhibited reduced nuclear localization compared to COP1 WT and was largely indifferent to Trb1 (Figures 7F and G).

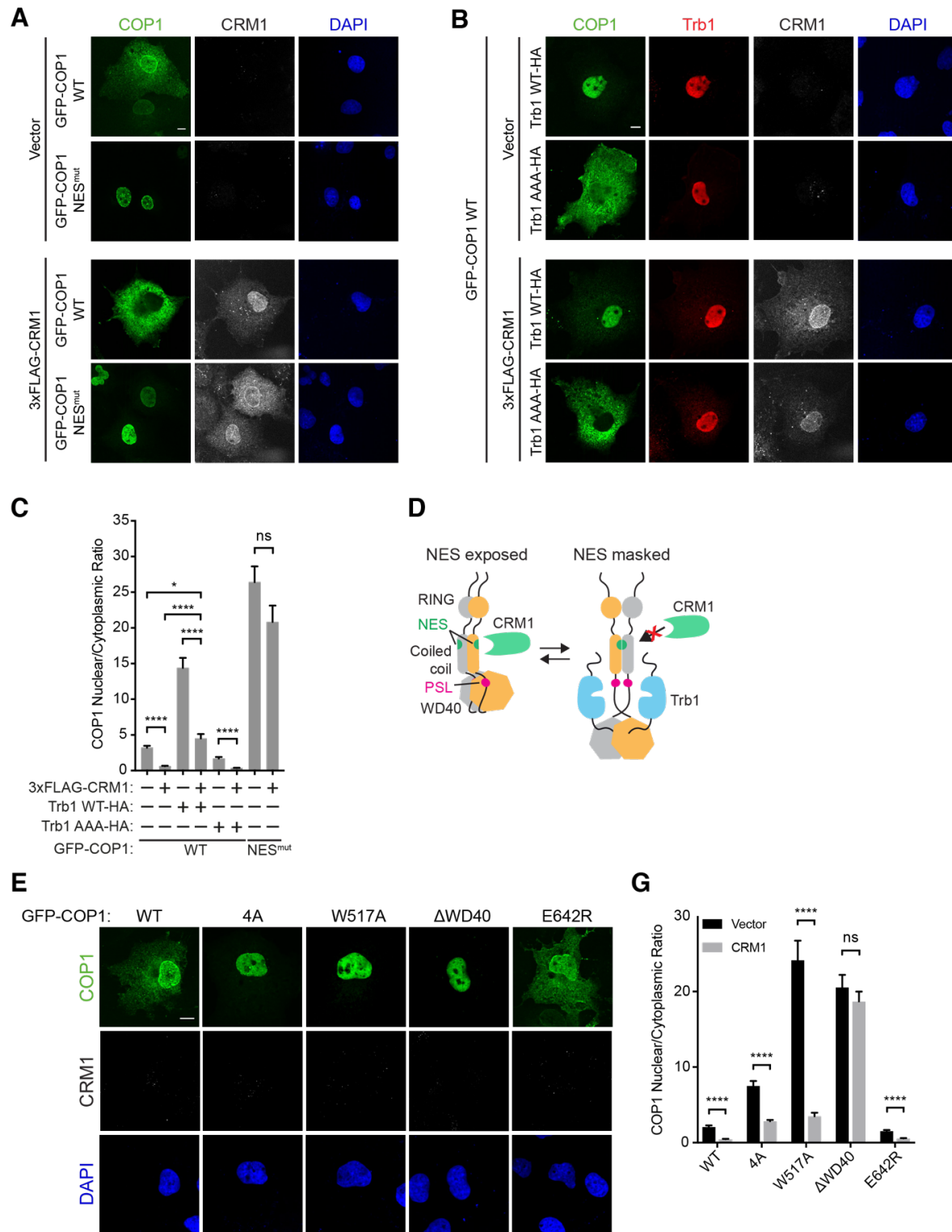
In contrast to glutamine substitution, replacement of S310 with a negatively charged residue should weaken the binding of the PSL to the WD40 domain and, consequently, enhance nuclear localization, even without Trb1 present. In agreement with this prediction, a S310E mutation resulted in increased nuclear COP1, and addition of Trb1 further potentiated this effect by less than 2-fold (Figures 7F and G). Due to the phosphomimetic potential of the S310E mutation, these data suggest that binding of the PSL to the WD40 domain could be regulated through phosphorylation of S310, which like Trb1 binding, would be expected to promote COP1 nuclear localization. This could be another reason why the S310Q mutation, which removes the

putative phosphorylation site, enhances PSL binding and results in efficient nuclear export of COP1.

### **Trb1 inhibits CRM1-mediated nuclear export of COP1**

Trb1 could increase COP1 nuclear localization by promoting nuclear import and/or inhibiting nuclear export of COP1. Since Trb1 is found primarily in the nucleus, Trb1 is more likely to regulate COP1 nuclear export. A leucine-rich nuclear export signal (NES) at the N-terminus of the COP1 coiled coil domain is recognized by the nuclear export receptor CRM1<sup>15,33</sup>. Mutation of the NES (COP1 NES<sup>mut</sup>) results in constitutively nuclear localization of COP1 (Figures 9A and C). To test if Trb1 influences COP1 localization through a CRM1-dependent pathway, we coexpressed COP1 and CRM1 with or without Trb1 and examined their localization via immunofluorescence. Overexpression of CRM1 shifts COP1 WT to predominantly cytoplasmic localization in a NES-dependent manner (Figures 9A and C). However, this shift is markedly reduced when COP1 is coexpressed with both CRM1 and Trb1 WT, but not Trb1 AAA (Figures 9A-C), suggesting that Trb1 binding to COP1 directly competes with CRM1-dependent nuclear export.

Recognition of cargo proteins by CRM1 is often regulated through masking or occlusion of the NES in the cargo. This can be achieved through intermolecular interactions that involve changes in oligomerization states, as observed for p53<sup>34</sup>, or through conformational changes, as shown for NFAT1<sup>35</sup>. Binding of the COP1 PSL to the WD40 domain could enable COP1 nuclear export by unmasking the NES and making it accessible to CRM1 (Figure 9D). Therefore, loss of the PSL/WD40 interaction should mask the NES and render COP1 less responsive to CRM1. To test this hypothesis, we coexpressed CRM1 with mutants of COP1 in which the PSL/WD40





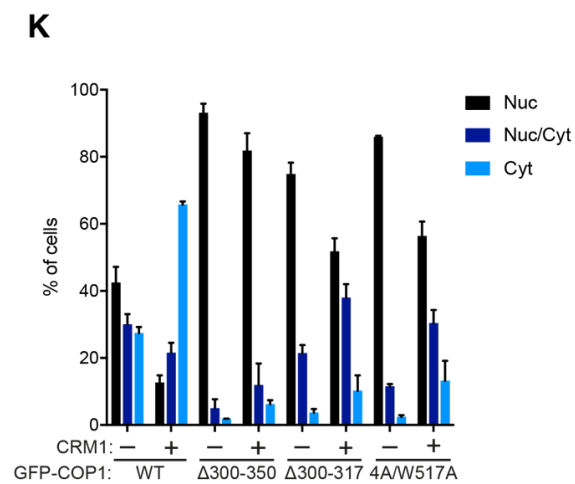
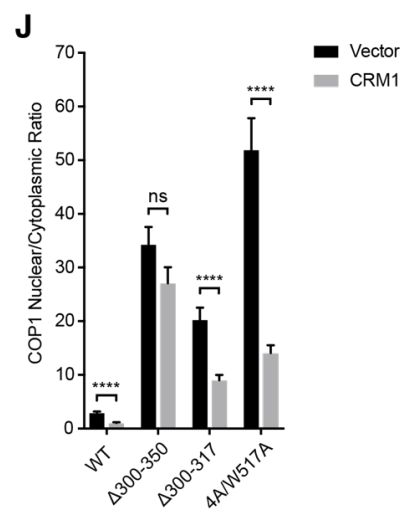
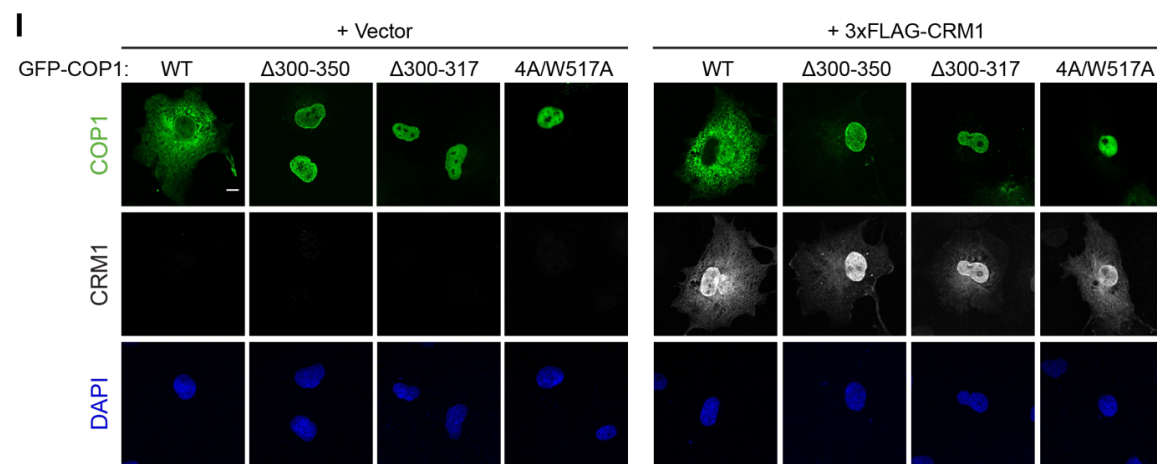
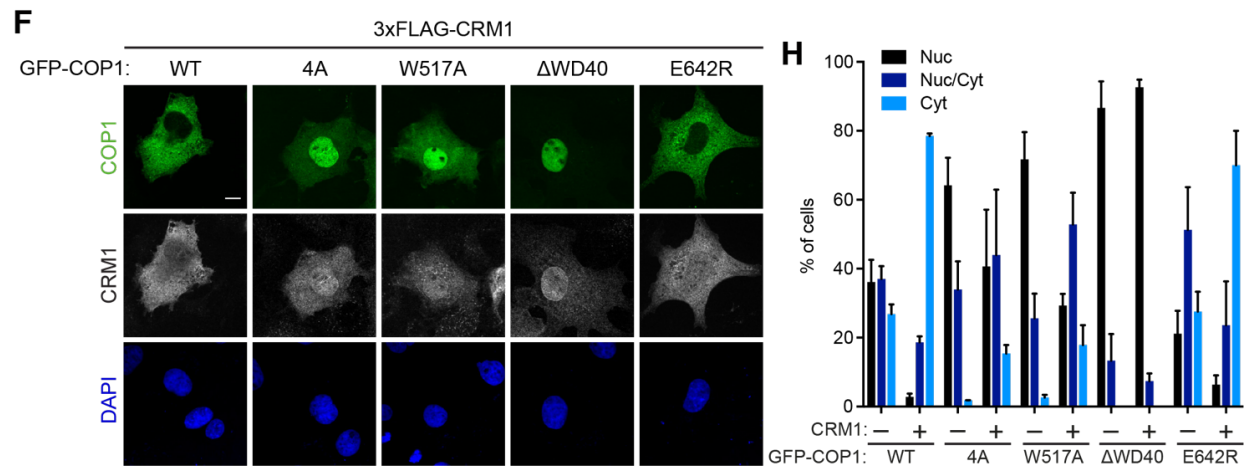


**Figure 9 | Trb1 inhibits CRM1-mediated nuclear export of COP1.**

- (A) Representative images of COS7 cells expressing GFP-COP1 WT or GFP-COP1 NES<sup>mut</sup> (V238A/L242A) (green) and empty vector or 3xFLAG-CRM1 (grayscale). Cells were stained with anti-FLAG (Cell Signaling) and anti-rabbit Alexa Fluor 680. Nuclei were counterstained with DAPI (blue). Scale bar, 10  $\mu$ m.
- (B) Representative images of COS7 cells expressing GFP-COP1 (green), the indicated Trb1-HA constructs (red), and empty vector or 3xFLAG-CRM1 (grayscale). Cells were stained with anti-FLAG (Cell Signaling), anti-HA (Sigma), anti-rabbit Alexa Fluor 680, and anti-mouse Alexa Fluor 568. Nuclei were counterstained with DAPI (blue). Scale bar, 10  $\mu$ m.
- (C) Quantification of the average ratio of nuclear/cytoplasmic fluorescence of GFP-COP1 constructs in (A) and (B). Mean values  $\pm$  S.E.M. are shown for three independent experiments where 50 individual cells per experiment were analyzed. Significance was calculated using the Student t test (ns, not significant; \* $p < 0.01$ ; \*\*\*\* $p < 0.00001$ ).
- (D) A hypothesized model for inhibition of COP1 nuclear export by Trb1 through NES masking. In this model, binding of the PSL to the WD40 domain stabilizes a conformation in which the NES, located in the distal coiled coil domain, is exposed. This could be achieved by an effective reduction of the distance between the WD40 domain and the coiled coil domain resulting from PSL binding. Loss of this proximity upon Trb1 binding could then induce a conformational change in the coiled coil domain resulting in NES masking. Relative changes in the dimerization interface within the previously reported COP1 coiled coil domain dimer, as a function of PSL binding, could be one mechanism for control of NES masking.
- (E) & (F) Representative images of COS7 cells expressing the indicated GFP-COP1 (green) constructs co-transfected with empty vector (E) or with 3xFLAG-CRM1 (F). Cells were stained with anti-FLAG (Sigma) and anti-mouse Alexa Fluor 568. Nuclei were counterstained with DAPI (blue). Scale bar, 10  $\mu$ m.
- (G) Quantification of the average ratio of nuclear/cytoplasmic fluorescence of GFP-COP1 constructs in (E) and (F). Mean values  $\pm$  S.E.M. are shown for three independent experiments where 50 individual cells per experiment were analyzed. Significance was calculated using the Student t test (ns, not significant; \*\*\*\* $p < 0.00001$ ).
- (H) Quantification of percentage of cells observed in (E) and (F) with the indicated GFP-COP1 construct exhibiting nuclear (Nuc), nuclear and cytoplasmic (Nuc/Cyt), or cytoplasmic (Cyt) localization. Mean values  $\pm$  S.E.M. are shown for three independent experiments where 50 individual cells per experiment were analyzed.
- (I) Representative images of COS7 cells expressing the indicated GFP-COP1 (green) constructs co-transfected with empty vector or 3xFLAG-CRM1 (grayscale). Cells were stained with anti-FLAG (Sigma) and anti-mouse Alexa Fluor 568. Nuclei were counterstained with DAPI (blue). Scale bar, 10  $\mu$ m.
- (J) Quantification of the average ratio of nuclear/cytoplasmic fluorescence of GFP-COP1 constructs in (I). Mean values  $\pm$  S.E.M. are shown for three independent experiments where 50 individual cells per experiment were analyzed. Significance was calculated using the Student t test (ns, not significant; \*\*\*\* $p < 0.00001$ ).
- (K) Quantification of percentage of cells observed in (I) with the indicated GFP-COP1 construct exhibiting nuclear (Nuc), nuclear and cytoplasmic (Nuc/Cyt), or cytoplasmic (Cyt) localization. Mean values  $\pm$  S.E.M. are shown for three independent experiments where 50 individual cells per experiment were analyzed.

interaction is disrupted (COP1 4A, COP1 W517A, and COP1  $\Delta$ WD40), as well as COP1 WT and COP1 E642R, in which this interaction is maintained. As expected, COP1 4A and COP1 W517A were less affected by the presence of CRM1 than COP1 WT and COP1 E624R (Figures 9E-G). Although the average nuclear to cytoplasmic ratio for COP1 4A and COP1 W517A still markedly decreased when CRM1 was coexpressed, both of these mutants remained substantially more nuclear than COP1 WT and COP1 E642R in the presence of CRM1 (Figure 9G). These differences were more striking when we considered how many cells showed exclusively cytosolic localization in the presence of CRM1, with ~80% of cells showing this phenotype for wild type COP1 and only ~20% for COP1 4A and COP1 W517A (Figure 9H). In contrast, COP1  $\Delta$ WD40 was completely unaffected by CRM1 overexpression and remained primarily nuclear under all conditions (Figures 9E-H), in agreement with this deletion being more potent than single WD40 point mutations in blocking binding of the COP1 binding motif (Figure 5B). Since COP1 4A and COP1 W517A could still be exported to a certain degree by CRM1 unlike COP1  $\Delta$ WD40, these mutations are likely less effective in abolishing the PSL/WD40 interaction. Thus, we generated a COP1 construct in which both the PSL and WD40 domain are mutated (COP1 4A/W517A). We also used the mutants in which the entire PSL is deleted (COP1  $\Delta$ 300-350, COP1  $\Delta$ 300-317). We then evaluated the localization of these mutants in the presence of CRM1 and found that, as predicted, they were more refractory to CRM1-mediated nuclear export than COP1 4A and COP1 W517A (Figures 9I-K). Collectively, these findings show that the PSL/WD40 interaction modulates COP1 responsiveness to CRM1.

## **Coevolution of Tribbles and the COP1 pseudosubstrate latch**

The Trb1-dependent control of the nuclear localization of human COP1 that we describe here is mechanistically very different from the light-exerted control of COP1 described in plants. COP1 is a highly conserved protein with homologs present in most animal and plant species, as well as some fungi. In contrast, Tribbles homologs have only been identified thus far in metazoans<sup>36</sup>. This evolutionary divergence led us to wonder whether appearance of the PSL site in COP1 coincides with appearance of Tribbles in evolution.

To ascertain the degree of conservation of the PSL in COP1, sequences of COP1 homologs from 100 diverse species were aligned and used to construct a phylogenetic tree (Figure 10). The sequence of each of these homologs was examined for the presence of a putative PSL, based on two criteria: (i) the site had to be present between the coiled coil and WD40 domains, and (ii) had to contain the VP dipeptide characteristic of the COP1-binding motif. We then determined if each of the species examined also possesses at least one Tribbles homolog, as well as whether these Tribbles homologs contain a COP1-binding motif in their C-terminal tail.

We found that, with only a few exceptions, the PSL in COP1 was present only in animal species that have at least one Tribbles homolog (Figure 10). In these species, Tribbles almost always had a COP1-binding motif, a feature that is remarkably well conserved in Tribbles homologs. The coevolution of Tribbles and the PSL site in COP1 supports the hypothesis that they are engaged in a conserved regulatory interaction. Notably, the sequence alignment also revealed that, in species where the PSL is present, the sequence of the entire linker connecting the coiled coil and WD40 domains is more conserved than in species where the PSL is absent, emphasizing the importance of this region in regulation of COP1 function in species in which Tribbles is also present.

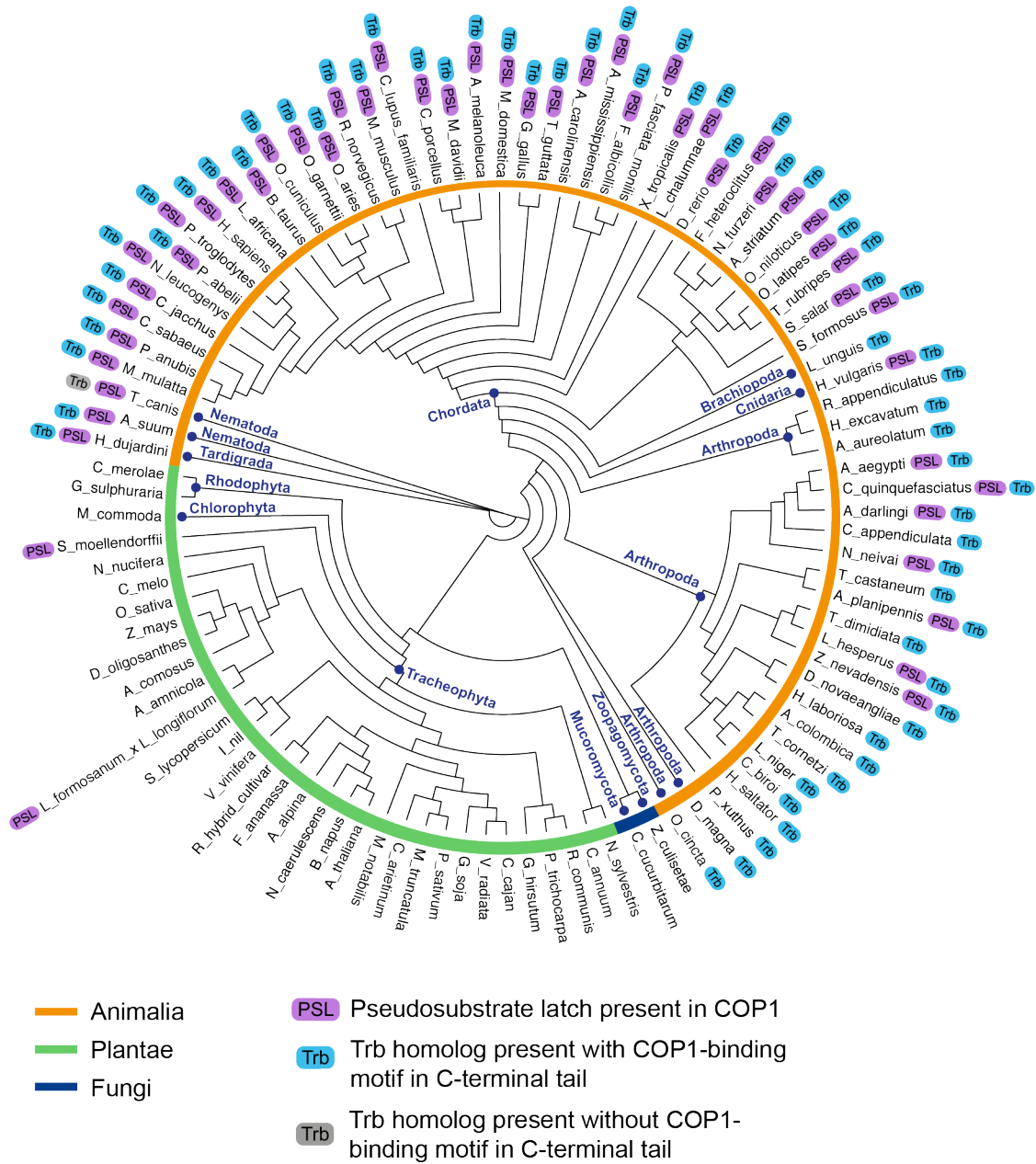


**Figure 10 | Coevolution of the COP1 pseudosubstrate latch and Tribbles.**

Phylogenetic tree of COP1 homologs from 100 species showing the presence of the pseudosubstrate latch (PSL) in COP1 and the presence of Tribbles homologs in the indicated species.

## **Potential role for conformational changes in the COP1 coiled coil domain in regulation of NES accessibility**

The COP1 NES is located at the N-terminus of the coiled coil domain, while the PSL is located immediately following the C-terminal end of the coiled coil and separated by a ~70 residue-long linker from the WD40 domain. Binding of the WD40 domain to the PSL would effectively shorten the linker region and bring the WD40 domain in close proximity to the coiled coil domain. Our data are consistent with a model in which this binding event is coupled to a conformational rearrangement in the coiled coil domain that would change the ability of the NES to interact with CRM1 and result in its “unmasking” when the PSL is bound to the WD40 domain. Since COP1 is believed to form a dimer through the coiled coil domain<sup>16</sup>, in which the NES is located, conformational changes within the coiled coil interface could be a way to regulate NES accessibility (Figure 9D).

Examination of the sequence of the COP1 coiled coil domain revealed that there is a heptad break resulting from a two-residue insertion near the C-terminus of the coiled coil domain (Figure 11A). Unlike one- or three-residue insertions, which are expected to cause local under- or overwinding of the coiled coil<sup>37</sup>, the effects of a two-residue insertion on the structure of a coiled coil are poorly understood. We speculated that this insertion might introduce a discontinuity that would enable the coiled coil domain to undergo conformational changes that affect the accessibility of the NES. Since the insertion occurs near the C-terminus of the coiled coil domain, we reasoned that binding of the WD40 domain to the PSL could sterically constrain the coiled coil into only one conformation, in which the NES is exposed. Consequently, if the C-terminal portion of the coiled coil following the insertion is important for changing the accessibility of the NES, then deleting this region should force the coiled coil domain to adopt

Predicted heptad register:    a b c d e f g a b c d e f g a b c d e f g a b c d e f g a b c    e f g a b c d e f g a b c d e

2 residue insertion

human            231    D N L D L A N V N L M L E L L V Q K K R Q L E A E S H A A Q L Q I L M E F L K V A R R N K R E Q L E Q I Q K E L S V L E  
 bovine            235    D N L D L A N V N L M L E L L V Q K K R Q L E A E S H A A Q L Q I L M E F L K V A R R N K R E Q L E Q I Q K E L S V L E  
 mouse            233    D N L D L A N V N L M L E L L V Q K K R Q L E A E S H A A Q L Q I L M E F L K V A R R N K R E Q L E Q I Q K E L S V L E  
 chicken          207    D N L D L A N V N L M L E L L V Q K K R Q L E A E S H A A Q L Q I L M E F L K V A R R N K R E Q L E Q I Q K E L S V L E  
 hydra            177    E N L D L S E V N N L L D A L I Q K K E S L E A D T E A V Q L E I L K E F L L Q L K N R K Q Q E F D K L K E E I R F L D  
 arabidopsis      134    C D V S I K E V D N L L T L L A E R R K R M E Q E A E R N M Q I L L D F L C L R K Q V D E L N E V Q T D L Q Y I K  
 pea               129    C E V T M K E L D T L L L L T E K K R K M E Q E A E R N M Q I L L D F L C L R K Q V D E L K E V Q T D L Q F I K  
 rice              142    N D M A V K E L D S L M T L I A E K K R R M E Q E S E T N M Q I L L V F L H C L R K Q V L E E L N E I Q T D L Q Y I K

NES

Predicted heptad register: a b c d e f g

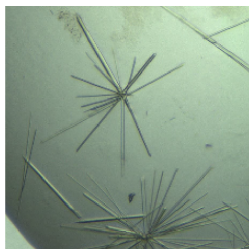
human	291	E	D	I	K	R	V	E	M	S	.	G	L	Y
bovine	295	E	D	I	K	R	V	E	M	S	.	G	L	Y
mouse	293	E	D	I	K	R	V	E	M	S	.	G	L	Y
chicken	267	E	D	I	K	R	V	E	M	S	.	G	L	Y
hydra	237	E	D	L	S	L	T	E	S	K	I	.	N	T
arabidopsis	194	E	D	I	N	A	V	E	R	H	R	I	D	L
pea	189	E	D	I	G	A	V	E	K	H	R	M	L	Y
rice	202	E	D	T	S	A	V	E	R	H	R	M	L	Y

**B**

C

Strain	COP1 Nuclear/Cytoplasmic Ratio
WT	~4
ACC30	~39 ****

D



**E**

● NES

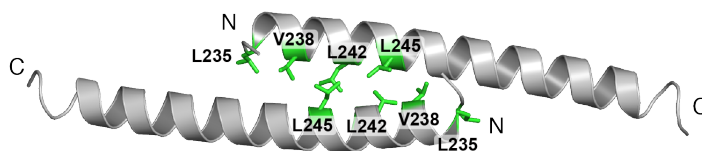


**Figure 11 | Identification of a heptad break in the COP1 coiled domain and its potential role in regulation of NES accessibility.**

- (A) Sequence alignment of the COP1 coiled coil domain from various species. The predicted heptad register of the coiled coil domain and the predicted site of a two-residue insertion is indicated above.
- (B) Representative images of COS7 cells expressing GFP-COP1 WT or GFP-COP1  $\Delta$ CC30. Nuclei were counterstained with DAPI (blue). Scale bar, 10  $\mu$ m.
- (C) Quantification of the average ratio of nuclear/cytoplasmic fluorescence of GFP-COP1 constructs in (B). Mean values  $\pm$  S.E.M. are shown for three independent experiments where 50 individual cells per experiment were analyzed. Significance was calculated using the Student t test (\*\*\*\*p < 0.00001).
- (D) Photo showing example of crystals obtained for COP1 CC  $\Delta$ 30.
- (E) Cartoon representation of crystal structure of COP1 CC  $\Delta$ 30 (gray). NES residues are shown in green sticks.

only one conformation. To test this idea, we deleted the last 30 residues of the coiled coil domain, which occur after the predicted heptad break, and found that this construct (COP1  $\Delta$ CC30) localized predominantly to the nucleus (Figure 11B and C), supporting a role for the C-terminal portion of the coiled coil domain in enabling nuclear export. This result indicates that loss of the C-terminal portion of the coiled coil domain causes the NES to become constitutively masked. To further investigate the structure of the coiled coil domain, we synthesized a peptide with the sequence of a fragment of the coiled coil domain lacking the region after the predicted insertion (COP1 CC  $\Delta$ 30) and solved its structure via x-ray crystallography (Figure 11D, Table 1). The structure revealed that this peptide is helical and forms an antiparallel dimer in which the NES residues are buried at the interface (Figure 11E). Whether the full-length COP1 coiled coil domain can adopt an analogous conformation remains unclear, but this structure demonstrates the tendency of the NES to become buried in the absence of the final 30 residues of the coiled coil domain.

### **Trb1 increases nuclear import of COP1**

Though we found that Trb1 inhibits COP1 nuclear export, it remains possible that Trb1 could also influence COP1 nuclear import to promote COP1 nuclear localization. COP1 nuclear import relies on a bipartite nuclear localization signal (NLS) with the two signal sequences located on either side of the RING domain<sup>15</sup> (Figure 12A). Mutation of either or both NLSs causes COP1 to become exclusively cytoplasmic (Figure 12B and C). Surprisingly, even though Trb1 is primarily nuclear, coexpression of Trb1 with the COP1 NLS mutants markedly increased their nuclear localization, albeit not to the same extent as COP1 WT (Figure 12B and C). This indicates that Trb1 enhances nuclear import of COP1. This could potentially be achieved if Trb1 and the COP1 NLS mutants can be imported as a complex, with Trb1 providing an NLS for recognition



**Table 1. Data collection and refinement statistics**

<b>Wavelength (Å)</b>	1.11583
<b>Resolution range (Å)</b>	33.94 - 1.8 (1.864 - 1.8)
<b>Space group</b>	P 43 21 2
<b>Unit cell</b>	35.165 35.165 129.487 90 90 90
<b>Total reflections</b>	16360 (1594)
<b>Unique reflections</b>	8180 (797)
<b>Multiplicity</b>	23.9 (24.3)
<b>Completeness (%)</b>	100.00 (100.00)
<b>Mean I/sigma(I)</b>	30.46 (3.88)
<b>Wilson B-factor</b>	29.42
<b>R-merge</b>	0.008133 (0.1697)
<b>R-meas</b>	0.0115
<b>CC1/2</b>	1 (0.973)
<b>CC*</b>	1 (0.993)
<b>R-work</b>	0.2369 (0.3503)
<b>R-free</b>	0.2733 (0.3175)
<b>Number of non-hydrogen atoms</b>	702
<b>macromolecules</b>	631
<b>water</b>	71
<b>Protein residues</b>	72
<b>RMS(bonds)</b>	0.012
<b>RMS(angles)</b>	1.37
<b>Ramachandran favored (%)</b>	1e+02
<b>Ramachandran outliers (%)</b>	0
<b>Clashscore</b>	2.27
<b>Average B-factor</b>	33.50
<b>macromolecules</b>	32.50
<b>solvent</b>	42.70

Statistics for the highest-resolution shell are shown in parentheses.

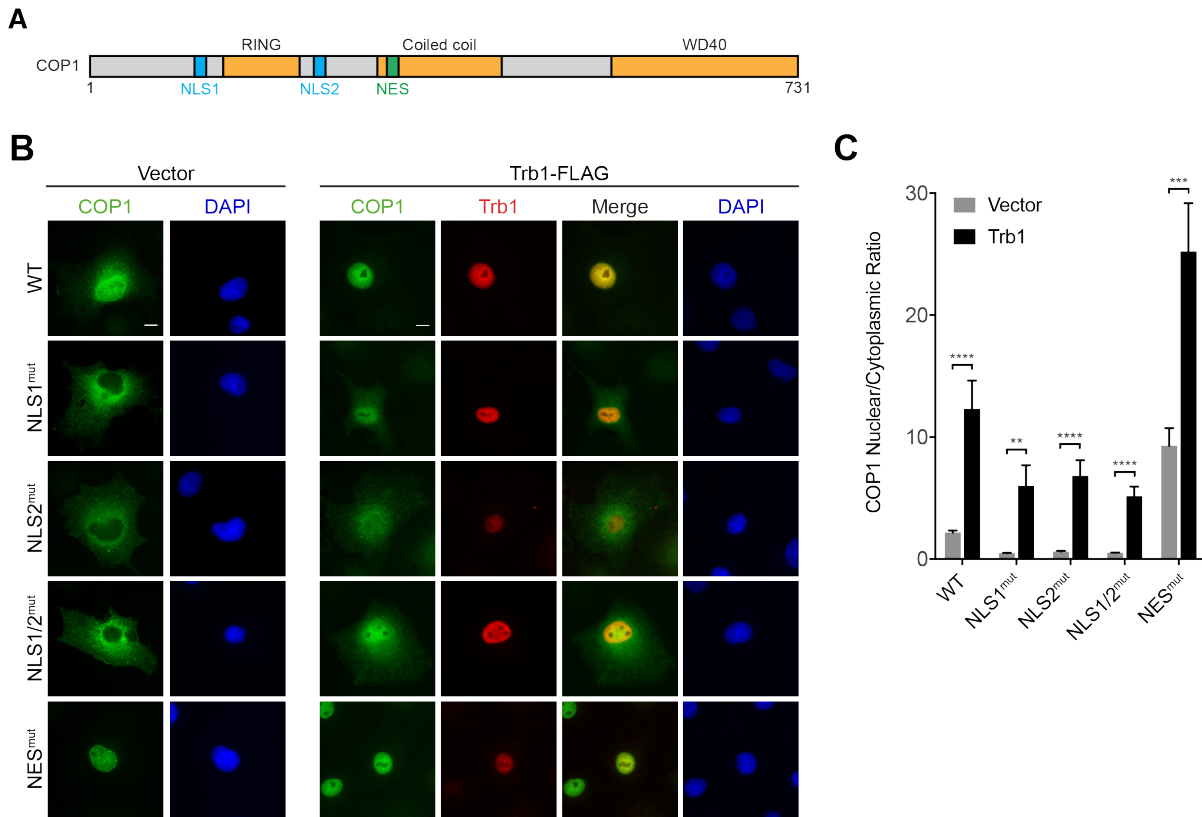


**Figure 12 | Trb1 promotes nuclear import of COP1.**

- (A) Schematic of COP1 illustrating locations of the nuclear localization signals (NLSs) and nuclear export signal (NES).
- (B) Representative images COS7 cells expressing the indicated GFP-COP1 constructs cotransfected with empty vector or with Trb1-FLAG. Cells were stained with mouse anti-FLAG (Sigma) and anti-mouse Alexa Fluor 568. Nuclei were counterstained with DAPI. Scale bar, 10  $\mu$ m.
- (C) Quantification of the average ratio of nuclear/cytoplasmic fluorescence of GFP-COP1 constructs in (B). Mean values  $\pm$  S.E.M. are shown for three independent experiments where 50 individual cells per experiment were analyzed. Significance was calculated using the Student t test (\*\* $p < 0.001$ ; \*\*\* $p < 0.0001$ ; \*\*\*\* $p < 0.00001$ ).

by nuclear import receptors. Alternatively, COP1 could be imported through another mechanism that is independent of its known NLSs, and loss of the bipartite NLS causes COP1 to be exported much more rapidly than it is imported. Further studies will be needed to establish whether the COP1 NLS mutants are still capable of being imported into the nucleus.

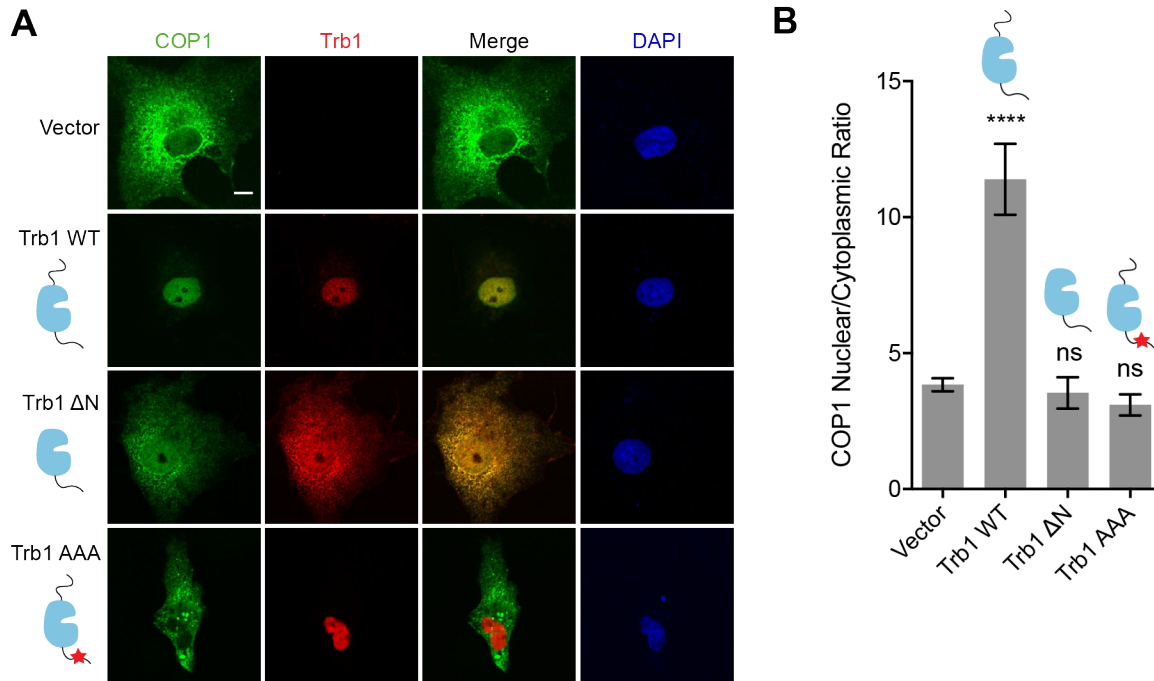


**Figure 13 | N-terminal region of Trb1 is necessary for promoting COP1 nuclear localization.**

**(A)** Representative images of COS7 cells coexpressing GFP-COP1 (green) with empty vector, Trb1 WT, or Trb1 ΔN (red). Cells were stained with mouse anti-FLAG (Sigma) and anti-mouse Alexa Fluor 568. Nuclei were counterstained with DAPI. Scale bar, 10 μm.

**(B)** Quantification of the average ratio of nuclear/cytoplasmic fluorescence of GFP-COP1 constructs in (A). Mean values ± S.E.M. are shown for three independent experiments where 50 individual cells per experiment were analyzed. Significance was calculated relative to GFP-COP1 with vector using the Student t test (ns, not significant; \*\*\*\* $p < 0.00001$ ).

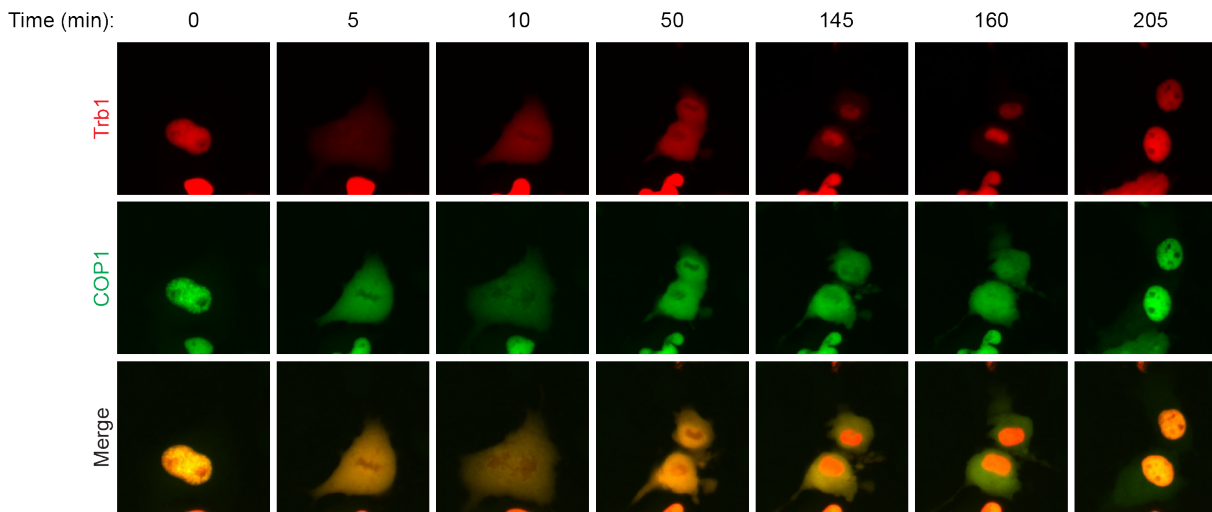
Trb1 has an NLS in its disordered N-terminal region. Deletion of this N-terminal region causes Trb1 to localize throughout the nucleus and cytoplasm rather than exclusively in the nucleus<sup>23</sup>. To determine whether Trb1 can still promote COP1 nuclear localization without its

NLS, we coexpressed COP1 with a Trb1 deletion mutant in which its N-terminal region (Trb1  $\Delta$ N) is deleted. Surprisingly, Trb1  $\Delta$ N was also unable to alter COP1 localization despite having an intact COP1-binding motif (Figure 13). This indicates that nuclear localization of Trb1 is necessary for it to promote COP1 nuclear localization. This result seems to conflict with our previous observation that the Trb1 C-terminal tail is sufficient to promote COP1 nuclear localization (Figure 3). This discrepancy could be explained by our observation that the GFP-tail construct, despite being able to localize throughout the nucleus and cytoplasm, is often more concentrated in the nucleus (Figure 3). Alternatively, it is possible that the C-terminal tail binds more readily to the pseudokinase domain when the N-terminal region of Trb1 is absent, reducing the ability of Trb1  $\Delta$ N to interact with COP1. Yet another potential explanation is that binding of Trb1 to COP1 alters not only NES accessibility but also NLS accessibility such that binding of Trb1  $\Delta$ N to COP1 in the cytoplasm prevents COP1 from being efficiently imported into the nucleus.

### **The Trb1/COP1 interaction is lost during the late stages of mitosis**

It remains unclear how the interaction between Trb1 and COP1 is regulated. In our imaging experiments, Trb1 and COP1 seems to associate constitutively when coexpressed, as indicated by localization of COP1 predominantly to the nucleus when Trb1 is present. Since localization of COP1 in plants is regulated by light and dark, we speculated that localization of human COP1 might also be controlled by a cyclical process. Thus, we examined how the subcellular localization of mCherry-Trb1 and GFP-COP1 changed over time through live cell imaging over a 24-hour period in COS7 cells. As observed in fixed cells, Trb1 and COP1 colocalized in the nucleus in cotransfected cells that were not undergoing mitosis. In dividing cells, both Trb1 and COP1 exit the nucleus upon breakdown of the nuclear envelope (Figure 14). Strikingly, after the nuclear

envelope reforms, Trb1 returns to the nucleus before COP1 does. This indicates that there is a period shortly after reformation of the nuclear envelope when Trb1 is unable to promote COP1 nuclear localization, possibly because they are unable to interact. This could potentially result from post-translational modifications to Trb1 or COP1 that prevent their association. Alternatively, COP1 nuclear import could be inhibited during mitosis, preventing it from interacting with Trb1, which has already relocated to the nucleus. Again, nuclear import of COP1 could be controlled through post-translational modifications, possibly by affecting the accessibility of its nuclear localization signals. Further studies will be needed to identify whether Trb1 and/or COP1 are modified during mitosis and how such modifications affect their ability to interact with each other.

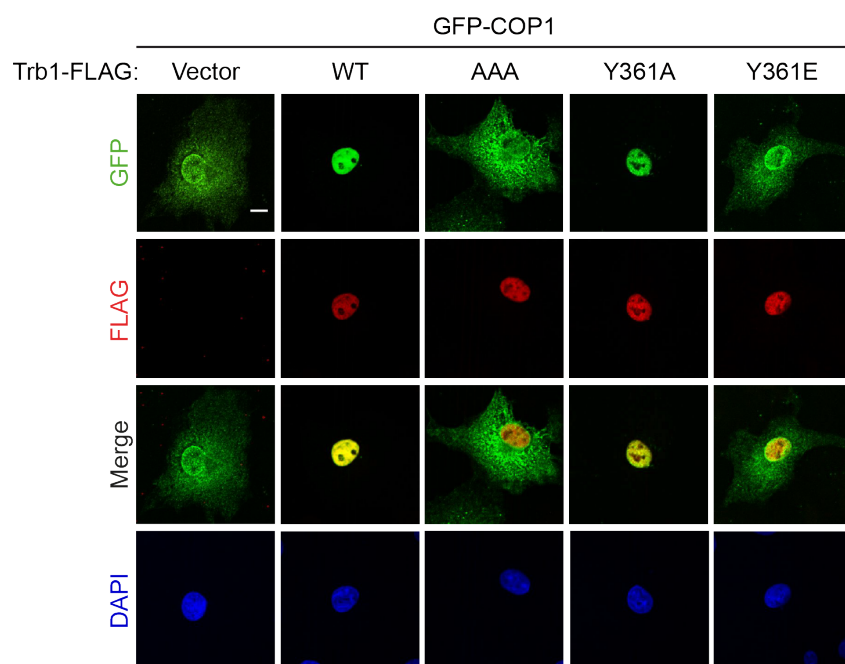
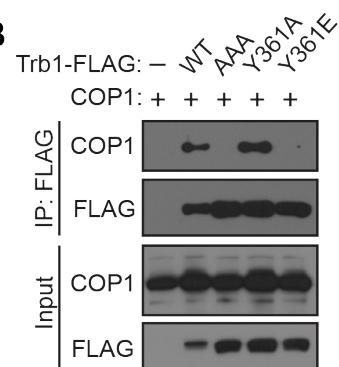
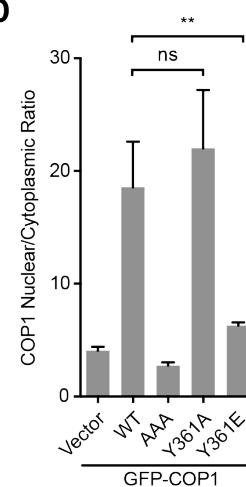
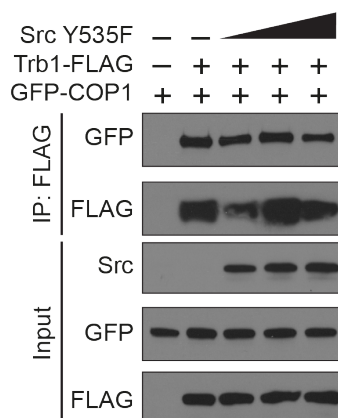
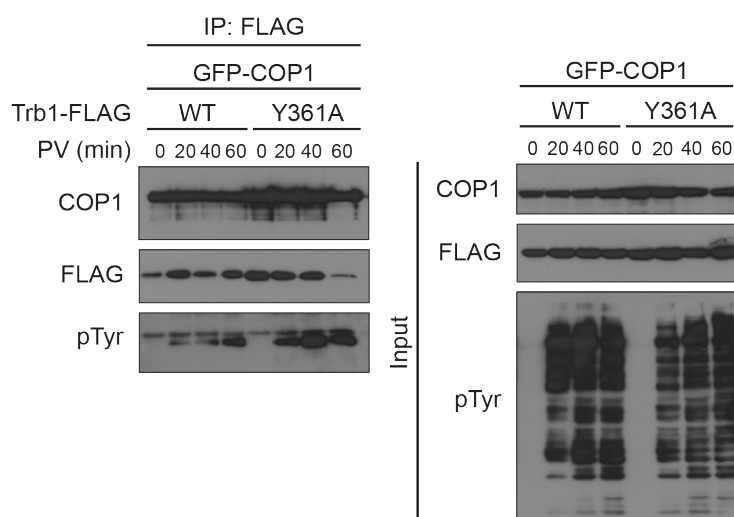


**Figure 14 | Cell cycle dependence of Trb1 and COP1 localization.**

Representative images of a COS7 cell coexpressing mCherry-Trb1 and GFP-COP1 at different timepoints after the cell begins undergoing mitosis.

**A**

	ETS1	273	SFNS	SLQR	VPSY	DSFDS	288
Trb1 homologs	<i>H. sapiens</i>	351	IGTSD	QI	VPEY	QEDSD	366
	<i>P. troglodytes</i>	351	IGTSD	QI	VPEY	QEDSD	366
	<i>M. musculus</i>	351	IGTSD	QI	VPEY	QEDSD	366
	<i>R. norvegicus</i>	351	VGTS	QI	VPEY	QDDND	366
	<i>F. catus</i>	351	IGTSD	QI	VPEY	QEDSD	366
	<i>B. taurus</i>	351	VGTS	QI	VPEY	QEDSD	366
	<i>G. gallus</i>	350	TGTSD	QI	VPEY	HGDND	365

**C****B****D****E****F**

**Figure 15 | A phosphomimetic mutation in the Trb1 C-terminal tail disrupts its interaction with COP1.**

- (A) Sequence alignment showing conservation of a Tyr residue following the COP1 binding motif in ETS1 and in homologs of Trb1. Residues in the sequences are colored to indicate residues conserved in the COP1-binding motif: Val-Pro dipeptide (red), acidic residues (blue), Tyr (magenta).
- (B) Coimmunoprecipitation of COP1 with the indicated Trb1-FLAG constructs in COS7 cells.
- (C) Representative images of COS7 cells expressing the indicated Trb1-FLAG constructs (red) and GFP-COP1 (red). Cells were stained with anti-FLAG and anti-mouse Alexa Fluor 568. Nuclei were counterstained with DAPI (blue). Scale bar, 10  $\mu$ m.
- (D) Quantification of the average ratio of nuclear/cytoplasmic fluorescence of GFP-COP1 in (C). Mean values  $\pm$  S.E.M. are shown for three independent experiments where 50 individual cells per experiment were analyzed. Significance relative to GFP-COP1 with empty vector was calculated using the Student t test (ns, not significant; \*\*p,  $p < 0.001$ ).
- (E) Coimmunoprecipitation of GFP-COP1 with Trb1-FLAG when coexpressed with empty vector or increasing amounts of constitutively active Src (Y535F) in COS7 cells.
- (F) Coimmunoprecipitation of GFP-COP1 with the indicated Trb1-FLAG constructs following treatment with 100  $\mu$ M sodium pervanadate for the indicated times in COS7 cells.

**A phosphomimetic mutation in the Trb1 C-terminal tail disrupts its interaction with COP1**

Phosphorylation of a tyrosine residue adjacent to the COP1-binding motif, described in some COP1 substrates, presents an opportunity for posttranslational control of binding to the WD40 domain of COP1. In ETS1, phosphorylation of a tyrosine residue neighboring the COP1-binding motif (Y283) disrupts its interaction with COP1<sup>38</sup>. The Trb1 C-terminal tail has a tyrosine residue (Y361) in an analogous position, and this residue is highly conserved in Trb1 across evolution (Figure 15A). When we mutated Y361 to glutamate to mimic the negative charge added by phosphorylation, Trb1 failed to pull down COP1 and could no longer promote COP1 nuclear localization as efficiently as Trb1 WT (Figure 15B-D). In contrast, Trb1 Y361A behaved similarly to Trb1 WT, underscoring the functional consequence of the negative charge introduced in this region by the Y361E mutation (Figure 15B-D). While Y283 in ETS1 is efficiently phosphorylated by Src family kinases<sup>38</sup>, co-expression of a constitutively active Src mutant in COS7 cells did not stimulate Trb1 Y361 phosphorylation and had no effect on the interaction between Trb1 and COP1

(Figure 15E). We were also unable to enrich for a Trb1 population phosphorylated on Y361 or disrupt the interaction between Trb1 and COP1 in the presence of sodium pervanadate, an irreversible tyrosine phosphatase inhibitor (Figure 15F). Although it remains unclear if Trb1 Y361 is phosphorylated, our results suggest that this posttranslational modification would be disruptive to interaction between Trb1 and COP1.

## DISCUSSION

Regulation of COP1 activity through nucleocytoplasmic shuttling was first characterized for *Arabidopsis* COP1. In plants, which do not have any Tribbles homologs, this process is controlled by light and involves several photoreceptors, including CRY1, phyA and phyB<sup>39</sup>. Like mammalian COP1, *Arabidopsis* COP1 has a cytoplasmic localization signal within its coiled coil domain that is necessary for its nuclear export and resembles the leucine-rich NESs recognized by CRM1<sup>40,41</sup>. The export of mammalian COP1 is primarily regulated by association with CRM1, as well as by 14-3-3 $\sigma$  under conditions of cell stress in response to DNA damage<sup>15,33,42</sup>. In plants, binding partners, such as SPA proteins and CSN1, that have been reported to modulate COP1 localization associate with the COP1 coiled coil domain<sup>43,44</sup>. In *Arabidopsis* COP1, control of COP1 subcellular localization seems to be exerted solely through coiled coil domain-mediated interactions, and the WD40 domain is not essential for light-regulated nucleocytoplasmic trafficking<sup>40,45</sup>. In stark contrast to *Arabidopsis* COP1, deletion of the WD40 domain prevents nuclear export of mammalian COP1, underscoring the importance of this domain for proper shuttling between the nucleus and cytoplasm<sup>15,16</sup>.

In this study, we elucidate the mechanism by which the WD40 domain controls nucleocytoplasmic shuttling of mammalian COP1. We show that the WD40 domain engages in an



intramolecular interaction that promotes nuclear export, and hence, its deletion results in nuclear enrichment of COP1. At this point, we can only speculate about the nature of the mechanism underlying this effect. Our data indicates that binding of the WD40 domain to the PSL, which is located adjacent to the C-terminus of the coiled coil domain, causes the NES to become accessible and disruption of that interaction causes the NES to become masked (Figure 9D). We speculate that the PSL/WD40 interaction regulates NES accessibility by modulating the conformation of the C-terminal region the coiled coil domain, which might be able to adopt different states due to a heptad break within the coiled coil domain. Currently, structural information for COP1 is limited to the WD40 domain and the coiled coil domain fragment presented here<sup>20</sup> (Figure 11D). Structural studies of the full-length coiled coil domain and, ideally, full-length COP1, are needed to reveal the conformational changes induced by the PSL/WD40 interaction and by binding of Trb1 to the WD40 domain, as well as how the accessibility of the COP1 NES is affected by these changes.

The implications of our data are that other proteins containing a COP1-binding motif should also control nuclear export of COP1. Indeed, Trb2 has been reported to increase COP1 nuclear localization through its C-terminal tail<sup>46</sup>. Trb3 and another Tribbles homolog STK40 (SgK495) also contain a COP1-binding motif in their C-terminal tails, and thus, have the potential to inhibit COP1 nuclear export. Several COP1 substrates, such as ETS1 and c-Jun, are also known to bind directly to COP1 through a consensus COP1-binding motif<sup>9,38</sup>. Their COP1-binding motifs bind to the COP1 WD40 domain with affinities that are higher than that of the COP1 PSL<sup>20</sup>. Thus, these substrates, which by and large, are localized to the nucleus, have the potential to compete with the PSL and thereby promote COP1 nuclear localization.

*Arabidopsis* COP1 binding partners like HY5 and UVR8, which bind to the WD40 domain via a COP1-binding motif similar to the one present in Tribbles, do not alter COP1 localization.

Instead, *Arabidopsis* COP1, which spontaneously localizes to nuclear puncta denoted as nuclear speckles, alters the localization of its substrates and recruits them to the speckles<sup>25,47</sup>. This speckle targeting has been speculated to regulate the function of *Arabidopsis* COP1 since loss of COP1 function correlates with loss of its localization to speckles<sup>48</sup>. We found that mammalian COP1 localizes to similar punctate nuclear structures, which are positive for a PML body marker, only when coexpressed with Trb1. Although it is not certain that the Trb1/COP1 nuclear puncta we observe represent the same compartment occupied by *Arabidopsis* COP1, these observations indicate that subnuclear localization might be important for regulating the function of Trb1 and COP1 in mammalian cells.

Like other pseudokinases, Tribbles have evolved to perform non-catalytic functions that often are unique, difficult to anticipate *a priori*, and challenging to understand mechanistically<sup>49-51</sup>. Sometimes, these functions are heavily influenced by adjacent domains, contributing to the challenges in characterizing the molecular mechanisms by which pseudokinases signal. We found that the pseudokinase Trb1 uses its C-terminal tail to control the nuclear export of COP1, in addition to its role as a scaffold that facilitates COP1 interaction with its substrates, which is primarily orchestrated by the pseudokinase domain<sup>7</sup>. It is unclear at present if the pseudokinase domain contributes to regulation of COP1 nuclear export. The crystal structure of the Trb1 pseudokinase domain and the C-terminal tail, however, offers a potential mechanism for this regulation. In the structure, the Trb1 C-terminal tail binds to a pocket formed by the  $\alpha$ C helix in the N-lobe of the pseudokinase domain in a manner reminiscent of binding of a conserved hydrophobic motif to the PIF pocket in AGC kinases<sup>31,52</sup>. Since the residues within the Trb1 C-terminal tail used to engage both the  $\alpha$ C pocket in the Trb1 pseudokinase domain and the COP1 WD40 domain partially overlap, these two interactions should be mutually exclusive. Thus,

binding of the C-terminal tail to the Trb1 pseudokinase domain could serve as an autoinhibitory mechanism restricting COP1 binding. Another regulatory step in COP1/Trb1 binding could involve phosphorylation. Our data provide evidence that phosphorylation of S310 in COP1 or Y361 in Trb1 has the potential to regulate binding of the C-terminal tail to COP1. Such post-translational modifications could potentially be cell cycle-dependent.

The differences in the nature of the nucleocytoplasmic shuttling mechanisms of COP1 in plants versus the one described here is remarkable given the high degree of structural similarity between plant and mammalian COP1. The net output of this regulation is modulation of the amount of COP1 in the nucleus, and hence the efficiency with which it can degrade transcription factors. This process is likely to be important in human leukemias where upregulation of Trb1 drives excessive COP1-dependent degradation of transcription factors and might be important to consider in efforts toward pharmacological targeting of this pseudokinase.

## **MATERIALS AND METHODS**

### **Plasmids, cell culture, and antibodies**

The human Trb1 coding sequence was synthesized by Genscript. Human cDNAs for COP1 and C/EBP $\alpha$  were purchased from Transomic (BC094728, BC160133). Constructs for each of these proteins were cloned into pcDNA3.1(+). 3xFLAG-CRM1 was a gift from Xin Wang (Addgene plasmid #17647). GFP-DAXX was a gift from Michael Rosen (UT Southwestern). Src Y535F was a gift from Kevan Shokat (UCSF). Mutations and deletions were introduced using Quikchange site-directed mutagenesis (Agilent). All constructs were verified by DNA sequencing. COS7 cells were maintained in DMEM supplemented with 10% fetal bovine serum, 100 U/mL penicillin, and 100  $\mu$ g/mL streptomycin. Transfections were carried out using Lipofectamine 3000 (Invitrogen).

The following primary antibodies were used: anti-FLAG (Sigma, F1804), anti-COP1 (Bethyl, A300-894A), anti-Trb1 (Abcam, ab137717), anti-GFP (Santa Cruz, sc-9996), anti-FLAG (Cell Signaling, 2368), anti-HA (Sigma, H9658), anti-HA (Santa Cruz, sc-7392), anti-C/EBP $\alpha$  (Cell Signaling, 2295), anti-nucleolin (Invitrogen, 39-6400), anti-SC-35 (Abcam, ab11826), anti-coilin (Abcam, ab11822), anti-Src (Cell Signaling, 2108), anti-p-Tyr-100 (Cell Signaling, 9411). For western blotting and immunoprecipitation, the following secondary antibodies were used: anti-mouse-HRP (GE Healthcare, NA931), anti-rabbit-HRP (Cell Signaling, 7074), anti-mouse IgG Veriblot (Abcam, ab131368), Veriblot for IP secondary (ab131366). GFP-tagged constructs were immunoprecipitated using GFP-trap beads (Chromotek). For immunofluorescence, anti-mouse Alexa Fluor 568 and anti-rabbit Alexa Fluor 680 secondary antibodies (Molecular Probes) were used.

### **Immunofluorescence**

COS7 cells were seeded onto glass coverslips in 6-well plates at  $9 \times 10^4$  cells/well and transfected with the indicated constructs. Approximately 24 hours post-transfection, cells were fixed in 3.7% formaldehyde, permeabilized in 0.1% Triton X-100, and blocked with 1% BSA. Cells were then incubated with the indicated primary antibodies for 1 hour at 37°C, washed with PBS, and incubated with the indicated secondary antibodies for 1 hour at 37°C. Nuclei were visualized using DAPI where indicated. Coverslips were mounted onto glass slides using ProLong Anti-Fade mounting medium (Thermo). Coverslips were imaged using a Nikon spinning disk confocal microscope.

To calculate nuclear/cytoplasmic ratios of COP1 fluorescence, confocal images were analyzed using FIJI (ImageJ). Binary image masks were created of DAPI-positive staining to define nuclear regions of interest (ROI) for analysis. This was done by applying a Gaussian Blur filter (2x2 pixel radius) to reduce noise followed by automatic thresholding using the Otsu algorithm to convert the image into a binary mask that included all fluorescence above background. This mask was then used to calculate the average fluorescence intensity for COP1 in the nucleus of each cell. The average fluorescence intensity of COP1 was then measured in a cytoplasmic ROI of equal size to the corresponding nuclear ROI for each cell. The average nuclear fluorescence intensity was then divided by the average cytoplasmic fluorescence intensity to determine the ratio of nuclear to cytoplasmic COP1 fluorescence in each cell. Data presented are the means  $\pm$  S.E.M. determined from at least three independent experiments. In each experiment, 50 cells per sample were randomly selected for analysis. Student t-tests were used to compare samples. Statistical analyses were performed using Graphpad Prism 7 (Graphpad).

### **Immunoprecipitation and western blotting**

COS7 cells were seeded onto 60 mm dishes at  $3.5 \times 10^5$  cells/dish and transfected with the indicated constructs. Approximately 24 hours post-transfection, cells were lysed in IP lysis buffer (50 mM Tris pH 7.5, 150 mM NaCl, 1% NP-40, 1 mM EDTA, 1 mM NaF, 1 mM  $\text{Na}_3\text{VO}_4$ ) supplemented with Roche complete mini EDTA-free protease inhibitor cocktail. The lysates were centrifuged for 10 min at 15000 rpm. The supernatants were then incubated with the indicated primary antibodies and Protein A sepharose beads (Invitrogen) or with GFP-trap beads (Chromotek) overnight rotating at 4°C. Beads were washed 3 times with wash buffer (50 mM Tris pH 7.5, 150 mM NaCl, 1 mM EDTA, 1 mM NaF, 1 mM  $\text{Na}_3\text{VO}_4$ ) supplemented with protease inhibitors.

Proteins were eluted using SDS-PAGE loading buffer, detected using standard western blotting protocols with the indicated antibodies, and visualized using enhanced chemiluminescence (ECL) reagent (GE Healthcare, Amersham). To reduce detection of IgG bands, Veriblot secondary antibodies (Abcam) were used to detect immunoprecipitated proteins. Where indicated, sodium pervanadate was prepared just prior to use by mixing equal volumes of 0.1 M H<sub>2</sub>O<sub>2</sub> and 0.1 M Na<sub>3</sub>VO<sub>4</sub>.

### **Protein purification**

His-tagged COP1 WD40 domain (residues 376-731) was expressed in Sf9 cells using the Bac-to-Bac expression system (Invitrogen) and purified with Talon beads (Clontech) followed by anion exchange chromatography on a Mono Q column (GE Healthcare). Purified proteins were then buffer exchanged into storage buffer (20 mM Tris pH 8.0, 250 mM NaCl, 5% glycerol, 2 mM TCEP), flash frozen, and stored at -80°C.

### **Fluorescence polarization**

Fluorescence polarization assays were performed using purified COP1 WD40 domain in FP assay buffer (20 mM Hepes pH 7.5, 150 mM NaCl, 2 mM TCEP, 0.1% Triton X-100). FITC-labeled and unlabeled peptides were synthesized by Elim Bio and purified to >90% purity, as assessed by HPLC. 25 nM FITC-Trb1 tail (residues 338-366) was pre-incubated with 1 μM COP1 WD40 domain before addition of indicated concentrations of the unlabeled COP1 PSL peptide (residues 302-320) or unlabeled Trb1 tail peptide. Experiments were performed in duplicate in 20 μL well volumes in black 384-well plates (Corning) on an Analyst AD plate reader (Molecular Devices) with excitation and emission wavelengths of 485 nm and 530 nm, respectively.

**Table 2. Peptides for fluorescence polarization competition assay.**

Peptide	Sequence
FITC-Trb1 tail	FITC-DSEIGTSDQIVPEYQEDSD
Unlabeled Trb1 tail	DSEIGTSDQIVPEYQEDSD
Unlabeled COP1 PSL	LYSPVSEDSTVPQFEAPSP
Unlabeled COP1 PSL 4A	LYSPVSAASTAAQFEAPSP

### **Phylogenetic Analysis**

Sequences of COP1 homologs were collected from the Uniprot and NCBI databases. These sequences were aligned using MUSCLE 3.8<sup>53</sup>, and this alignment was used to generate a phylogenetic tree using the phylogeny software PhyML 3.0, which built the tree based on the maximum likelihood principle<sup>54</sup>. The tree was visualized using Dendroscope 3<sup>55</sup>.

### **Crystallization and structure determination of COP1 CC $\Delta$ 30**

A peptide corresponding to residues 233-268 of COP1 was synthesized through solid phase peptide synthesis (Bobo Dang, DeGrado Lab, UCSF). The lyophilized peptide was solubilized in 20 mM Tris pH 9.0. Crystals were obtained by sitting drop vapor diffusion at room temperature in drops consisting of 0.5  $\mu$ L peptide (5 mg/mL) and 0.5  $\mu$ L mother liquor (0.1 M sodium cacodylate pH 7.0, 27% isopropanol, and 0.2 M sodium citrate). Diffraction data were collected at beamline 8.3.1 at the Advanced Light Source at Lawrence Berkeley National Laboratory. Data were processed using XDS<sup>56</sup>. The structure was solved by molecular replacement using AMPLE<sup>57</sup> to identify a

polyalanine helix as a search model. Coot was used for graphical modeling following iterative rounds of refinement using Refmac5, PHENIX, and translation-liberation-screw (TLS) refinement to improve model quality<sup>58-61</sup>. Data collection and refinement statistics are presented in Table 1. The structure has two molecules in the asymmetric unit that are related by translational non-crystallographic symmetry. This resulted in higher than expected values of R and R<sub>free</sub> due to the systematic strengthening and weakening of reflections, which results in a bimodal intensity distribution (Table 1).

### **Live cell imaging**

COS7 cells were transfected in suspension with mCherry-Trb1 and GFP-COP1 before being seeded into a Lab-tek chambered coverglass at 8000 cells/well. After 24 hours, the cells were washed with PBS, and the media on the cells was replaced with FluoroBrite DMEM (Thermo) supplemented with 10% FBS, 100 U/mL penicillin, 100 µg/mL streptomycin, and 2 mM L-glutamine. The cells were then imaged on a Nikon epifluorescence widefield microscope with images acquired at various regions of interest every five minutes for 24 hours. The cells were maintained at 37°C with 5% CO<sub>2</sub> throughout imaging.

### **ACKNOWLEDGEMENTS**

We thank Nathan Schmidt and Bill DeGrado for their insights on coiled coils, Bobo Dang for synthesizing the COP1 CC Δ30 peptide, Kelvin Cho for his work on the live cell imaging experiments and initial characterization of Trb1 phosphomimetic mutations, DeLaine Larsen and Kari Herrington for their assistance with the microscopes, Terri Lee and Dyche Mullins for providing subnuclear markers, and the staff at ALS beamline 8.3.1 for their assistance with x-ray



diffraction experiments. We also thank all members of the Jura Lab for helpful discussions, especially Lijun Liu for his assistance in data collection and solving the COP1 CC  $\Delta$ 30 structure.

## REFERENCES

1. Migliorini, D. *et al.* Cop1 constitutively regulates c-Jun protein stability and functions as a tumor suppressor in mice. *J. Clin. Invest.* **121**, 1329–1343 (2011).
2. Dornan, D. *et al.* ATM engages autodegradation of the E3 ubiquitin ligase COP1 after DNA damage. *Science* **313**, 1122–1126 (2006).
3. Dornan, D. *et al.* COP1, the negative regulator of p53, is overexpressed in breast and ovarian adenocarcinomas. *Cancer Research* **64**, 7226–7230 (2004).
4. Lee, Y.-H. *et al.* Definition of ubiquitination modulator COP1 as a novel therapeutic target in human hepatocellular carcinoma. *Cancer Research* **70**, 8264–8269 (2010).
5. Su, C.-H. *et al.* 14-3-3sigma exerts tumor-suppressor activity mediated by regulation of COP1 stability. *Cancer Research* **71**, 884–894 (2011).
6. Vitari, A. C. *et al.* COP1 is a tumour suppressor that causes degradation of ETS transcription factors. *Nature* **474**, 403–406 (2011).
7. Keeshan, K. *et al.* Transformation by Tribbles homolog 2 (Trib2) requires both the Trib2 kinase domain and COP1 binding. *Blood* **116**, 4948–4957 (2010).
8. Dornan, D. *et al.* The ubiquitin ligase COP1 is a critical negative regulator of p53. *Nature* **429**, 86–92 (2004).
9. Wertz, I. E. *et al.* Human De-etiolated-1 regulates c-Jun by assembling a CUL4A ubiquitin ligase. *Science* **303**, 1371–1374 (2004).

10. Deng, X. W., Caspar, T. & Quail, P. H. cop1: a regulatory locus involved in light-controlled development and gene expression in Arabidopsis. *Genes & Development* **5**, 1172–1182 (1991).
11. Ma, L. *et al.* Genomic evidence for COP1 as a repressor of light-regulated gene expression and development in Arabidopsis. *Plant Cell* **14**, 2383–2398 (2002).
12. Lau, O. S. & Deng, X. W. The photomorphogenic repressors COP1 and DET1: 20 years later. *Trends Plant Sci.* **17**, 584–593 (2012).
13. Arnim, Von, A. G. & Deng, X. W. Light inactivation of Arabidopsis photomorphogenic repressor COP1 involves a cell-specific regulation of its nucleocytoplasmic partitioning. *Cell* **79**, 1035–1045 (1994).
14. Pacín, M., Legris, M. & Casal, J. J. Rapid decline in nuclear constitutive photomorphogenesis1 abundance anticipates the stabilization of its target elongated hypocotyl5 in the light. *Plant Physiol.* **164**, 1134–1138 (2014).
15. Yi, C., Wang, H., Wei, N. & Deng, X. W. An initial biochemical and cell biological characterization of the mammalian homologue of a central plant developmental switch, COP1. *BMC Cell Biol.* **3**, 30 (2002).
16. Bianchi, E. *et al.* Characterization of human constitutive photomorphogenesis protein 1, a RING finger ubiquitin ligase that interacts with Jun transcription factors and modulates their transcriptional activity. *J. Biol. Chem.* **278**, 19682–19690 (2003).
17. Dedhia, P. H. *et al.* Differential ability of Tribbles family members to promote degradation of C/EBPalpha and induce acute myelogenous leukemia. *Blood* **116**, 1321–1328 (2010).

18. Yoshida, A., Kato, J.-Y., Nakamae, I. & Yoneda-Kato, N. COP1 targets C/EBP $\alpha$  for degradation and induces acute myeloid leukemia via Trib1. *Blood* **122**, 1750–1760 (2013).
19. Satoh, T. *et al.* Critical role of Trib1 in differentiation of tissue-resident M2-like macrophages. *Nature* **495**, 524–528 (2013).
20. Uljon, S. *et al.* Structural Basis for Substrate Selectivity of the E3 Ligase COP1. *Structure* **24**, 687–696 (2016).
21. Holm, M., Hardtke, C. S., Gaudet, R. & Deng, X. W. Identification of a structural motif that confers specific interaction with the WD40 repeat domain of Arabidopsis COP1. *EMBO J.* **20**, 118–127 (2001).
22. Qi, L. *et al.* TRB3 links the E3 ubiquitin ligase COP1 to lipid metabolism. *Science* **312**, 1763–1766 (2006).
23. Kiss-Toth, E. *et al.* Functional mapping and identification of novel regulators for the Toll/Interleukin-1 signalling network by transcription expression cloning. *Cellular Signalling* **18**, 202–214 (2006).
24. Soubeyrand, S., Martinuk, A., Lau, P. & McPherson, R. TRIB1 Is Regulated Post-Transcriptionally by Proteasomal and Non-Proteasomal Pathways. *PLoS ONE* **11**, e0152346 (2016).
25. Ang, L. H. *et al.* Molecular interaction between COP1 and HY5 defines a regulatory switch for light control of Arabidopsis development. *Molecular Cell* **1**, 213–222 (1998).
26. Wang, H., Ma, L. G., Li, J. M., Zhao, H. Y. & Deng, X. W. Direct interaction of Arabidopsis cryptochromes with COP1 in light control development. *Science* **294**, 154–158 (2001).

27. Seo, H. S. *et al.* LAF1 ubiquitination by COP1 controls photomorphogenesis and is stimulated by SPA1. *Nature* **423**, 995–999 (2003).
28. Keeshan, K. *et al.* Tribbles homolog 2 inactivates C/EBP $\alpha$  and causes acute myelogenous leukemia. *Cancer Cell* **10**, 401–411 (2006).
29. Das, R., Sebo, Z., Pence, L. & Dobens, L. L. Drosophila Tribbles Antagonizes Insulin Signaling-Mediated Growth and Metabolism via Interactions with Akt Kinase. *PLoS ONE* **9**, e109530 (2014).
30. Masoner, V. *et al.* The kinase domain of Drosophila Tribbles is required for turnover of fly C/EBP during cell migration. *Developmental Biology* **375**, 33–44 (2013).
31. Murphy, J. M. *et al.* Molecular Mechanism of CCAAT-Enhancer Binding Protein Recruitment by the TRIB1 Pseudokinase. *Structure* **23**, 2111–2121 (2015).
32. Baker, N. A., Sept, D., Joseph, S., Holst, M. J. & McCammon, J. A. Electrostatics of nanosystems: application to microtubules and the ribosome. *Proceedings of the National Academy of Sciences* **98**, 10037–10041 (2001).
33. Kirli, K. *et al.* A deep proteomics perspective on CRM1-mediated nuclear export and nucleocytoplasmic partitioning. *eLife* **4**, 1195 (2015).
34. Stommel, J. M. *et al.* A leucine-rich nuclear export signal in the p53 tetramerization domain: regulation of subcellular localization and p53 activity by NES masking. *EMBO J.* **18**, 1660–1672 (1999).
35. Okamura, H. *et al.* Concerted dephosphorylation of the transcription factor NFAT1 induces a conformational switch that regulates transcriptional activity. *Molecular Cell* **6**, 539–550 (2000).

36. Eyers, P. A., Keeshan, K. & Kannan, N. Tribbles in the 21st Century: The Evolving Roles of Tribbles Pseudokinases in Biology and Disease. *Trends in Cell Biology* (2016). doi:10.1016/j.tcb.2016.11.002
37. Brown, J. H., Cohen, C. & Parry, D. A. Heptad breaks in alpha-helical coiled coils: stutters and stammers. *Proteins* **26**, 134–145 (1996).
38. Lu, G. *et al.* Phosphorylation of ETS1 by Src Family Kinases Prevents Its Recognition by the COP1 Tumor Suppressor. *Cancer Cell* **26**, 222–234 (2014).
39. Osterlund, M. T. & Deng, X. W. Multiple photoreceptors mediate the light-induced reduction of GUS-COP1 from Arabidopsis hypocotyl nuclei. *Plant J.* **16**, 201–208 (1998).
40. Stacey, M. G., Hicks, S. N. & Arnim, Von, A. G. Discrete domains mediate the light-responsive nuclear and cytoplasmic localization of Arabidopsis COP1. *Plant Cell* **11**, 349–364 (1999).
41. Subramanian, C. *et al.* The Arabidopsis repressor of light signaling, COP1, is regulated by nuclear exclusion: mutational analysis by bioluminescence resonance energy transfer. *Proceedings of the National Academy of Sciences* **101**, 6798–6802 (2004).
42. Su, C.-H. *et al.* Nuclear export regulation of COP1 by 14-3-3 $\sigma$  in response to DNA damage. *Mol. Cancer* **9**, 243 (2010).
43. Wang, X. *et al.* Regulation of COP1 nuclear localization by the COP9 signalosome via direct interaction with CSN1. *Plant J.* **58**, 655–667 (2009).
44. Balcerowicz, M., Kerner, K., Schenkel, C. & Hoecker, U. SPA Proteins Affect the Subcellular Localization of COP1 in the COP1/SPA Ubiquitin Ligase Complex during Photomorphogenesis. *Plant Physiol.* **174**, 1314–1321 (2017).

45. Torii, K. U., McNellis, T. W. & Deng, X. W. Functional dissection of Arabidopsis COP1 reveals specific roles of its three structural modules in light control of seedling development. *EMBO J.* **17**, 5577–5587 (1998).
46. Xu, S. *et al.* TRIB2 inhibits Wnt/ $\beta$ -Catenin/TCF4 signaling through its associated ubiquitin E3 ligases,  $\beta$ -TrCP, COP1 and Smurf1, in liver cancer cells. *FEBS Letters* **588**, 4334–4341 (2014).
47. Favory, J.-J. *et al.* Interaction of COP1 and UVR8 regulates UV-B-induced photomorphogenesis and stress acclimation in Arabidopsis. *EMBO J.* **28**, 591–601 (2009).
48. Stacey, M. G. & Arnim, Von, A. G. A novel motif mediates the targeting of the Arabidopsis COP1 protein to subnuclear foci. *J. Biol. Chem.* **274**, 27231–27236 (1999).
49. Kung, J. E. & Jura, N. Structural Basis for the Non-catalytic Functions of Protein Kinases. *Structure* **24**, 7–24 (2016).
50. Jacobsen, A. V. & Murphy, J. M. The secret life of kinases: insights into non-catalytic signalling functions from pseudokinases. *Biochem. Soc. Trans.* **45**, 665–681 (2017).
51. Reiterer, V., Eysers, P. A. & Farhan, H. Day of the dead: pseudokinases and pseudophosphatases in physiology and disease. *Trends in Cell Biology* **24**, 489–505 (2014).
52. Pearce, L. R., Komander, D. & Alessi, D. R. The nuts and bolts of AGC protein kinases. *Nat Rev Mol Cell Biol* **11**, 9–22 (2010).
53. Edgar, R. C. MUSCLE: multiple sequence alignment with high accuracy and high throughput. *Nucleic Acids Research* **32**, 1792–1797 (2004).
54. Guindon, S. *et al.* New algorithms and methods to estimate maximum-likelihood phylogenies: assessing the performance of PhyML 3.0. *Syst. Biol.* **59**, 307–321 (2010).

55. Huson, D. H. & Scornavacca, C. Dendroscope 3: an interactive tool for rooted phylogenetic trees and networks. *Syst. Biol.* **61**, 1061–1067 (2012).
56. Kabsch, W. IUCr. XDS. *Acta Crystallogr Sect D Biol Crystallogr* **66**, 125–132 (2010).
57. Thomas, J. M. H. *et al.* Routine phasing of coiled-coil protein crystal structures with AMPLE. *IUCrJ* **2**, 198–206 (2015).
58. Emsley, P. & Cowtan, K. Coot: model-building tools for molecular graphics. *Acta Crystallogr Sect D Biol Crystallogr* **60**, 2126–2132 (2004).
59. Vagin, A. A. *et al.* REFMAC5 dictionary: organization of prior chemical knowledge and guidelines for its use. *Acta Crystallogr Sect D Biol Crystallogr* **60**, 2184–2195 (2004).
60. Adams, P. D. *et al.* PHENIX: a comprehensive Python-based system for macromolecular structure solution. *Acta Crystallogr Sect D Biol Crystallogr* **66**, 213–221 (2010).
61. Painter, J. & Merritt, E. A. Optimal description of a protein structure in terms of multiple groups undergoing TLS motion. *Acta Crystallogr Sect D Biol Crystallogr* **62**, 439–450 (2006).

### **Chapter 3: Biophysical and structural characterization of Trb1**



## INTRODUCTION

Though Tribbles pseudokinases are thought to be catalytically inactive, their pseudokinase domains are essential for several of their functions, including promoting ubiquitination of C/EBP transcription factors, regulation of Akt activation, and modulation of MAPK signaling<sup>1-5</sup>. This is underscored by the fact that mutations of conserved residues in their pseudokinase domains have been reported to perturb Tribbles function. When the conserved aspartate in the HRD motif of the putative active site is mutated to asparagine, *Drosophila* Tribbles can no longer interact with the C/EBP homolog Slbo or facilitate Slbo degradation<sup>4</sup>. The same mutation also prevents *Drosophila* Tribbles from interacting with and inhibiting Akt<sup>2</sup>. Mutating other conserved residues in the catalytic loop near the HRD motif also reduces degradation of C/EBP $\alpha$  by murine Trb2<sup>1</sup>. Additionally, a gain-of-function mutation at a conserved arginine residue (R107L) in the pseudokinase domain of Trb1 was identified in a case of acute megakaryocytic leukemia. This mutation occurs in N-lobe of Trb1 at a site distant (~15 Å) from the putative active site and was found to cause enhanced depletion of C/EBP $\alpha$ <sup>6</sup>. Mutation of the same residue in Trb3 (Q84R) is associated with insulin resistance and enhances the ability of Trb3 to inhibit Akt signaling<sup>7</sup>.

Understanding the mechanisms underlying the effects of these pseudokinase domain mutations would provide valuable insight into the molecular basis of Tribbles function. In canonical active kinases, mutations in the active site would likely interfere with catalytic activity, but it is unclear how these mutations would disrupt the function of a pseudokinase like Tribbles. The effects of these mutations could be explained by changes in Tribbles' affinity for their binding partners or in their conformational state. Additionally, *Drosophila* Tribbles was recently shown to self-associate in a yeast two-hybrid assay, and mutation of the HRD aspartate to asparagine disrupted that interaction<sup>4</sup>. Although the role of oligomerization in Tribbles function is currently

unknown, oligomerization is critical for the function of numerous kinases and pseudokinases<sup>8</sup>, and this result suggests that oligomerization might be essential for Tribbles' role as a scaffold. Furthermore, the functions of several pseudokinases, including HER3, STRAD $\alpha$ , and JAK2, are influenced by occupancy of their nucleotide-binding pockets<sup>9-11</sup>. A recent report demonstrates that the same might be true for Trb2<sup>12</sup>. Thus, in my research, in order to gain insight into the molecular mechanisms of Tribbles function, I sought to investigate the structure and function of the pseudokinase domain of Trb1.

## RESULTS

### Optimization of Trb1 purification and crystallization

Full-length Trb1 (Trb1 FL) and the Trb1 pseudokinase domain (Trb1 KD) were recombinantly expressed and purified from *E. coli*. We screened a variety of buffers, salts, and other additives using a thermal shift assay to identify buffer conditions that increased the thermostability of Trb1. We found that Trb1 was most stable under basic conditions (pH > 8.5)

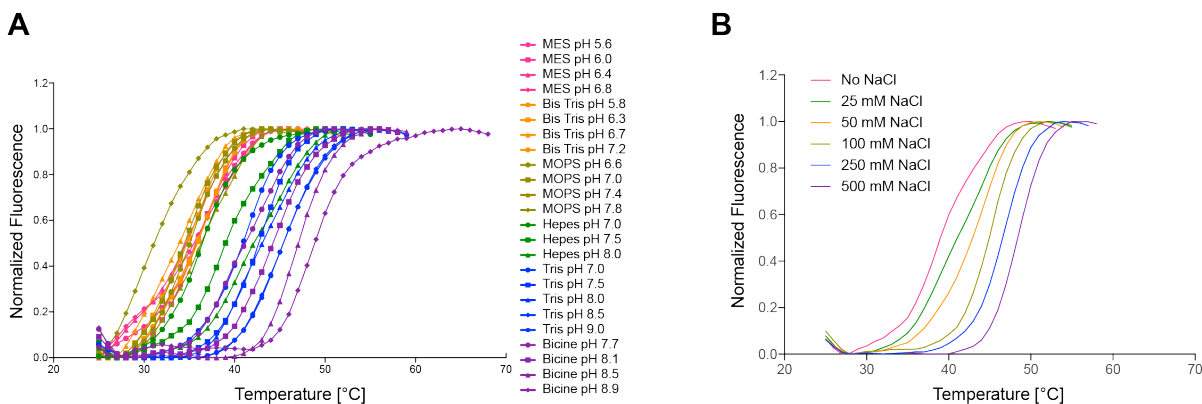


**Figure 1 | Trb1 buffer optimization.**

Thermal shift assay for full-length Trb1 diluted into (A) different buffers and pHs and (B) buffers containing varying amounts of NaCl.

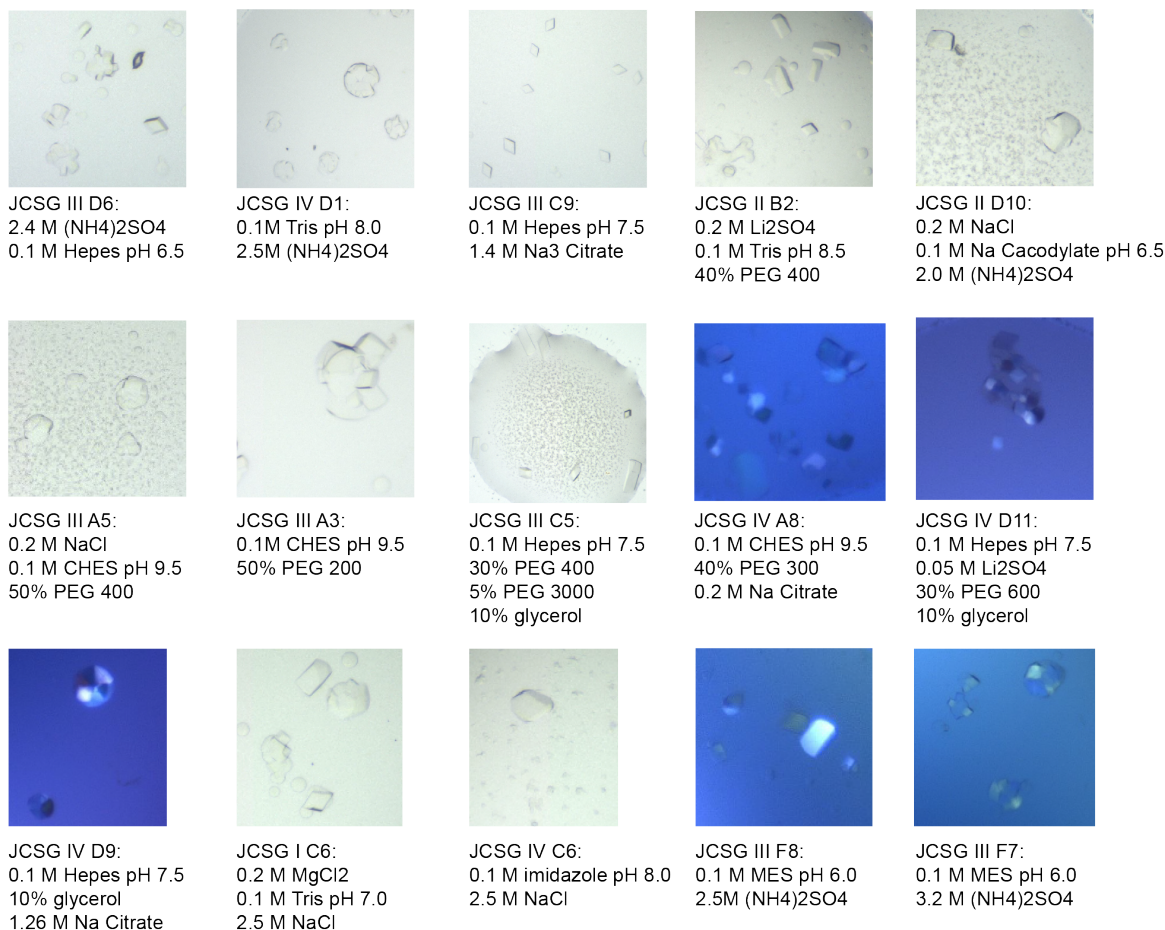


**Figure 2 | Trb1 KD crystals and crystallization conditions.**

Images showing examples of crystals of the Trb1 pseudokinase domain (Trb1 KD) and the corresponding crystallization conditions.

and with high salt concentrations (500 mM NaCl) (Figure 1). We were able to crystallize Trb1 KD in a variety of conditions in commercial 96 well screens (Figure 2). The crystals were confirmed using UV imaging to be protein crystals, and several crystals were selected to attempt structure determination. However, no crystals diffracted to a resolution high enough to solve the structure. The highest resolution that was achieved was approximately 5 Å for crystals grown in 0.1 M Hepes pH 7.5 and 1.4 M sodium citrate with the protein at a concentration of 5.5 mg/mL at room temperature. Unfortunately, though the crystals could be reproduced in commercial 96 well

screens, we were unable to reproduce these crystals in custom screens in 96 well or 24 well plates and, thus, were unable to optimize the crystallization conditions.

### Characterization of Trb1 kinase activity and nucleotide binding

To determine whether Trb1 is catalytically active, the autophosphorylation activity of Trb1 FL or Trb1 KD was measured using a continuous coupled kinase assay in which conversion of ATP to ADP is linked to NADH oxidation. Autophosphorylation was measured since many kinases are known to autophosphorylate, and because there are no known substrates of Tribbles-mediated phosphorylation. The purified kinase domain of the Ser/Thr kinase BMPR2 (BMPR2 KD) was used as a positive control since BMPR2 is known to autophosphorylate. Even at the highest protein concentrations used in the assay, no autophosphorylation could be detected for either Trb1 FL or Trb1 KD (Figure 3).

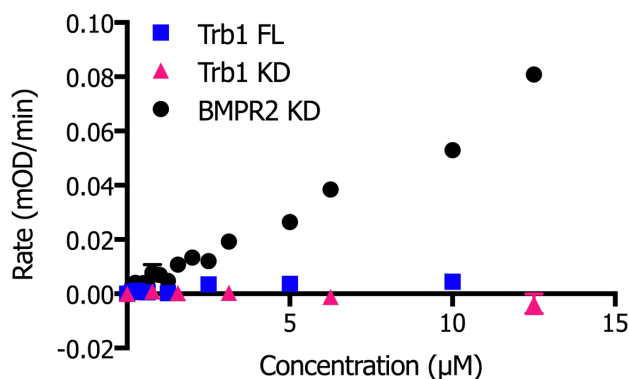


**Figure 3 | Trb1 does not autophosphorylate.**

In vitro enzyme-coupled kinase assay measuring kinase activity of full-length Trb1 (Trb1 FL), the Trb1 pseudokinase domain (Trb1 KD), and BMPR2 kinase domain (BMPR2 KD).

Although Trb1 did not autophosphorylate under these experimental conditions, it is possible that the catalytic activity of Trb1 only manifests itself in the presence of specific substrates or binding partners. However, if Trb1 does in fact possess catalytic activity, it would need to be able to bind ATP. Recent studies demonstrated that Trb2 is capable of binding to ATP and catalyzing phosphorylation only in the presence of EDTA and that the Trb2 pseudokinase domain can bind to known inhibitors of EGFR and HER2<sup>12,13</sup>. Additionally, several kinases have been shown to be allosterically regulated by binding of small molecules in their ATP-binding pocket<sup>14</sup>. Therefore, even if Trb1 is catalytically inactive, ATP-binding could allosterically regulate the

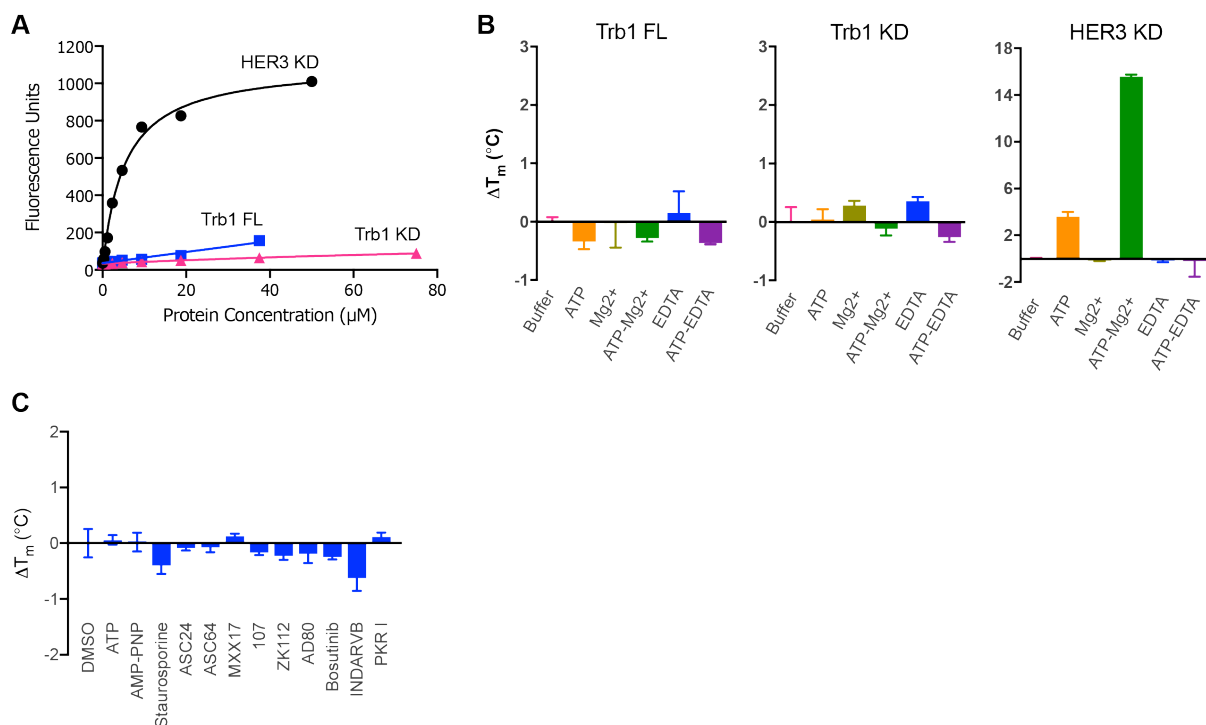


**Figure 4 | Trb1 does not bind to ATP or ATP-competitive small molecules. (A)** Mant-ATP binding assay showing that, unlike the HER3 pseudokinase domain, full-length Trb1 (Trb1 FL) and the Trb1 pseudokinase domain (Trb1 KD) fail to bind mant-ATP. **(B)** Thermal shift assays showing that the melting temperatures of Trb1 FL and Trb1 KD are unaffected by Mg<sup>2+</sup>, ATP, or EDTA, whereas HER3 KD thermostability increases in the presence of ATP and Mg<sup>2+</sup>-ATP. **(C)** Thermal shift assay showing that an array of known ATP-competitive small molecule kinase inhibitors failed to shift the melting temperature of Trb1 KD.

scaffolding functions of Trb1. To resolve whether or not Trb1 can bind ATP, recombinant Trb1 FL and Trb1 KD were incubated with  $Mg^{2+}$  and (2'-(3')-*O*-(*N*-methylantraniloyl)-ATP (mant-ATP), a fluorescent ATP analog, whose fluorescence increases upon binding to a protein. The pseudokinase HER3 was used as a positive control since HER3 is known to bind ATP<sup>15</sup>. While HER3 bound mant-ATP with a  $K_d$  of  $\sim 5 \mu M$ , no appreciable binding of mant-ATP could be detected for Trb1 FL or Trb1 KD even at very high protein concentrations (Figure 4A).

As an orthogonal method, the ability of Trb1 FL and Trb1 KD to bind ATP was also tested through a thermal shift assay in which ligand binding would be expected to increase the melting temperature of Trb1. Consistent with the mant-ATP binding assay, neither Trb1 FL or Trb1 KD exhibited a significant increase in melting temperature upon addition of  $Mg^{2+}$  and/or ATP, whereas the melting temperature of HER3 increased markedly in the presence of ATP and  $Mg^{2+}$  (Figure 4B). Unlike Trb2, addition of EDTA also had no effect on the ability of Trb1 to bind ATP. To examine whether the Trb1 nucleotide-binding pocket could accommodate other ligands, we also tested several promiscuous ATP-competitive small molecule kinase inhibitors for their ability to bind to Trb1 KD through thermal shift assays. However, none of these compounds had a significant effect on the thermostability of Trb1 KD with or without divalent cations present (Figure 4C). Collectively, these results demonstrate that Trb1 is indeed catalytically inactive and indicate that its putative nucleotide-binding pocket is inaccessible to typical ATP-competitive small molecule kinase inhibitors.

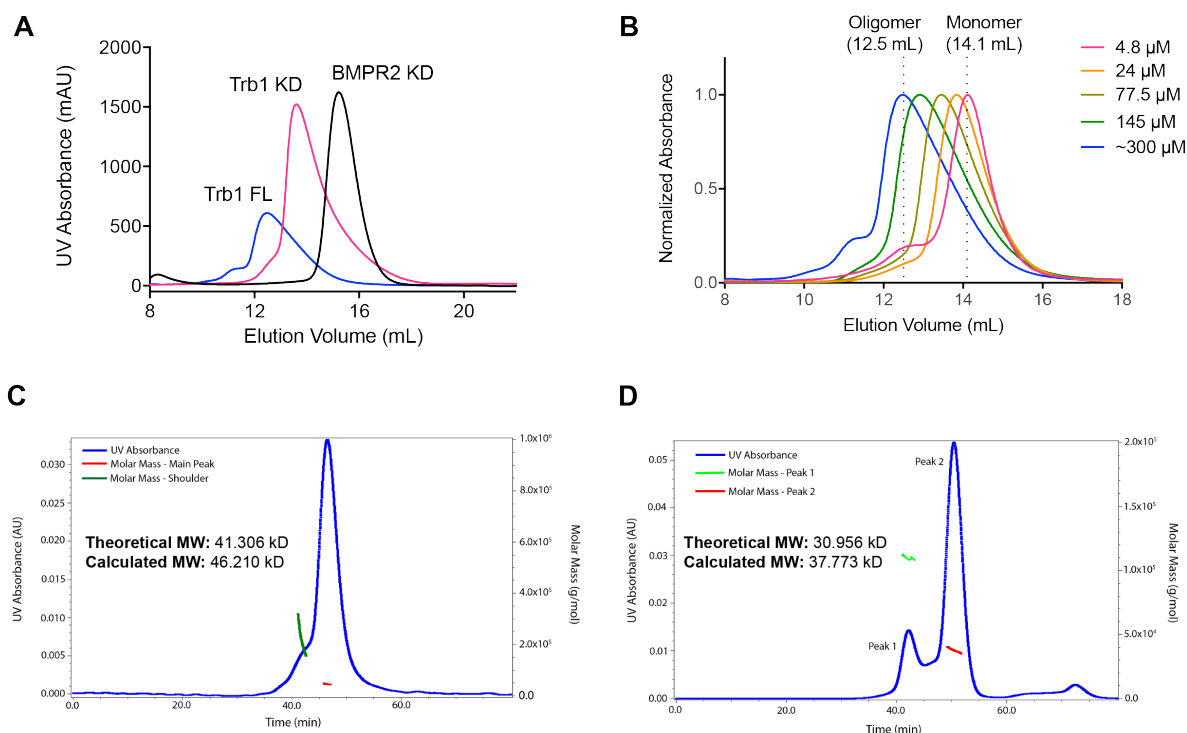


**Figure 5 | Analysis of Trb1 oligomerization.**

- (A) Size exclusion profiles of full-length Trb1 (Trb1 FL), the Trb1 pseudokinase domain (Trb1 KD), and the BMPR2 kinase domain (BMPR2 KD).
- (B) Size exclusion profiles of Trb1 FL at indicated concentrations.
- (C) & (D) SEC-MALS analysis of Trb1 FL and Trb1 KD with their theoretical molecular weight and that calculated based on light scattering.

### Trb1 forms oligomers in solution

While purifying Trb1, we found that both Trb1 FL and Trb1 KD eluted much earlier during size exclusion column chromatography than would be expected for their respective molecular weights if they were behaving as monomers (Figure 5A). In both cases, this phenomenon did not appear to be the result of aggregation, as both constructs eluted after the void volume. This indicates that Trb1 readily forms oligomers in solution, and that the N- and C-terminal domains are not required for oligomerization. Multi-angle light scattering showed that when only 100  $\mu$ g of Trb1 FL or Trb1 KD were loaded onto the size exclusion column, both were monomeric (Figure 5C and D). To examine the concentration dependence of Trb1 oligomerization, several different

amounts of Trb1 FL were analyzed using size exclusion chromatography. As the amount of Trb1 FL decreased, the protein eluted later from the column, indicating that the proportion of monomeric Trb1 FL increases at lower concentrations (Figure 5B). If the Trb1 oligomer were stable, one would expect to see two peaks at intermediate protein concentrations, corresponding to the oligomeric and monomeric Trb1. Instead, Trb1 elutes as a single peak with a large shoulder whose center shifts in response to protein concentration. This indicates that Trb1 likely has a low affinity for itself under the conditions tested and that the Trb1 oligomer dissociates rapidly. The role of this oligomer in Tribbles function is currently unknown. However, oligomerization is important for the function of many kinases<sup>8</sup>, and oligomerization might be important for interaction with COP1 and C/EBP $\alpha$ , which are both known to form dimers.

Interestingly, the *Drosophila* homolog of Tribbles was recently reported to interact with itself in a yeast two-hybrid assay where Tribbles was placed in both the bait and the prey vectors. This interaction could be disrupted by mutating the conserved aspartate in the HRD motif of the pseudokinase domain to asparagine<sup>4</sup>. When I introduced this same mutation (D205N) into Trb1 FL, I found that the Trb1 FL D205N mutant eluted significantly later than the wild type protein during size exclusion chromatography even when the same amount of each protein was loaded onto the column (Figure 6A). In agreement with what was observed for *Drosophila* Tribbles, this mutation impairs ability of Trb1 to oligomerize. This mutation does not, however, completely eliminate oligomerization, as the D205N mutant still elutes earlier than would be expected for monomeric Trb1. The same mutation was also shown to interfere with the interaction of Tribbles with Akt and Tribbles-mediated degradation of the C/EBP homolog Slbo, as well as Tribbles' interaction with Slbo<sup>2,4</sup>. This suggests that oligomerization plays an important role in Tribbles



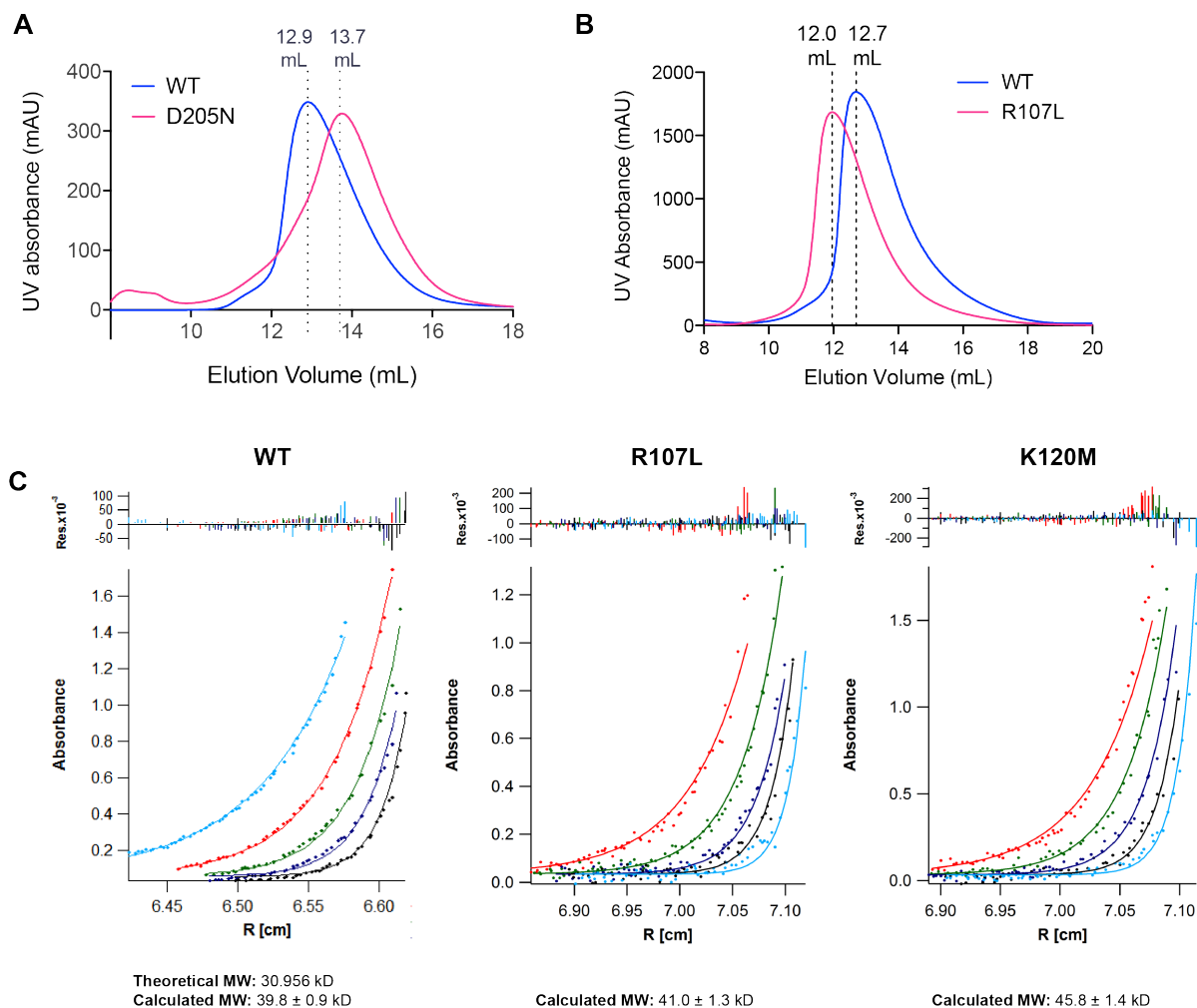


**Figure 6 | Effects of Trb1 KD mutations on oligomerization.**

**(A) & (B)** Size exclusion profiles for Trb1 KD D205N and R107L.

**(C)** Sedimentation equilibrium analytical ultracentrifugation analysis of Trb1 KD WT, R107L, and K120M.

function by facilitating interactions with binding partners. Alternatively, it is possible that Tribbles utilizes the same interface for oligomerization and for interaction with C/EBP transcription factors and Akt.

To further investigate Trb1 oligomerization, we also examined whether mutation of other conserved residues in the pseudokinase domain affected the oligomerization state of Trb1 through analytical size exclusion chromatography. Unlike D205N, Trb1 R107L eluted earlier than Trb1

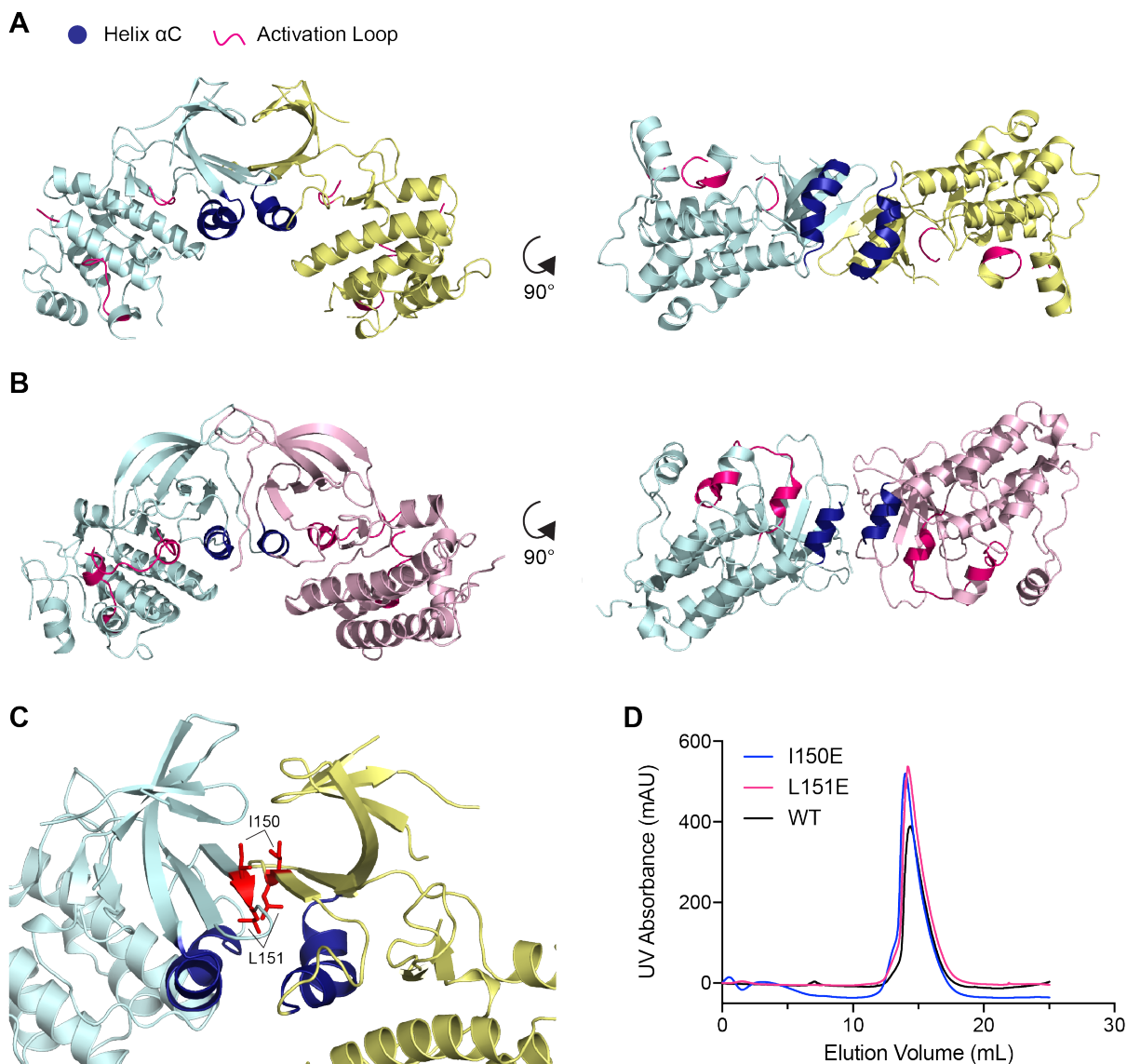


**Figure 7 | Characterization of potential Trb1 dimer interface.**

(A) Cartoon representation of putative Trb1 dimer (PDB: 5CEK).

(B) Cartoon representation of HER3 N-lobe dimer (PDB: 3KEX).

(C) Close-up view of location of I150 and L151 at the putative Trb1 dimer interface.

(D) Size exclusion profiles for Trb1 KD WT, I150E, and L151E.

WT, indicating that this mutation enhances Trb1 oligomerization (Figure 6B). The oligomerization state of Trb1 WT, Trb1 R107L, and Trb1 K120M were also characterized through sedimentation equilibrium analytical ultracentrifugation (AUC) (Figure 6C). The calculated molecular weights for each of these constructs indicated that they were primarily monomeric. However, the calculated

molecular weights for both Trb1 R107L and K120M were both a slightly higher than that for Trb1 WT, indicating that these mutations might increase the propensity of Trb1 to oligomerize. For AUC, these constructs were limited to a concentration of only 37  $\mu$ M in order to stay within the linear range of the detector. It is possible that higher concentrations of Trb1 are necessary to observe oligomer formation.

During the course of this work, crystal structures of the Trb1 pseudokinase domain with and without its C-terminal tail were solved<sup>16</sup>. In the crystal structure of the Trb1 pseudokinase domain, we identified a potential dimer interface between the N-lobes of two molecules of Trb1 in the crystal lattice (Figure 7A). This interface resembles an N-lobe dimer interface previously observed in a crystal structure of the pseudokinase domain of HER3 (Figure 7B) and is not present in the structure of Trb1 that includes its C-terminal tail<sup>16,17</sup>. To test whether this potential interface is responsible for mediating Trb1 oligomerization, we introduced two mutations I150E and L151E that we expected would disrupt dimerization through this interface (Figure 7C). However, we found that both mutants still behaved similarly to Trb1 WT during size exclusion chromatography (Figure 7D), indicating that these mutations had no effect on Trb1 oligomerization.

## DISCUSSION

The functions of pseudokinases are often regulated through occupancy of the nucleotide-binding pocket and through self-association. In our studies of Trb1, we have verified that Trb1 is catalytically inactive since it is incapable of binding to ATP. These findings are consistent with recent work examining the biochemical properties of Trb1 and with crystal structures of Trb1 that show that its nucleotide-binding pocket is highly occluded<sup>16</sup>. We also found that the putative nucleotide-binding pocket of Trb1 is unable to bind to known ATP-competitive small molecule

kinase inhibitors even though the inhibitors that we screened have been shown to be bind promiscuously to a diverse array of kinases. Consequently, typical kinase inhibitor scaffolds are unlikely to be able to target the Trb1 pseudoactive site. A recent study found that binding of the transcription factor C/EBP $\alpha$  to the C-lobe of Trb1 induces a conformational change in the activation loop of Trb1<sup>18</sup>. This finding demonstrates the ability of the Trb1 pseudoactive site to undergo major structural rearrangements. Further structural studies of the different potential conformations of the Trb1 pseudokinase domain will be needed to ascertain whether any of these conformational states are more amenable to targeting with ATP-competitive small molecules.

Our findings also indicate a potential role for self-association in Trb1 function. Both COP1 and C/EBP transcription factors are known to function as dimers. Consequently, it would not be surprising if Tribbles pseudokinases must also dimerize to interact with these binding partners. A functional role for Tribbles self-association was first suggested by studies of *Drosophila* Tribbles that found that mutation of the HRD aspartate prevented Tribbles self-association and impaired Tribbles-mediated degradation of Slbo and inhibition of Akt<sup>2,4</sup>. We found that an analogous mutation in human Trb1 reduces the propensity of Trb1 to oligomerize, while a gain-of-function mutation, R107L, first discovered in a patient with acute megakaryocytic leukemia had the opposite effect and seemed to enhance Trb1 oligomerization. Similarly, mutation of the  $\beta$ 3 lysine, K120M, also appeared to increase Trb1 oligomerization. Collectively, these results indicate that oligomerization could enhance Trb1 function and that mutations in the pseudoactive site can modulate the ability of the pseudokinase domain to self-associate. Since both K120M and D205N are located within the pseudoactive site, they are unlikely to be directly involved in an oligomerization interface. Instead, these mutations likely bias the pseudokinase domain toward different conformations that affect its ability to self-associate. R107L is located on the surface of

the N-lobe and, thus, could potentially be involved in interacting with another monomer of Trb1. Notably, R107 corresponds to Q84 in Trb3, and the Trb3 Q84R mutation has been implicated in insulin resistance due to enhanced inhibition of Akt<sup>7</sup>. It is currently unknown whether Trb3 also oligomerizes, but it is tempting to speculate that the Q84R mutation might enhance Trb3 function by promoting its oligomerization. Further studies will be needed to characterize the oligomeric state of Tribbles pseudokinases, identify oligomerization interfaces, and determine how disease mutations and mutations within the pseudoactive site affect the conformation of the pseudokinase domain. Though it remains unknown whether Tribbles pseudokinases self-associate in cells, we have observed that Trb1 and COP1 colocalize in PML bodies in the nucleus (Chapter 2, Figure 2). Proteins that localize to PML bodies are known to form higher order oligomers through multivalent interactions, and thus, Trb1 self-association might be important for determining its subnuclear localization<sup>19</sup>. Additional cellular studies of Trb1 will be necessary to determine whether Trb1 self-associates in cells and how this self-association might affect Trb1 function and localization.

## **MATERIALS AND METHODS**

### **Protein expression and purification**

Trb1 FL (residues 1-372) and Trb1 KD (residues 81-350) were cloned into a modified pET28a vector containing an N-terminal 10xHis tag followed by a TEV protease cleavage site. Both constructs were expressed in BL21 (DE3) pLysS. Cultures were grown at 37°C until the OD<sub>600</sub> reached 0.4 - 0.6. The cultures were then cooled to 18°C and induced with 0.5 mM IPTG overnight. The pellets were flash frozen and stored at -80°C until lysis. The pellets were resuspended in Lysis Buffer (50 mM Tris pH 8.8, 500 mM NaCl, 5% glycerol, and 5 mM  $\beta$ -mercaptoethanol) and lysed using an EmulsiFlex-C5 (Avestin). After centrifugation, proteins were purified using Talon resin

(Clontech) followed by cleavage of the His tag with TEV protease. To remove uncleaved protein and TEV, the protein was incubated with Ni<sup>2+</sup> affinity resin, and the flowthrough was collected. The cleaved protein was then purified via size exclusion chromatography on a Hiload 16/600 Superdex 200 pg column (GE Healthcare) equilibrated in 20 mM Tris pH 8.8, 500 mM NaCl, 5% glycerol, and 2 mM DTT. The protein was then diluted into buffer containing 20 mM Tris pH 8.8, 5% glycerol, and 2 mM DTT and purified via anion exchange on a Resource Q column (Bio-Rad). The purified protein was buffer exchanged into 20 mM Tris pH 8.8, 500 mM NaCl, 5% glycerol, and 2 mM TCEP, concentrated, flash frozen, and stored in aliquots at -80°C. The identity and mass of the purified proteins was verified via mass spectrometry.

#### **In vitro kinase assay**

Kinase activity was measured using a continuous enzyme-coupled reaction system, in which conversion of ATP into ADP results in NADH oxidation, as previously described<sup>20</sup>. The reaction buffer contained 20 mM Tris pH 7.5, 10 mM MgCl<sub>2</sub>, and 0.5 mM ATP. NADH absorbance at 340 nm was measured for 15 minutes at 30°C in a Molecular Devices SpectraMax plate reader.

#### **Mant-ATP binding assay**

Binding assays were carried out in buffer containing 20 mM Tris pH 8.8, 5% glycerol, 150 mM NaCl, 2 mM DTT, 0.6 μM (2'-(3')-O-(*N*-methylantraniloyl)-ATP (mant-ATP) (Invitrogen), and 5 mM MgCl<sub>2</sub>. Fluorescence was measured with an excitation wavelength of 280 nm and an emission wavelength of 450 nm using a FlexStation 3 plate reader. Data shown are representative of two independent experiments.

### **Thermal shift assay**

Thermal shift assays were performed with proteins diluted to 2  $\mu$ M in buffer containing 20 mM Tris pH 8.0, 150 mM NaCl, and 1 mM DTT and assayed with the indicated concentration of ligand in a total reaction volume of 25  $\mu$ L. Sypro Orange (Molecular Probes) was used at a final concentration of 2x with fluorescence detected at 530 nm. The temperature was raised in steps of 1°C/minute from 25°C to 95°C with fluorescence readings taken at each interval. Changes in melting temperature were assessed relative a buffer or DMSO control. The melting temperature ( $T_m$ ) for each sample, which corresponds to the midpoint of the protein unfolding transition, was determined by plotting the fluorescence as a function of temperature and fitting the resulting melt curve to a Boltzmann equation using GraphPad Prism, as previously described<sup>21</sup>. Data shown represent at least two independent experiments.

### **Analytical size exclusion chromatography**

Trb1 oligomerization was examined by running various concentrations of the indicated construct on a Superdex 200 10/300 gl column (GE Healthcare) equilibrated in buffer containing 20 mM Hepes pH 8.0, 5% glycerol, 150 mM NaCl, and 2 mM DTT at a flow rate 0.5 mL/min.

### **Size exclusion chromatography-multi-angle light scattering (SEC-MALS)**

Purified proteins were injected onto a Superdex 200 10/300 gl column (GE Healthcare) equilibrated in buffer containing 20 mM Hepes pH 8.0, 150 mM NaCl, 5% glycerol, and 0.1 mM TCEP at a flow rate of 0.3 mL/min. Multi-angle light scattering profiles were recored using a miniDAWN TREOS laser photometer (Wyatt Technology) and an Optilab rEX refractive index

detector (Wyatt Technology). Data were processed using ASTRA software package 6.0.6.13 (Wyatt Technology).

### **Analytical ultracentrifugation**

Sedimentation equilibrium experiments were carried out using a Beckman XL-I Analytical Ultracentrifuge with the indicated Trb1 constructs at 37  $\mu$ M in buffer containing 20 mM Tris pH 8.8, 500 mM NaCl, 5% glycerol, and 2 mM TCEP at speeds of 25,000, 30,000, 35,000, 40,000, and 45,000 rpm at 25°C. Data collected on UV absorbance at 280 nm for each sample from the five speeds were fit globally to single-species equilibrium sedimentation by a nonlinear least-squares method using Igor Pro (Wavemetrics).

### **ACKNOWLEDGEMENTS**

We would like to thank Erin Thompson for purifying several Trb1 mutants and her assistance with examining their oligomerization, Yao Fan for providing mant-ATP and assisting with mant-ATP binding assays, Chris Kimberlin for assistance with SEC-MALS and AUC, Shao-Qing Zhang for performing sedimentation equilibrium AUC experiments, Juan Oses-Prieto for performing mass spectrometry, and Chris Novotny and Kevan Shokat for providing kinase inhibitors for the thermal shift assays. We would also like to thank all members of the Jura Lab for their advice and helpful discussions, especially Tarjani Thaker for her assistance with setting up the thermal shift assays, Peter Littlefield for providing purified HER3, as well as Chris Agnew and Lijun Liu for their help with crystallography and x-ray data collection.



## REFERENCES

1. Keeshan, K. *et al.* Transformation by Tribbles homolog 2 (Trib2) requires both the Trib2 kinase domain and COP1 binding. *Blood* **116**, 4948–4957 (2010).
2. Das, R., Sebo, Z., Pence, L. & Dobens, L. L. *Drosophila* Tribbles Antagonizes Insulin Signaling-Mediated Growth and Metabolism via Interactions with Akt Kinase. *PLoS ONE* **9**, e109530 (2014).
3. Du, K., Herzig, S., Kulkarni, R. N. & Montminy, M. TRB3: a tribbles homolog that inhibits Akt/PKB activation by insulin in liver. *Science* **300**, 1574–1577 (2003).
4. Masoner, V. *et al.* The kinase domain of *Drosophila* Tribbles is required for turnover of fly C/EBP during cell migration. *Developmental Biology* **375**, 33–44 (2013).
5. Yokoyama, T. *et al.* Trib1 links the MEK1/ERK pathway in myeloid leukemogenesis. *Blood* **116**, 2768–2775 (2010).
6. Yokoyama, T. *et al.* Identification of TRIB1 R107L gain-of-function mutation in human acute megakaryocytic leukemia. *Blood* **119**, 2608–2611 (2012).
7. Prudente, S. *et al.* The functional Q84R polymorphism of mammalian Tribbles homolog TRB3 is associated with insulin resistance and related cardiovascular risk in Caucasians from Italy. *Diabetes* **54**, 2807–2811 (2005).
8. Lavoie, H., Li, J. J., Thevakumaran, N., Therrien, M. & Sicheri, F. Dimerization-induced allostery in protein kinase regulation. *Trends in Biochemical Sciences* (2014). doi:10.1016/j.tibs.2014.08.004
9. Claus, J. *et al.* Inhibitor-induced HER2-HER3 heterodimerisation promotes proliferation through a novel dimer interface. *eLife* **7**, 16ra7–23 (2018).

10. Zeqiraj, E. *et al.* ATP and MO25 $\alpha$  Regulate the Conformational State of the STRAD $\alpha$  Pseudokinase and Activation of the LKB1 Tumour Suppressor. *PLoS Biol.* **7**, e1000126 (2009).
11. Hammarén, H. M. *et al.* ATP binding to the pseudokinase domain of JAK2 is critical for pathogenic activation. *Proc. Natl. Acad. Sci. U.S.A.* (2015). doi:10.1073/pnas.1423201112
12. Foulkes, D. M. *et al.* Repurposing covalent EGFR/HER2 inhibitors for on-target degradation of human Tribbles 2 (TRIB2) pseudokinase. *bioRxiv* 305243 (2018). doi:10.1101/305243
13. Bailey, F. P. *et al.* The Tribbles 2 (TRB2) pseudokinase binds to ATP and autophosphorylates in a metal-independent manner. *Biochem. J.* (2015). doi:10.1042/BJ20141441
14. Cameron, A. J. M. & Cameron, A. J. M. Occupational hazards: allosteric regulation of protein kinases through the nucleotide-binding pocket. *Biochem. Soc. Trans.* **39**, 472–476 (2011).
15. Shi, F. *et al.* ErbB3/HER3 intracellular domain is competent to bind ATP and catalyze autophosphorylation. *Proceedings of the National Academy of Sciences* **107**, 7692–7697 (2010).
16. Murphy, J. M. *et al.* Molecular Mechanism of CCAAT-Enhancer Binding Protein Recruitment by the TRIB1 Pseudokinase. *Structure* **23**, 2111–2121 (2015).
17. Jura, N., Shan, Y., Cao, X., Shaw, D. E. & Kuriyan, J. Structural analysis of the catalytically inactive kinase domain of the human EGF receptor 3. *Proc. Natl. Acad. Sci. U.S.A.* **106**, 21608–21613 (2009).

18. Jamieson, S. A. *et al.* Substrate binding allosterically relieves autoinhibition of the TRIB1 pseudokinase. *bioRxiv* 313767 (2018). doi:10.1101/313767
19. Lallemand-Breitenbach, V. & de Thé, H. PML nuclear bodies. *Cold Spring Harb Perspect Biol* **2**, a000661 (2010).
20. Zhang, X., Gureasko, J., Shen, K., Cole, P. A. & Kuriyan, J. An allosteric mechanism for activation of the kinase domain of epidermal growth factor receptor. *Cell* **125**, 1137–1149 (2006).
21. Niesen, F. H. *et al.* The use of differential scanning fluorimetry to detect ligand interactions that promote protein stability. *Nat Protoc* **2**, 2212–2221 (2007).



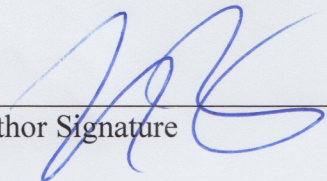
**Publishing Agreement**

*It is the policy of the University to encourage the distribution of all theses, dissertations, and manuscripts. Copies of all UCSF theses, dissertations, and manuscripts will be routed to the library via the Graduate Division. The library will make all theses, dissertations, and manuscripts accessible to the public and will preserve these to the best of their abilities, in perpetuity.*

***Please sign the following statement:***

*I hereby grant permission to the Graduate Division of the University of California, San Francisco to release copies of my thesis, dissertation, or manuscript to the Campus Library to provide access and preservation, in whole or in part, in perpetuity.*

Author Signature



Date

6/7/18